Air water flow conditions on spillway channels downstream of Piano key weirs

Auteur : Dalem, Juliette
Promoteur(s) : Erpicum, Sebastien
Faculté : Faculté des Sciences appliquées
Diplôme : Master en ingénieur civil des constructions, à finalité spécialisée en "civil engineering"
Année académique : 2022-2023
URI/URL : http://hdl.handle.net/2268.2/17726

University of Liège, Faculty of Applied Sciences

Air water flow conditions on spillway channels downstream of Piano key weirs

Master thesis conducted by

DALEM Juliette

with the aim of obtaining the degree of Master in Civil Engineering

Promotor:
S.Erpicum - ULiège

Jury:
B.Dewals - ULiège
F.Nguyen - ULiège
D.Bung - FH Aachen

Academic year 2022-2023

Acknowledgements

First of all, I would like to express my deep gratitude to my supervisor, Pr. Sebastien Erpicum, for his precious advice and guidance throughout this work.

I would also like to thank the team of the hydraulic laboratory (Maxime Mathieu, Gregory Thonard and Claude Lhermerout) for their patience and help during this work. Without them, the experimental part would not have been possible.

I am extremely thankful to Pr. Daniel Bung for lending me the probes and also for his follow-up and advices during this work.

I would like to thank Pauline and Caroline for taking the time to carefully read over my work.

Finally, other more familiar actors were present and important for my well-being during the period of this project. I would like to thank my friends and my family for supporting and helping me during my five years at the University of Liège.

Abstract

Piano Key Weirs (PKWs) are an improvement of labyrinth key weirs. This type of weir can be placed on the dams needing to be restored, which is an advantage given the number of ageing dams. PKWs are used as the crest of spillways in order to manage water discharge, mitigate flood risks, and maintain the structural integrity of the dams. However, few studies have been carried out on flow properties downstream of this type of weir.

The main aim of this research work is to compare different flow properties as the clear water depths, the velocities, the air concentration profiles or the dissipated energy for different spillway types for a steep slope. Three weirs are tested: a Creager weir and two PKWs with different geometries. For each weir, a smooth and a stepped spillway are placed, making a total of six configurations tested. The results are obtained with a double-tips conductivity probe.

Different conclusions were drawn from the results obtained in this work. Firstly, more air is entrained in the flow for stepped spillways than for smooth spillways. Moreover, in the case of smooth spillway, the air entrainment is more important for PKWs while, for the stepped spillways, the air entrainment can be considered to be the same for the different weirs. Then, a non-uniformity of heads across the width of the channel appears downstream the PKWs. The head variation is greater for smooth spillways than for stepped spillways. Finally, the stepped spillways dissipate more energy than smooth spillways. Moreover, the type of weir seems to have a small influence on the dissipated energy. Even if the difference is not very important, the dissipated energy is slightly greater in the case of a Creager weir than PKWs.

Résumé

Les déversoirs en touches de piano (PKWs) sont une amélioration des déversoirs en labyrinthe. Ce type de déversoir peut être installé sur les barrages nécessitant une restauration, ce qui est un avantage compte tenu du nombre croissant de barrages vieillissants. Les PKWs sont utilisés comme crête des déversoirs pour gérer l'évacuation de l'eau, atténuer les risques d'inondation et maintenir l'intégrité structurelle des barrages. Cependant, peu d'études ont été menées sur les caractéristiques d'écoulement en aval de ce type de déversoir.

L'objectif principal de ce travail de recherche est de comparer différentes caractéristiques d'écoulement telles que les hauteurs d'eau claire, les vitesses, les profils de concentration d'air ou l'énergie dissipée pour différents types d'évacuateurs de crue sur une pente raide. Trois déversoirs sont testés : un déversoir Creager et deux PKWs avec des géométries différentes. Pour chaque déversoir, un coursier lisse et un coursier en marches d'escalier sont installés, ce qui fait un total de six configurations testées. Les résultats sont obtenus à l'aide d'une sonde de conductivité à double pointe.

Différentes conclusions ont été tirées des résultats obtenus dans ce travail. Tout d'abord, plus d'air est entraîné dans l'écoulement pour les coursiers en marches d'escalier que pour les coursiers lisses. De plus, dans le cas des coursiers lisses, l'entraînement d'air est plus important pour les PKWs que pour le seuil Creager. Pour les coursiers en marches d'escalier, l'entraînement d'air peut être considéré comme étant le même pour les différents déversoirs. Ensuite, une non-uniformité des hauteurs d'eau sur la largeur du canal apparaît en aval des PKWs, la variation de charge est plus importante pour les coursiers lisses que pour les coursiers en marches d'escalier. Enfin, les coursiers en marches d'escalier dissipent plus d'énergie que les coursiers lisses. De plus, le type de déversoir semble avoir une faible influence sur l'énergie dissipée. Bien que la différence ne soit pas très importante, l'énergie dissipée est légèrement plus élevée dans le cas d'un déversoir Creager que pour les PKWs.

Contents

Chapter 1

Introduction

Dams have certainly existed since prehistory. For oldest known dams, there is the Sadd el-Kafara dam in Egypt constructed in 3000 BC. According to N. Schnitter-Reinhardt, the oldest dam would be in Jordan and would have been built at the end of the 4th millennium BC (Wikipedia, accessed in March 2023). More recently, an important number of large dams were built between about 1955 and 1990. For these years, the construction of new dams is still present but decreasing, especially for the last decade. Indeed, Figure 1.1 resumes the annual construction of large dams, which means a dam with a height of 15 meters or greater, from the lowest foundation to crest, or a dam between 5 meters and 15 meters impounding more than 3 million cubic metres according to ICOLD, accessed in March 2023 (International Commission On Large Dams). Thus far, this commission has identified nearly 60,000 large dams in the world.

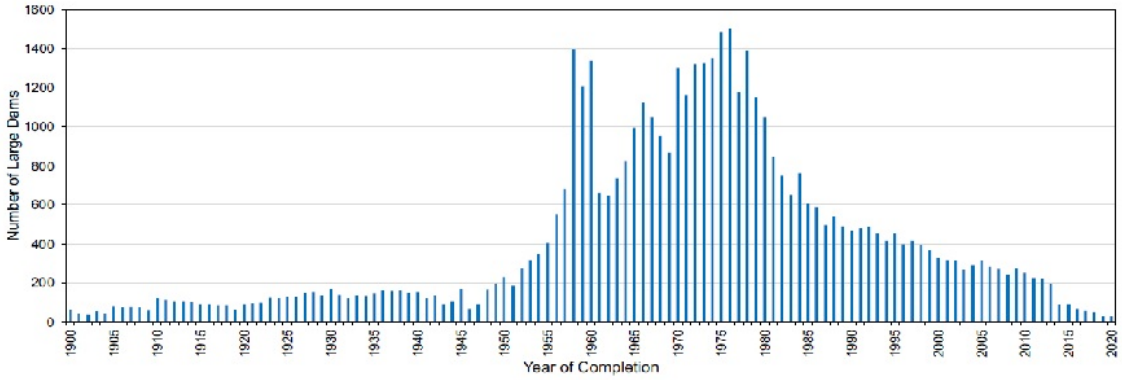

FIGURE 1.1: Annual construction of large dams (ICOLD, accessed in March 2023).

All these different dams may have different uses. Indeed, dams are built for flood control, water supply, irrigation, navigation, hydropower, fish farming or even recreation. Moreover, a dam can serve several purposes at the same time (ICOLD, accessed in March 2023).

Until now, many dams need to be rehabilitated and improved due to different reasons. Firstly, the demand for water rises due to the increase in world population and the demographic trends. Furthermore, the vast majority of dams were built about 50 years ago, and things have changed since then. Indeed, the safety has been improved to avoid accident and dam overtopping which leads to significant damages. Moreover, another aspect which leads to change the current dams structures is the fact that the peak flow values are higher than before. The reasons are the availability of more extensive hydrologic data series and the climate change. As a result, the current dams have to be modified to increase the storage of water and to increase the capacity to pass the flow. (Anderson and Tullis, 2013, Crookston et al., 2019 and Singh and Kumar, 2022).

An important part of the dams is the spillway. Spillways provide safe release of floodwaters from a dam to a downstream area by controlling overflows. A spillway has three components:

- Weir
- Spillway channel
- Energy dissipation structure

There are two main categories of spillways: free-flow spillways or gated spillways. Gated spillways are equipped with gates that regulate the flow rate. Indeed, they can be lowered or raised to enable discharge control. For free-flow spillways, the water drains from the reservoir when its level reaches the crest of the spillway. There are two families of free-flow spillways: the linear weirs (Creager weir) and non-linear weirs (labyrinth key weir or piano key weirs). Free-flow spillways weirs prove to be the best option in terms of reliability, simplicity, safety, construction costs, and maintenance. However, unlike gated spillways, they do not allow any control of the flow discharged, which decreases their discharge capacity (Cfbr, accessed in June 2023). A spillway with a high discharge capacity enables greater water storage in the reservoir while maintaining acceptable levels of dam overtopping and other upstream flood-related risks (Erpicum et al., 2020).

Then, the spillway channel can be of various types: it is possible to have smooth or stepped spillways.

Existing dams with different types of spillways are shown on Figures 1.2 to 1.5.

FIGURE 1.2: Beaver dam (US) – gated spillway (finartamerica, accessed in June 2023).

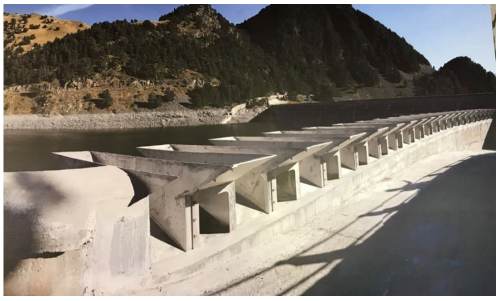

FIGURE 1.3: Oule dam - PKW (Defi12, accessed in June 2023).

FIGURE 1.4: Riou dam (France) - stepped spillway (IAHR, accessed in June 2023).

FIGURE 1.5: Charmines dam (France) - PKW and smooth spillway (LeProgrès, accessed in June 2023).

1.1 Summary diagram

To help with the understanding of the different parts of this thesis, Figure 1.6 includes the most important geometric parameters of a stepped spillway with a Creager weir. Firstly, the coordinates x, y and z are represented: x is the direction of the flow from the top of the spillway, y the height from the bottom of the channel or the pseudo bottom calculated perpendicularly to it. Finally, z is the distance from the left side of the channel. After that, the geometric parameters are:

- s: vertical step height
- ϕ: inclination of the spillway
- H_{dam}: vertical height of the spillway
- L: the width of the channel
- H: upstream head which depends on the discharge

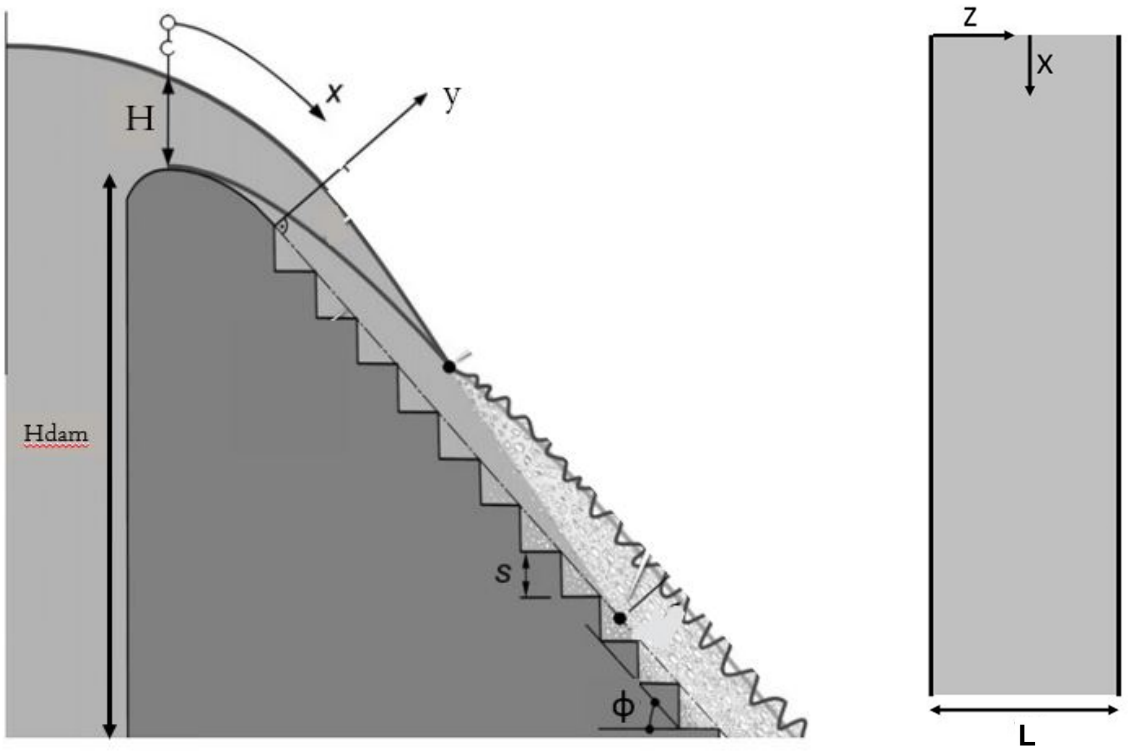

FIGURE 1.6: Definition sketch (Pfister and Hager, 2011).

Chapter 2

State of the Art

2.1 Stepped spillway

The stepped spillways have been used for centuries because of different advantages. At the beginning, the reasons why people used them were for the ease of construction and the simplicity of design. In a second time, they were used because stepped spillways increase the energy dissipation compared to smooth spillways. This generates smaller dimensions of the dissipation basin at the toe of the dam. This energy dissipation increase is due to the macro-roughness of the steps (Chanson, 2001). Indeed, the friction coefficient for a stepped spillway is higher than for a smooth spillway which generates a decrease in velocity, an increase in flow height and more energy dissipation.

Another advantage is that stepped spillways reduce the potential risk of cavitation thanks to the significant aeration. Indeed, due to the compressibility of the air-water mixture, a bottom air concentration of about 5-8% is considered sufficient to avoid cavitation damage (Boes and Hager, 2003b).

For stepped spillways, three different flow regimes were determined according to a dimensionless flow rate corresponding to the ratio between the critical height (h_c) and the vertical step height (s). The critical height itself depends on the unit discharge ($h_c = (q_W^2/g)^{1/3}$). The three different flow regimes are called nappe flow, transition flow and skimming flow (Chanson, 2001).

2.1.1 The nappe flow

The nappe flow appears for low discharges and large steps. It corresponds to a succession of free-falling jets over each step of the spillway. Under all these jets, some air nappes appear, as it can be seen on Figure 2.1. In this case, the flow energy is dissipated by jet breakup in air, jet impact, mixing and the formation of a fully developed or partial hydraulic jump on the steps. Stepped spillways with nappe flow can be analysed as a series of drop structures (Chanson, 1994).

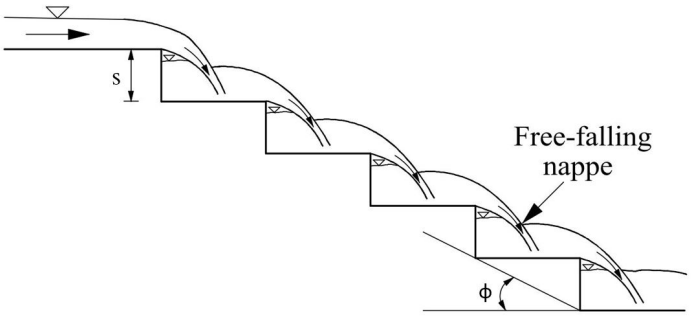

FIGURE 2.1: Nappe flow (Baylar et al., 2009).

As already mentioned, for stepped spillways, the flow aeration is very important. In the case of the nappe flow, some air bubbles enter into the flow at each step at the toe of each free-falling (Chanson, 1994).

2.1.2 The skimming flow

The skimming flow appears for large discharges and small steps. According to Boes and Hager, 2003a, Equation 2.1 has to be verified to have a skimming flow,

$$\frac{h_c}{s} > 0.91 - 0.14tan(\phi) \tag{2.1}$$

The water flows as a coherent stream above the pseudo-bottom formed by the edges of the steps. Some recirculation zones are formed between the pseudo-bottom and the steps in the triangular zones (Figure 2.2). These vortices are maintained thanks to the important shear stresses between the pseudo-bottom and the coherent flow. In this case, the flow energy is dissipated by the recirculating vortices (Bung, 2011, Boes and Hager, 2003a, Chanson and Gonzalez, 2005).

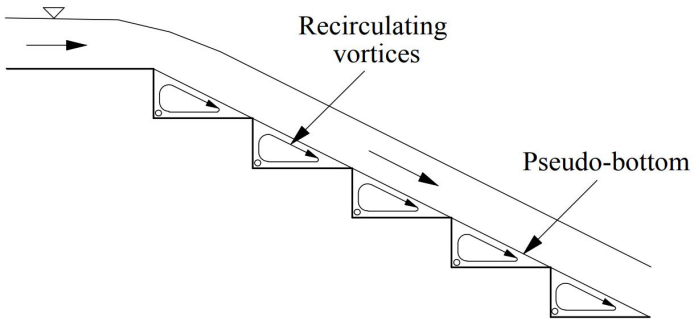

FIGURE 2.2: Skimming flow (Baylar et al., 2009).

A skimming flow is divided in three different parts (Figure 2.3). At the upper part of the spillway, the flow is unaerated and the water in this part is called clear water. For this flow region, the velocity increases, which generates a height decrease. On this part, the turbulent boundary layer starts to grow until it reaches the water surface. At this moment, the degree of turbulence is high enough to entrain air into the flow. The point where the aeration begins is called inception point. The air-water flow after this point is called white water. The location of the inception point (L_i) on stepped spillways is closer to the spillway crest than on smooth chutes (Chanson, 1994).

This location depends on the channel slope (ϕ), the step height (s) and the critical height ($h_c = (q_W^2/g)^{1/3}$), as described by Equation 2.2 proposed by Boes and Hager, 2003b

$$L_i = \frac{5.90 h_c^{1.2}}{(sin\phi)^{1.4} s^{0.2}} \tag{2.2}$$

The second part of the skimming flow is the gradually varied flow: the aeration is more and more important. In this part, the height increases until it reaches a plateau which corresponds to the uniform height. Thus, the third and last part is the uniform flow region: the characteristics of flow (depth, velocity and air concentration) stay the same along this part of the spillway. These characteristics only depend on the flow rate, the slope of the spillway and the step height.

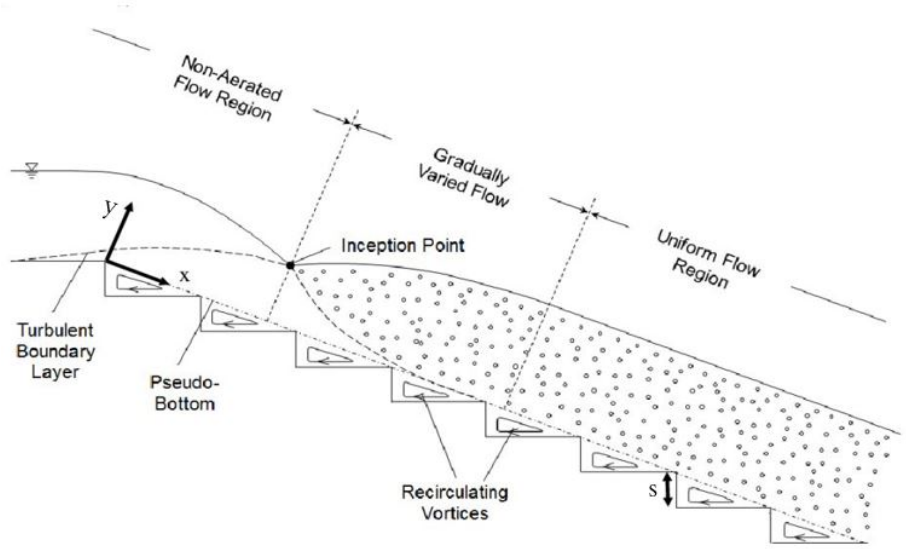

FIGURE 2.3: Skimming flow over a stepped spillway identifying key flow features such as the inception point, recirculating vortices and air entrainment (Van Alwon et al., 2017).

Analytic model

An analytic model was developed in the article of Boes and Hager, 2003a to calculate the different uniform flow characteristics. Firstly, the vertical height from the top to reach the uniform flow ($H_{dam,u}$) is defined by Equation 2.3.

$$\frac{H_{dam,u}}{h_c} = 24 sin\phi^{2/3} \tag{2.3}$$

Two characteristic uniform flow depths can be calculated: the uniform equivalent clear water depth ($h_{w,u}$) and the uniform mixture-flow depth ($h_{90,u}$). The index 90 means that the air concentration is equal to 90% at $y = h_{90,u}$.

$$\frac{h_{w,u}}{s} = 0.23 F_*^{0.65} \tag{2.4}$$

$$\frac{h_{90,u}}{s} = 0.5 F_*^{(0.1 tan\phi + 0.5)} \tag{2.5}$$

In Equations 2.4 and 2.5, F_* corresponds to the characteristic roughness Froude number. This number depends on the discharge, the slope and the vertical step height.

$$F_* = \frac{q_w}{\sqrt{g sin\phi s^3}} \tag{2.6}$$

Air concentration profile

The air concentration depends on the transverse coordinate (y) originating at the pseudo-bottom and perpendicular to it. Firstly, Wood, 1991 proposed an equation to approximate the air concentration. This model is based on the one used for the distribution of suspended sediment in a flowing stream. Then, the air concentration distribution was given by the air bubble advective-diffusion equation (Chanson, 1995a). This method was approved for the stepped spillway by Chanson, 1995b. Later on, an advanced air concentration distribution for stepped spillway was developed by Chanson and Toombes, 2002 and verify by Bung, 2011. The different equations for each model are in Equation 2.7 to Equation 2.14.

1. Wood, 1991

$$C(y) = \frac{\beta}{\beta + exp(\gamma cos\phi y'^2)} \tag{2.7}$$

In Equation 2.7, y' is the non-dimensional depth ($y' = y/y_{90}$), y_{90} corresponds to the flow height where the air concentration is equal to 0.9. β and γ are constants. To find these two constants, two relations are needed. The first one is the condition $C(y' = 1) = 0.9$ and the second one is described by Figure 2.4 which allows to find $\gamma cos\phi$ for a desired mean air concentration (C_{mean}).

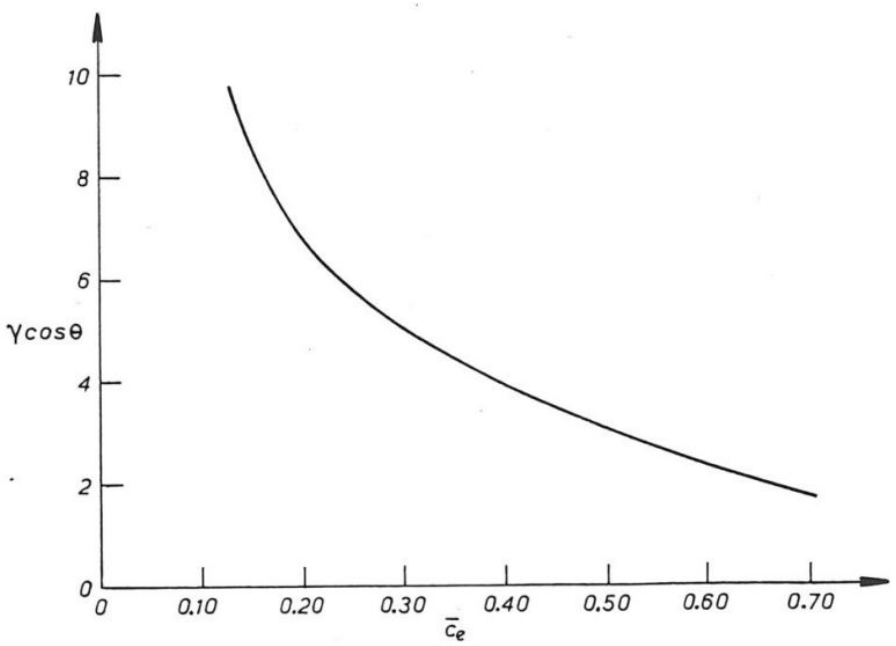

FIGURE 2.4: Plot of $\gamma cos\phi$ [-] vs. the equilibrium air concentration C_{mean} [-] (Wood, 1991).

2. Chanson, 1995a

$$C(y) = 1 - tanh^2\left(K' - \frac{y/y_{90}}{2D'}\right) \tag{2.8}$$

$$K^* = arctanh(\sqrt{0.1}) \qquad K' = K^* + \frac{1}{2D'} \tag{2.9}$$

$$C_{mean} = 2D'\left(tanh\left(K^* + \frac{1}{2D'} - tanh(K^*)\right)\right) \tag{2.10}$$

3. Chanson and Toombes, 2002

$$C(y) = 1 - tanh^2\left(K' - \frac{y/h_{90}}{2D_0} + \frac{(y/y_{90} - 1/3)^3}{3D_0}\right) \tag{2.11}$$

$$K^* = arctanh(\sqrt{0.1}) \qquad K' = K^* + \frac{1}{2D_0} - \frac{8}{81D_0} \tag{2.12}$$

$$C_{mean} = 0.7622(1.0434 - exp(-3.614D_0)) \tag{2.13}$$

For the three different models, the average air concentration is calculated with Equation 2.14.

$$C_{mean} = \frac{1}{y_{90}} \int_{y=0}^{y=y_{90}} C(z)dz \tag{2.14}$$

Moreover, the average air concentration can be used to calculate the clear water depth (h_w) from the flow height corresponding to an air concentration equal to 0.9 (Equation 2.15).

$$h_w = y_{90}(1 - C_{mean}) \tag{2.15}$$

An example of comparison between these three air concentration profiles is shown at Figure 2.5.

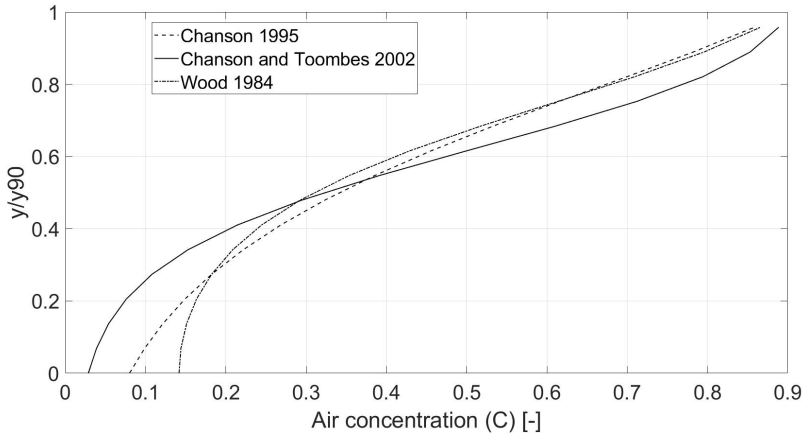

FIGURE 2.5: Example of air concentration distributions.

As it can be seen on Figure 2.5, the air concentration increases when the distance from the pseudo-bottom increases. From the air concentration profile, three distinct flow regions can be distinguished (Boes and Hager, 2003b):

- $C < 0.3 - 0.4$: Mainly clear water flow comprising small air bubbles.
- $C > 0.6 - 0.7$: Mainly air flow comprising water droplets.
- Intermediate region with a true two-phase flow.

Velocity profile
The velocity distribution for a stepped spillway follows a power law (Equation 2.16). In this equation, V_{90} represents the velocity for an air concentration equals to 90%. Depending on the research, different values of N have been found. These values are displayed in Table 2.6. Figure 2.7 is an example of the different velocity distribution depending on N.

$$\frac{V}{V_{90}} = \left(\frac{y}{y_{90}}\right)^{1/N} \tag{2.16}$$

Articles	Value of N
Carosi and Chanson, 2008	10
Chanson and Felder, 2010	7
Matos, 2000	5.1
Boes, 2000	5.8

FIGURE 2.6: Different values of N.

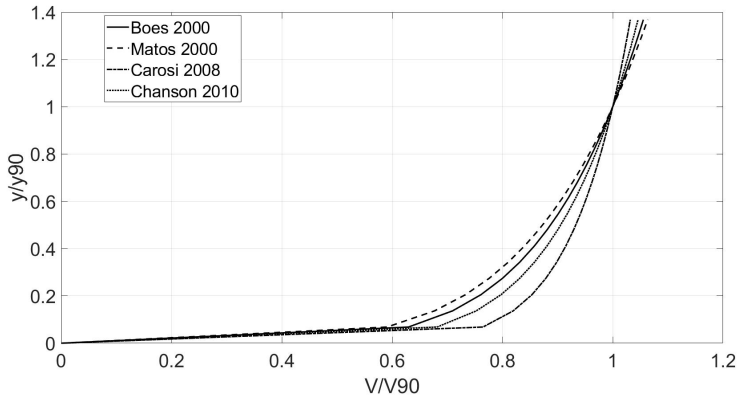

FIGURE 2.7: Example of velocity distributions.

This velocity profile allows to calculate another important parameter for a skimming flow: the average velocity, which can be calculated with Equation 2.17.

$$V_{mean} = \frac{1}{y_{90}} \int_{y=0}^{y=y_{90}} V(z)dz \tag{2.17}$$

2.1.3 The transition flow

The transition flow is the third flow regime in a skimming flow. It is a mixing between the nappe flow and the skimming flow. In fact, the free surface of the flow is not parallel to the pseudo bottom, but the flow can not be assimilated to a sum of free-falling. Under the pseudo-bottom, it is possible to have flow recirculation as for skimming flow but also air cavitation as the nappe flow (Figure 2.8). This flow is characterized by a chaotic behaviour and strong splashing and droplets projections. In general, this flow condition should be avoided (Chanson and Gonzalez, 2005).

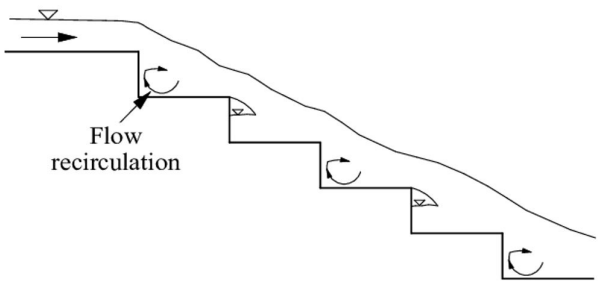

FIGURE 2.8: Transition flow (Baylar et al., 2009).

2.2 Piano Key Weir (PKW)

"With rising demands for more reservoir water storage, increasing magnitudes of probable maximum flood events and the continuing need to improve dam safety, the capacities of many existing spillways are currently inadequate and in need of upgrade or replacement"(Anderson and Tullis, 2013). In order to solve this problem, three solutions can be considered :

- Increase the width of the spillway
- Lower the spillway crest elevation
- Increase the crest length

The width increase is often complicated to realise because of the geometry of the dam and the costs involved. Moreover, lowering the spillway crest height decreases the water storage capacity of the dam. This disadvantage is often avoided because this water storage is used for hydroelectricity, water supply,... (Anderson and Tullis, 2013). Then, the best solution for the rehabilitation of the existing dams is increasing the crest length. With that knowledge, a new type of free crest spillway has been designed: the labyrinth key weir (Figure 2.9, left). This type of weir was initially investigated by Gentilini in 1941. Following the publication of significant research by the US Bureau of Reclamation and the American Society of Civil Engineers (ASCE) in the 1980s, as well as the construction of Ute Dam (USA), the number of Labyrinth weir projects experienced an exponential growth (Erpicum et al., 2020).

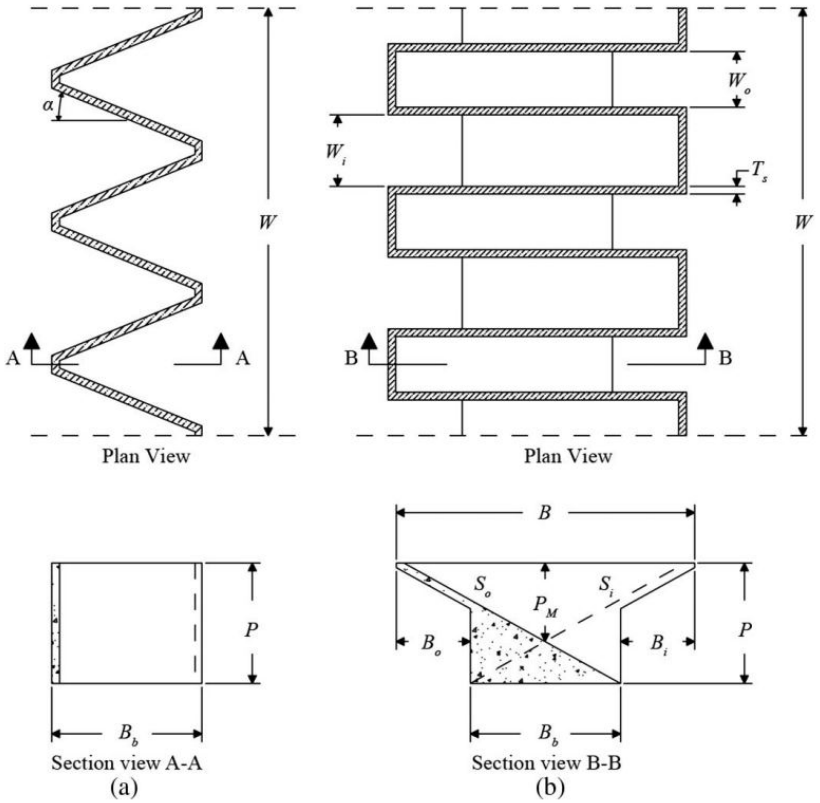

FIGURE 2.9: Typical weir geometries: (a) trapezoidal labyrinth (top and bottom); (b) PK (top and bottom) (Anderson and Tullis, 2013).

With a view to further improving the type of weir at the crest of the dam, from 1999, the NGO Hydrocoop began investigations to improve the traditional Labyrinth concept, in close collaboration with the Electricité de France - Laboratoire National d'Hydraulique (EDF-LNH) in France, the Indian Institute of Technology Roorkee in India and the Biskra University in Algeria. Thanks to these investigations, Lempérière and Ouamane, 2003 proposed for the first time the Piano Key weir (noted also PKW) (Erpicum et al., 2020). Unlike labyrinth weirs, PKWs can be placed on the dams needing to be restored or they can be used for new dams. PKWs are a development of the labyrinth weirs with a rectangular labyrinth, vertical walls connected by alternating inclined bottom plates which create inlets and outlets. These characteristics explain the name of this type of spillway because it seems like piano keys (Figure 2.9, right). The first dam with this installation was built in 2006 at Goulours in France (Figure 2.10) (Laugier et al., 2013).

FIGURE 2.10: Goulours dam in France (link).

The type of weir strongly influences the aeration of the flow. Indeed, the full aeration begins upper on the spillway with a PKW than with ogee crested weir (Silvestri et al., 2013). As a reminder, at the beginning of the stepped spillway a non-aerated zone is firstly present, followed by a gradually aerated zone and finally a fully-aerated zone for a stepped spillway with a Creager weir.

The PKWs present several advantages. The main advantage is the increase in spillway discharge capacity. Indeed, the increase of the crest length allows a better discharge capacity. Then, the sloping floors create cantilevers, which leads to a smaller footprint of the foundation. This aspect can especially help in reduced build area (Lempérière and Ouamane, 2003). Moreover, this type of crest decreases the cost because of the prefabricated formwork. This can be used because of the repetitive cycles even if the geometry is complex. Consequently, the construction time is relatively short (Laugier et al., 2013). The PKWs also increase the safety at low cost, the flood prevention and the storage of reservoirs (Ouamane and Lempérière, 2006). Then, their construction is simple and requires minimal maintenance. Moreover, the PKWs increase the aeration of the flow which reduces the risk of erosion downstream.

2.2.1 Types of PKW

Two types of PKW can be identified according to the overhang of keys. The first one, called PKW type A, has similar upstream and downstream overhangs. This solution is often chosen because this type of PKW can be built with precast concrete elements due to the self balanced structure (Figure 2.12, left). The second type, called PKW type B, has only upstream overhangs (Figure 2.12, right) (Lempérière and Ouamane, 2003).

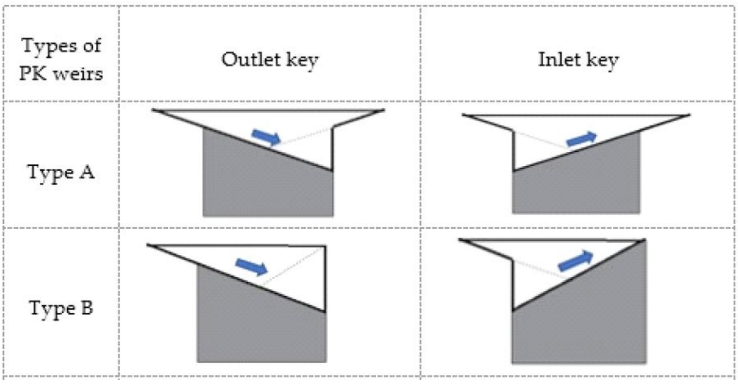

FIGURE 2.11: Two main types of PKW (Bhukya et al., 2022).

2.2.2 Notation of PKW

Even for one solution it exists a lot of PKW's settings depending on different parameters: the number of "PKW unit" (W_u) composed of two transversal walls, an inlet and two half outlets but also weir height (P), lateral crest length (B), inlet and outlet widths (W_i, W_o), up- and downstream overhang lengths (B_o, B_i) and wall thickness (T_s). All these notations are shown in Figure 2.12.

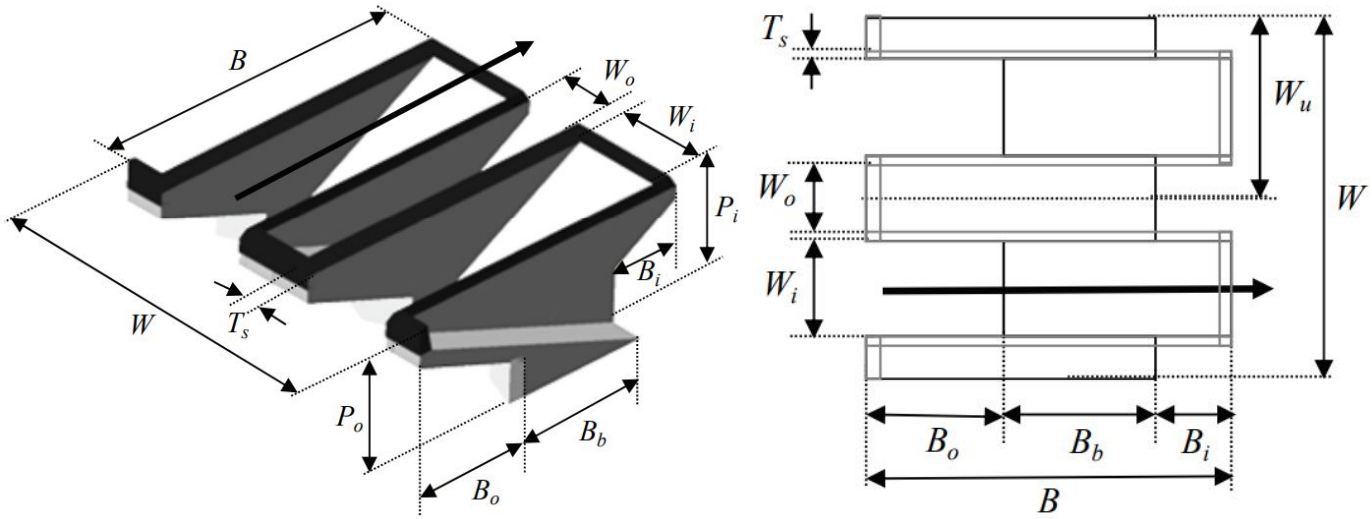

FIGURE 2.12: Geometric parameters of PKW (Pralong et al., 2011).

Two different approaches can described the hydraulic performance of a PKW (Schleiss, 2011):

1. The Poleni equation is considered as the base and the different PKW parameters are taking into account in the discharge coefficient (C_w). In Equation 2.18, L is the crest lenght, H the total upstream head and g the gravitational constant.

$$Q = C_w L \sqrt{2gH^3} \tag{2.18}$$

2. A discharge enhancement ratio (r) is calculated between the PKW discharge (Q_{PKW}) and the corresponding sharp-crested weir discharge (Q_w), as shown in Equation 2.19.

$$r = \frac{Q_{PKW}}{Q_W} \tag{2.19}$$

2.2.3 Flow patterns

The PKWs were designed in order to increase the crest length which has the effect, for low head, to increase significantly the discharge capacity. However, the passing capacity decreases when the discharge increases due to the interaction between the different nappes. Indeed, when the head increases, the opposite nappes begin to interact until they disappear (Figure 2.13). The more the distance between two inlets is important, the more the discharge has to be important to have an interaction between the jets. Finally, when the flow rate is too important, the efficiency decreases rapidly and the crest length tends to the channel width, which corresponds to the crest length for a standard linear crest (Schleiss, 2011).

FIGURE 2.13: Nappes interactions depending on the discharge (Silvestri, 2011-2012).

Lopes et al., 2011 described the flow properties downstream of labyrinths weirs, in particular under the trapezoidal labyrinth weirs. Above the crest, the flow is two-dimensional but in the chute and downstream the crest, the flow becomes three-dimensional. When the flow is supercritical, the nappe interference and the jet impact on the spillway create water splashing and jet deflection which leads to shockwaves and areas of air entrainment. Downstream this, shockwaves propagate and create some local maxima and minima flow depths when they intersect each other. Further downstream, a two-dimensional flow appears and this flow can be characterized by a relation between the total upstream head H [m] over the weir crest, the weir height P [m] and the magnification ratio (L/W).

Once enough experimental results have been obtained, Lopes et al., 2011 estimated the residual energy under trapezoidal labyrinth weirs. They concluded that this residual energy increases non-linearly as the upstream specific energy increases. Moreover, an empirical equation was found to fit with the experimental results to be able to calculate the residual energy under trapezoidal labyrinth weirs.

Approximatively ten years later, Merkel et al., 2018 studied the rectangular labyrinth weirs and arrived at the conclusion that the behaviours under this type of weir are more or less the same as those of trapezoidal labyrinth weirs.

Finally, R. Eslinger and Crookston, 2020 studied the energy dissipation under PKW thanks to different Type A PKW models with different width ratios (W_i/W_o). In this study, the channel downstream of the PKW is horizontal. Firstly, they compared the flow pattern at the toe of PKWs and of labyrinth weirs. Some differences were found as the position of the jets. The PKW jets are aligned with the outlet keys, while they are aligned to the apexes for labyrinth weirs. In addition to this, the intensity of the jets seems to be more important for PKWs. Finally, the deflection angles caused by the shockwaves are smaller for PKWs which leads to reduction in downstream interactions jets. Figure 2.14 shows the downstream flow fields of a PKW.

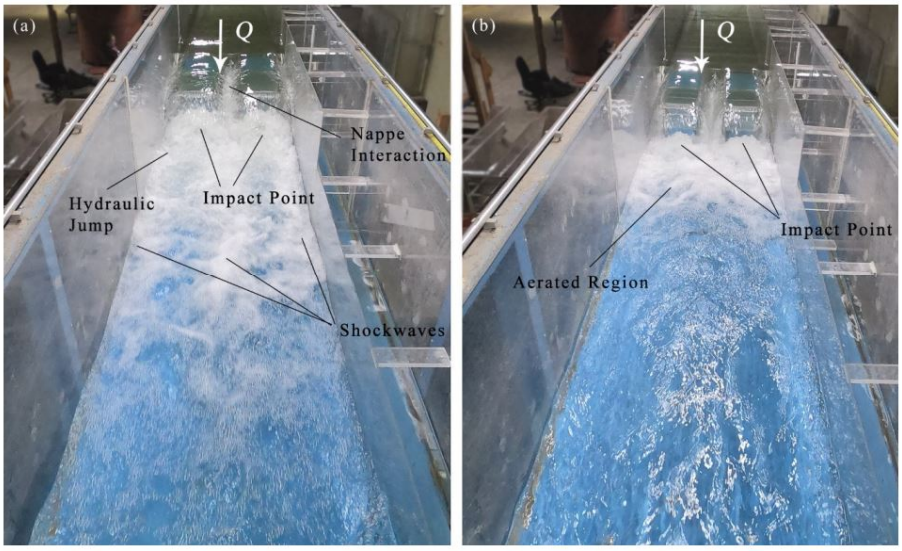

FIGURE 2.14: Downstream flow field of Type A PKW for (a) H/P = 0.23 and (b) H/P = 0.12 (R. Eslinger and Crookston, 2020).

After the comparison of the pattern of flows, R. Eslinger and Crookston, 2020 analysed the energy dissipation under the different PKWs. Their results are displayed on Figure 2.15. On this figure, some results for labyrinth weirs are also present to compare them to the PKWs results.

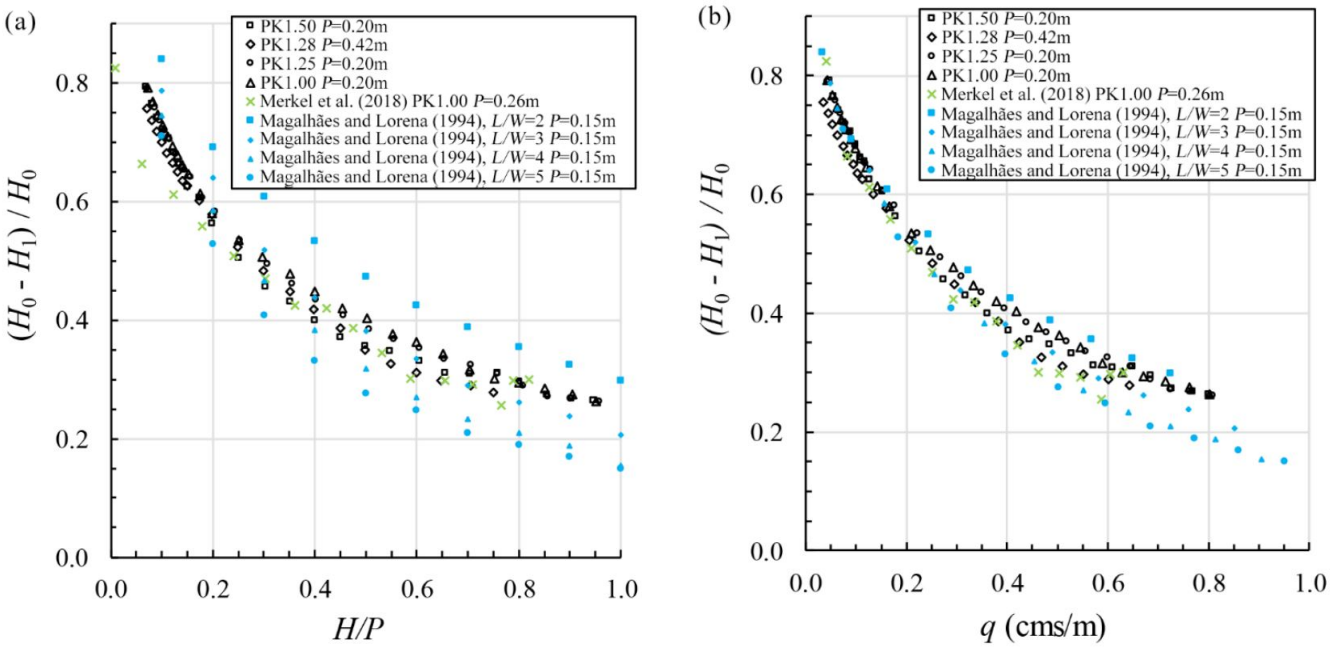

FIGURE 2.15: Relative energy dissipation $[(H0 - H1)/H0]$ [-] with respect to (a) the head water ratio (H/P) [-] and (b) unit discharge (q) [cms/m] for Type A PKW (R. Eslinger and Crookston, 2020).

These results lead to several conclusions. Firstly, when the discharge increases, the volumetric space of the outlet decreases, which leads to a smaller jet interaction and therefore to a decrease in energy dissipation. This also explains why the PKWs are less effective at dissipating energy at higher heads as it can be observed on Figure 2.15. Moreover, the relative energy dissipation is inversely proportional to the ratio H/P with a nonlinear trend.

Secondly, these results allow the drawing of conclusions about the differences between the PKWs. Indeed, the results at the extremities of the curves are very close, which means that the values at the extremities are independent of the ratio W_i/W_o. However, for $0.2 \leq H/P \leq 0.9$, the energy dissipation depends on the PKWs geometry. The greater the width of the inlets compared to that of the outlets, the lower the energy dissipation. This can be clearly remarked on Figure 2.15 where the rectangles ($W_i/W_o = 1.5$) are the lowest and the triangles ($W_i/W_o = 1$) are the highest (R. Eslinger and Crookston, 2020).

In conclusion, a lot of studies and designs were conducted about PKWs, especially about the discharge capacity. However, only a few studies are available about the energy dissipation downstream of PKWs. This unknown is problematic in terms of the design of the energy dissipative structures and the protection measures downstream.

The purpose of this thesis is therefore a first step in characterising the flow properties downstream Piano Key Weirs, particularly for a steep slope. For this characterization, the flows downstream, using three different weirs, are going to be studied: a Creager weir and two Piano Key Weirs with different geometries. The purpose of having three different weirs is to be able to compare them. The flow study will be done with a double-tips conductivity probe. This probe is used to take air concentration and velocity measurements in the present work.

Chapter 3

Methodology

3.1 Experimental setup

The setup used for the present study has been constructed for Dewals et al., 2004 and has been used by Erpicum et al., 2011, Silvestri et al., 2013 and Faure, 2015-2016.

The water is brought through conduits to a reservoir. When there is enough water, it passes over the weir and it flows along the spillway. At the end of the spillway, the water arrives in a horizontal channel and it is evacuated. The channel is 0.492m wide, its vertical height is 2.01m and its inclination is equal to 52°. For the stepped spillway, the vertical and horizontal heights of the steps are respectively 3 cm and 2.4 cm. The sides of the channel are made of plexiglass and PVC while the smooth spillway is made of aluminium in order to minimise the friction of the flow. The friction coefficient for this material is equal to $90m^{1/3}/s$.

FIGURE 3.1: Model used in the present study.

In the present study, two different types of weir are used : a Creager weir that will be the reference and two PKWs with different geometries. The first one has 1.5 inlets and 1.5 outlets and the second one has 2.5 inlets and 2.5 outlets. All the geometry characteristics for both PKWs are in Table 3.1.

1. Creager weir

FIGURE 3.2: Creager weir used for the study.

2. PK weir

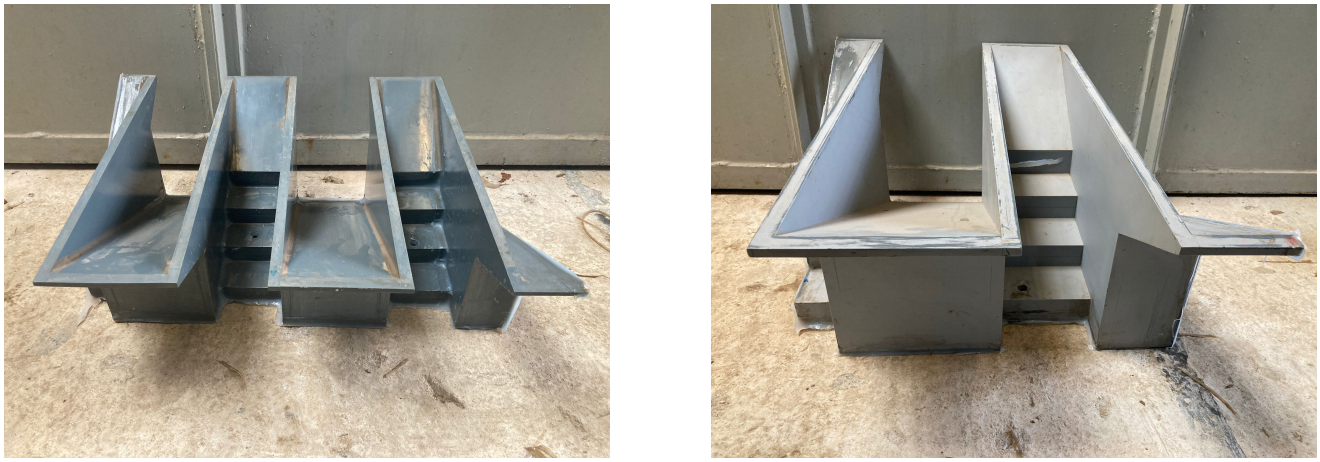

FIGURE 3.3: PKWs used for the study.

	W_i [cm]	W_o [cm]	T_s [cm]	P [cm]	B [cm]	B_i [cm]	B_o [cm]	W_i/W_o [-]	P/W_i [-]	T_s/W_i [-]	L_u/W_u [-]
PKW 1	9.7	7.7	1	16.3	38.3	11	13.9	1.26	1.66	0.1	4.88
PKW 2	16.9	12.3	1.5	26.2	62.3	6.8	8.7	1.37	1.55	0.09	4.78

TABLE 3.1: PKWs geometry.

The three weirs have different heights and depths, their positioning above the spillway is thus not the same. Figure 3.4 takes up these different positions. In Table 3.2, the different weir heights are resumed.

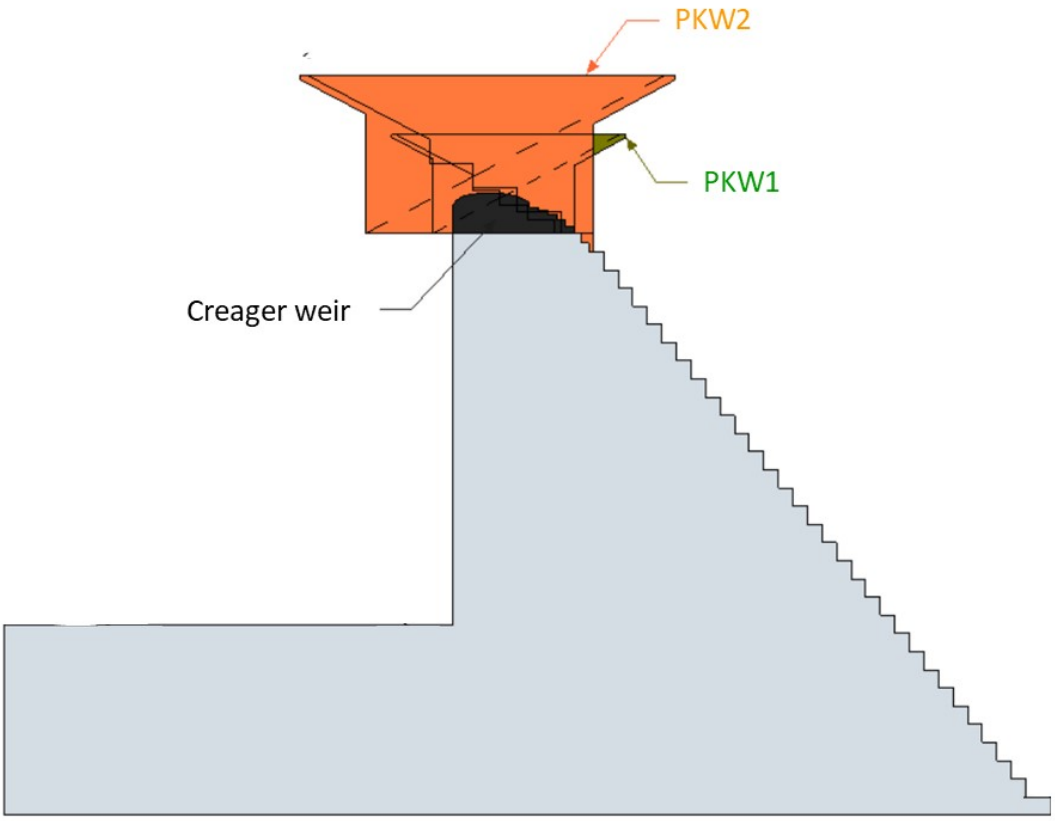

FIGURE 3.4: Positioning of the three weirs above the spillway.

Weirs	**P [m]**
Creager weir	0.067
PKW1	0.163
PKW2	0.262

TABLE 3.2: Heights of weirs [m].

3.2 Instrumentation

3.2.1 Double-tips conductivity probe

In the present study, the different properties of the flow are measured using a double-tips conductivity probe (Figure 3.5). The two tips have to be placed parallel to the flow direction and a spacing Δx can be measured between them. The tips are some electrodes, which means that depending on the nature of the surrounding fluid, the voltage is low (air) or high (water). When the correlation between the two electrodes is done, it is possible to find the travelling time of the bubbles between the two tips. With these parameters, it is possible to calculate the air-water mixture flow velocity as the ration between the distance and the travelling time (Bung, 2011). This type of probe also allows to have the air concentration, the number of air bubbles.

FIGURE 3.5: Double-tips conductivity probe.

The results are obtained under some hypothesis:
— No slip between air bubbles and water
— Both tips pierce the same bubble despite the small perpendicular distance between the tips

The distance Δx between the two tips has to be determined. The solution found to measure this is to use an optical microscope (Figure 3.6). For the first probe, the distance between the two tips is 5.02 mm and for the second one is 4.94 mm.

Sensibility of the probe

To use the probe, a frequency and an acquisition time have to be chosen. Figures 3.7, 3.8, 3.9 and 3.10 show the dependence of air concentration and velocity on the frequency. Figures 3.11, 3.12, 3.13 and 3.14 show the different parameters depending on the acquisition time. For each acquisition time and frequency, four measurements were taken (blue points on the graphs). From these four measurements, the dispersion (orange lines on the graphs) and the mean were calculated.

Choice of frequency

Based on the above figures, a frequency of 45 kHz has been chosen. Figure 3.8 shows that the air concentration stabilizes for a frequency equal to 20 kHz and the dispersion of the measurements which is represented on Figure 3.7 does not reduce after a certain frequency. However, it is not the case for the velocity (Figure 3.10), which reaches a plateau at more or less 40kHz/45kHz. Moreover, Figure 3.9 shows that the dispersion is slightly reduced from 45kHz, the chosen value of frequency.

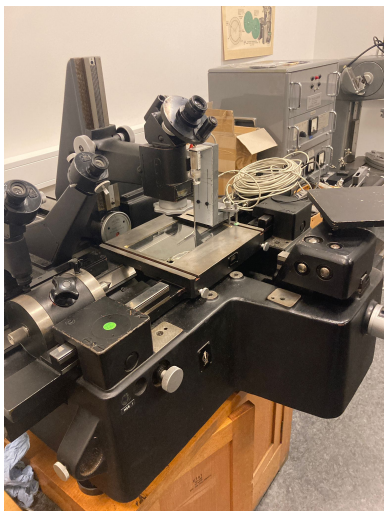

FIGURE 3.6: Optical microscope.

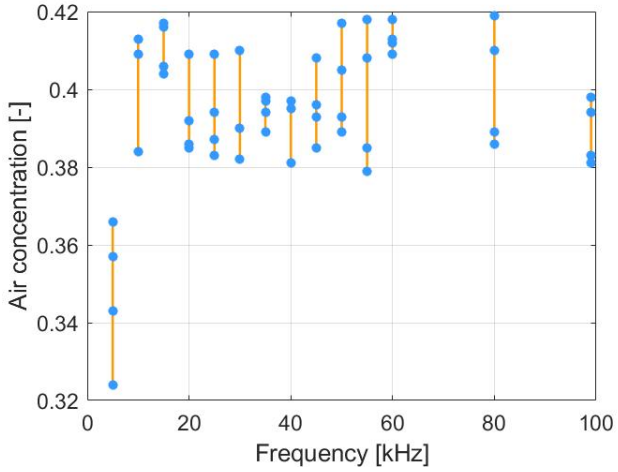

FIGURE 3.7: Air concentration [-] as a function of frequency [kHz].

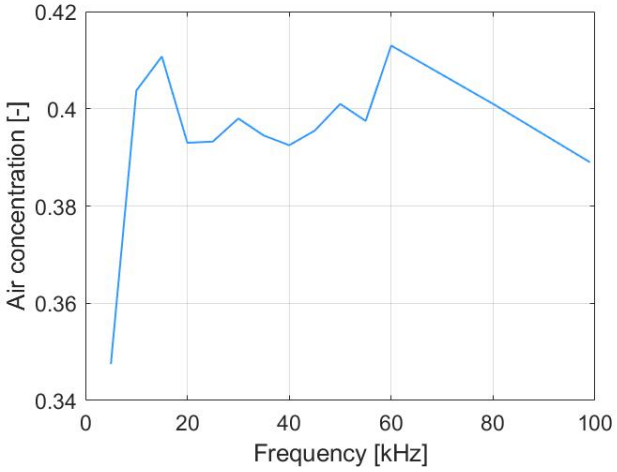

FIGURE 3.8: Air concentration [-] as a function of frequency (mean) [kHz].

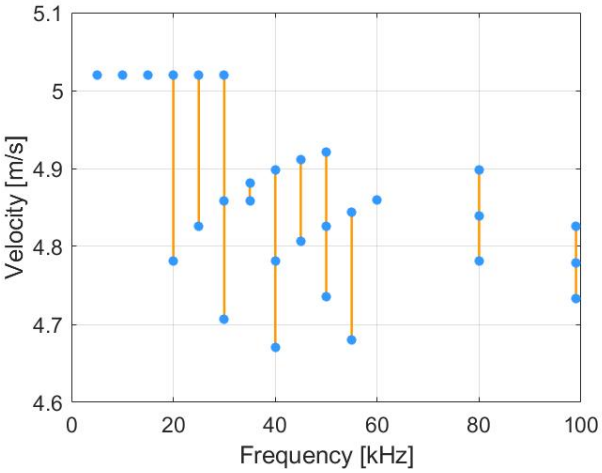

FIGURE 3.9: Velocity [m/s] as a function of frequency [kHz].

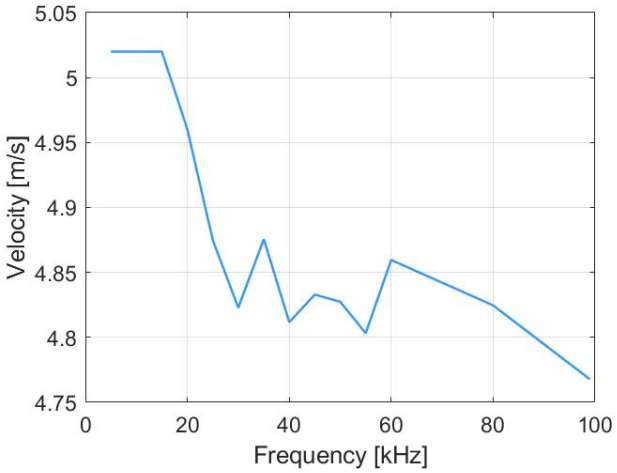

FIGURE 3.10: Velocity [m/s] as a function of frequency (mean) [kHz].

Choice of acquisition time

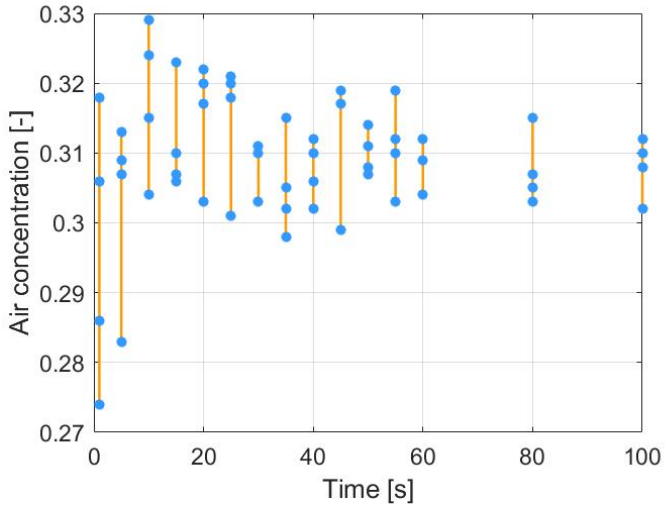

FIGURE 3.11: Air concentration [-] as a function of acquisition time [s].

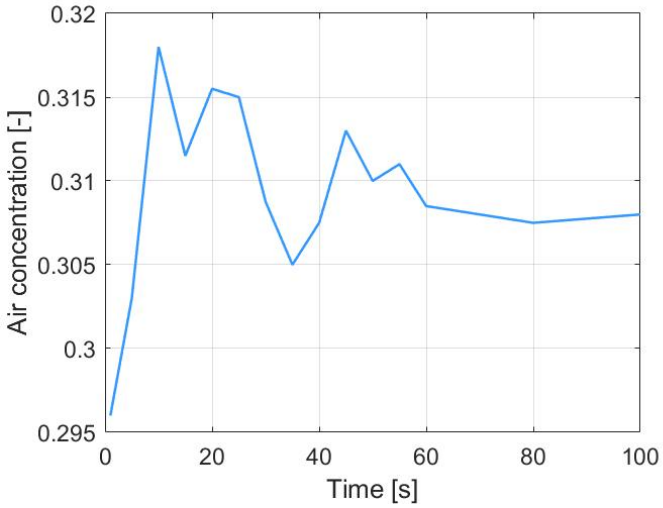

FIGURE 3.12: Air concentration [-] as a function of acquisition time (mean) [s].

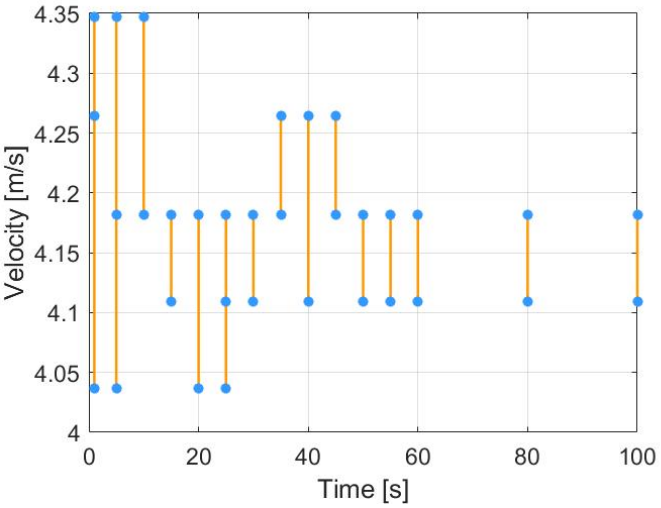

FIGURE 3.13: Velocity [m/s] as a function of acquisition time [s].

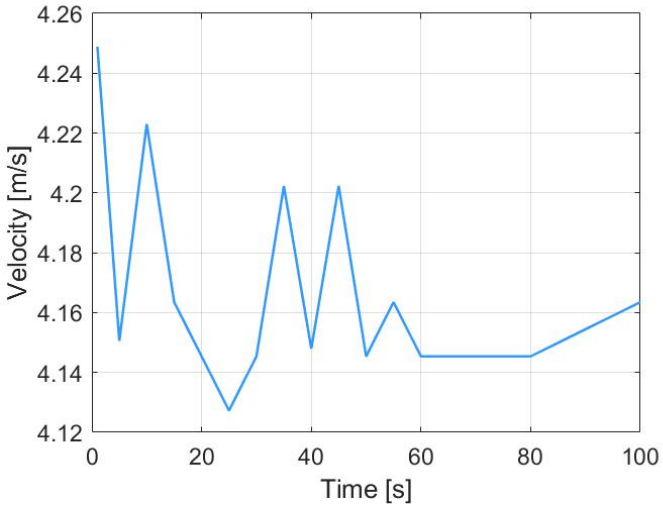

FIGURE 3.14: Velocity [m/s] as a function of acquisition time (mean) [s].

The choice of the acquisition time is less obvious. Indeed, the above figures do not reveal a significant time dependence of the void fraction and the velocity. In fact, Figure 3.11 shows a difference between 0.28 and 0.33 and the mean (Figure 3.12) has a difference of about 2%. For the velocity, it is known that this type of probe can provide data in the order of 5 to 10 %. Therefore, it is not possible to conclude about an optimal acquisition time with these figures. Henceforth, an acquisition time of 30s is so chosen for all measurements in this work.

3.2.2 Probe holder

In order to have reproducibility between tests, hold the probe and put it back at the same place, a probe holder was designed in collaboration with the lab technician. This probe holder allows taking measurements on the width from 31 mm to 463 mm from the left side of the channel. Firstly, all the measurements were taken at 176 cm from the top of the spillway but after that, it was decided to vary the position along the spillway. This explained that three different horizontal bars are placed on Figure 3.15 on the right. In conclusion, this probe holder allows to have results at x=176cm, 158cm and 140cm and z comprised between 31mm and 460mm.

FIGURE 3.15: Probe holder.

3.2.3 Flowmeter

To know the discharge in the channel, a flowmeter is installed on the water pipe. This flowmeter gives the discharge in L/s. Its error is 1% on its flow range.

FIGURE 3.16: Flowmeter.

3.3 Tests

3.3.1 Different configurations

During this work, different configurations of the setup were studied in order to compare the different results. These configurations are summarized in Table 3.3.

	Weir	**Spillway**
Configuration 1	Creager	smooth
Configuration 2	PKW1	smooth
Configuration 3	PKW2	smooth
Configuration 4	Creager	stepped
Configuration 5	PKW1	stepped
Configuration 6	PKW2	stepped

TABLE 3.3: Configurations tested.

3.3.2 Procedure of a test

For each configuration described in Table 3.3, an experimental protocol is followed in order to have reproducibility between tests and be able to conduct them again in same conditions, but also to compare the different configurations. Indeed, the different measurements should be taken the same way so that the comparison is precise and correct. The following steps are performed for each test:

1. **Probe installation at the desired position on the width.** To make sure this position is correct, the distance is always measured with the same tape measure, even if some marks were done on the probe holder. Moreover, bolts are tightened around the device to reduce vibration.

2. **Probe installation at the position closest to the pseudo bottom for the configurations with the stepped spillway and closest to the bottom for the configurations with the smooth spillway.**

3. **Switching on the pump and opening of the valve in order to obtain the desired discharge.** After that, some seconds are taken to wait for the stabilisation of the discharge, which can be read on the flowmeter.

4. **Probe signal recording for an acquisition time of 30s at a frequency of 45Hz for the vertical position which is the closest to the bottom and collection of the results given by the program.** This recording is achieved thanks to the program VFM2 on loan from the Aachen University as well as the probes. This program gives the air concentration and the velocity by making a correlation between the signals of the two tips of the probe.

5. All the measurements are taken twice to be able to compare them and verify that there is not any change between them.

6. **Change of the probe position in the vertical direction perpendicularly to the bottom using a limnimeter (Figure 3.17).** In general, the probe is raised by 2 mm. However, sometimes, when the difference of air concentration is too high between two measurements (more than 0.1), the probe is raised by only 1 mm. This step is repeated until arrive to an air concentration of 0.95.

FIGURE 3.17: Limnimeter.

7. **Switching off the pump and closing of the valve before changing the probe position.**

8. **Starting again from 1.**

3.4 Preliminary calculations

Before taking measurements, a range of flow has to be determined to have a skimming and uniform flow before the end of the spillway in the configuration with the stepped spillway and the Creager weir.

Skimming Flow
According to Boes and Hager, 2003a, Equation 3.1 has to be verified to have a skimming flow. As a reminder, the properties of the setup are the following ones: the vertical step height(s) is equal to 0.03m and the channel slope (ϕ) is equal to 52°.

$$\frac{h_c}{s} > 0.91 - 0.14tg(\phi) \tag{3.1}$$

$$\frac{h_c}{s} > 0.73$$

$$q_d > \sqrt{(0.73 \times 0.03)^3 \times 9.81} = 0.01m^2/s$$

$$Q_d > q_d L = 0.01 \times 0.491 = 4.91L/s$$

Uniform flow
According to Boes and Hager, 2003a, Equation 3.2 has to be verified to have a uniform flow before the end of the spillway ($H_{dam,u} = 2,05m$). Indeed, the different characteristics in the part of uniform flow are going to be analysed.

$$\frac{H_{dam,u}}{h_c} = 24sin(\phi)^{2/3} = 20.5 \tag{3.2}$$

$$2.05 > 20.5h_c$$

$$q_d < \sqrt{\left(\frac{2.05}{20.5}\right)^3 g} = 0.099m^2/s$$

$$Q_d < q_d L = 0.099 \times 0.491 = 49L/s$$

In conclusion, the flow has to be between 4.94 L/s and 49 L/s to have a skimming and uniform flow. To decide the flow used, the uniform mixture-flow depth is calculated with Equation 2.5 and Equation 2.6. The results are synthetized in Table 3.4.

$Q_d[L/s]$	$q_d[m^3/s]$	$h_c[m]$	$H_{dam,u}[m]$	$h_{90,u}[mm]$
10	0.02	0.035	0.71	18.4
20	0.04	0.055	1.13	28.4
25	0.05	0.064	1.31	32.7
30	0.06	0.072	1.48	36.7
40	0.08	0.087	1.79	43.9

TABLE 3.4: Values of uniform mixture-flow depth [mm] for different discharges [L/s].

Finally, the flow depth has to be as high as possible to be able to take enough measurements according to the y-coordinates. However, it is important to have enough place to take the measurements in the uniform flow at the end of the spillway. Therefore, a discharge equal to 25 L/s was chosen for the entire study.

Chapter 4

Results

4.1 Introduction

In this chapter, the results for the configurations described in Table 3.3 are presented. The results dealt with in this study are the air concentration and the velocity for different positions on the spillway. The results will be shown property by property in this chapter, starting with the air concentration, then the velocity and finally the discharge. As a reminder, all the results are obtained with a discharge equal to 25 L/s.

In the Section 4.3 and Section 4.4, the results are shown, but it's important to know and understand the different positions of the measures for each configuration. Firstly, for the Creager weir, the first idea is that the flow is uniform on the width, but a verification of this hypothesis has to be realised with at least two measures with different positions on x. For the PKWs the choice of the positions on the width are more complicated because, as it can be observed on Figure 4.1 and Figure 4.2, some lighter jets appears. The flow downstream a PKW is therefore not uniform along the width, the measurements have to be at the good place to prove it.

FIGURE 4.1: Flow downstream PKW1.

FIGURE 4.2: Flow downstream PKW2.

In view of the non-uniformity across the width, the choice of measurement positions had to be made. In order to minimize the time, the choice to take measurements at points that seem most appropriate and not at points separated by a constant distance was done. The chosen positions are thus downstream the middle of the inlet, the middle of the outlet and downstream the separations between an inlet and an outlet for both PKWs. The selected positions along z-coordinates are listed and shown in Figure 4.3 for PKW1 and in Figure 4.4 for PKW2.

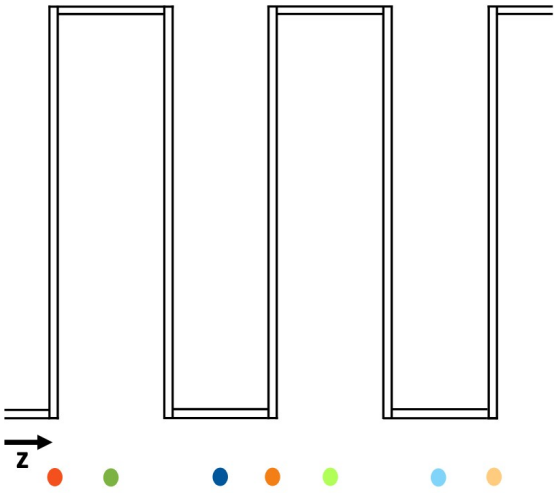

z [mm]	z' [-]	Repair in relation to PKW geometry	
47	0.22	edge	●
100	0.5	outlet	●
197	1	inlet	●
240	1.22	edge	●
294	1.5	outlet	●
392	2	inlet	●
435	2.22	edge	●

FIGURE 4.3: Different measure positions on the width for the PKW 1.

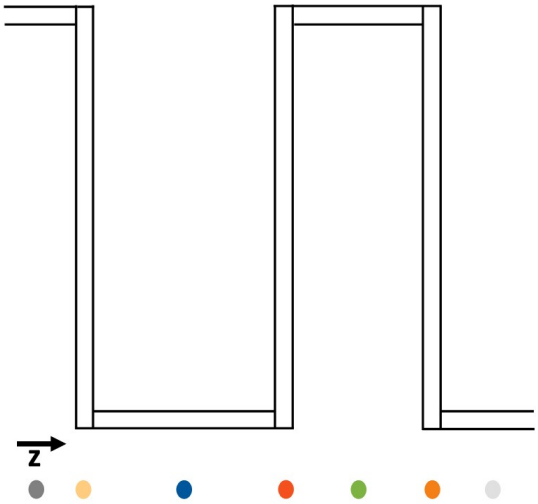

z [mm]	z' [-]	Repair in relation to PKW geometry	
31	-0.42	side	●
74	-0.29	edge	●
166	0	inlet	●
258	0.29	edge	●
327	0.5	outlet	●
396	0.71	edge	●
460	0.91	side	●

FIGURE 4.4: Different measure positions on the width for the PKW 2.

In order to improve the readability of future graphs, two things have been set up: firstly, the different shades of colour corresponds to a specific position depending on the geometry of the PKW. The shades of green correspond to the middle of the outlets, the shades of blue to the middle of the inlets, the shades of orange to the separations between the inlets and outlets and the shades of grey to the extreme side. Secondly, the z-coordinates are dimensionless in order to better understand the positions of the measures (z' in Figure 4.3 and Figure 4.4). The whole numbers correspond to the middle of the inlets, the numbers with .5 to the middle of the outlets and the other numbers to separations between the inlets and outlets.

A summary of the configurations and of the measures realised is presented at Table 4.1.

	Weir	**Spillway**	**Discharge**	**number of positions on z**	**number of positions on x**	**number of repetitions**
Config 1	Creager	smooth	$25L/s$	2	1	2
Config 2	PKW1			18	3	2
Config 3	PKW2			6	3	1
Config 4	Creager	stepped		2	1	2
Config 5	PKW1			7	3	2
Config 6	PKW2			6	3	1

TABLE 4.1: Configurations tested.

4.2 General comparisons

Before discussing the results for each configuration, some comparisons available for all the configurations are going to be analysed. Two comparisons are going to be realised on the stepped spillway with the Creager weir: a comparison between the results obtained with the two different probes and a comparison between the measures taken above a step niche or above a step edge for the stepped spillway configurations.

4.2.1 Comparison between the results of two probes

The first comparison is the comparison between the two different probes. The purpose of this comparison is to be sure that the probes give the same results in case the first probe is damaged. Indeed, the probes are fragile, especially the two tips that can easily bend and/or break. It is therefore important to ensure that a change of probe between two configurations will not bias the results. The results for the two probes are shown on Figures 4.5 and 4.6.

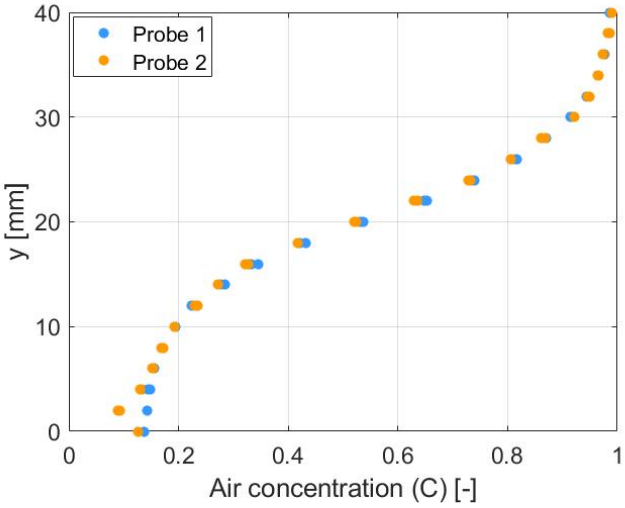

FIGURE 4.5: Comparison between the 2 probes: Air concentration [-].

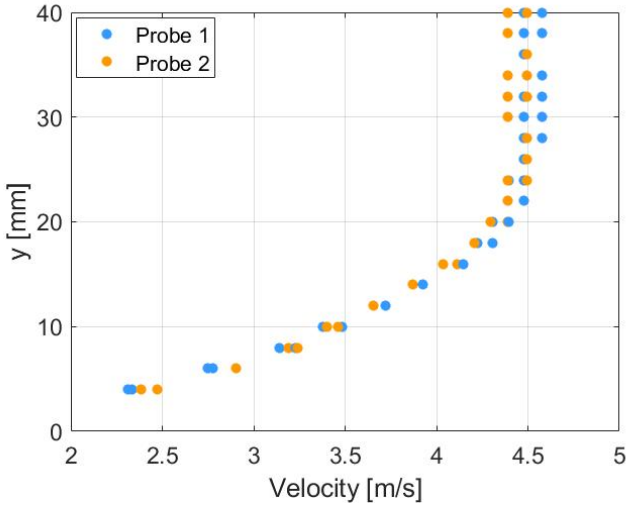

FIGURE 4.6: Comparison between the 2 probes: Velocity [m/s].

The quasi-perfect S-shape on Figure 4.5 confirms that the two probes gives the same results for the air concentration. For the velocity, shown on Figure 4.6, a small difference appears. However, a small difference also exists between the points which are measured with the same probe and at the exact same place (2 points of the same colour for the same y/y_{90}). As a reminder, all the measurements were taken twice. Moreover, the colour points are mixed and no trend can be drawn from this graph. In conclusion, the difference between the velocity measured by the two probes can be explained by the accuracy of the probe. In conclusion, in case of a problem with one probe, the second one can be used without any change in the results.

4.2.2 Comparison between the results above step edges and above step niches

The second comparison is a slight change of the x-coordinate , i.e a change in the flow direction. Indeed, as it can be seen on Figure 4.7, the probe is moved from a position where it is above a step edge to a position where it is above a step niche. This comparison is realised because, for example, Bung, 2011 found some differences between these positions. The results are shown on Figures 4.8 and 4.9.

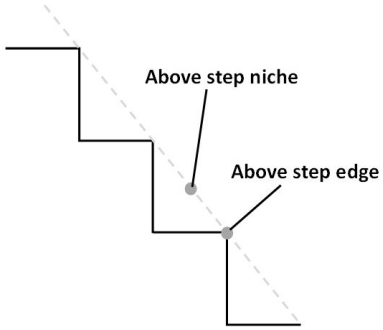

FIGURE 4.7: Position above a step edge VS position above a step niche.

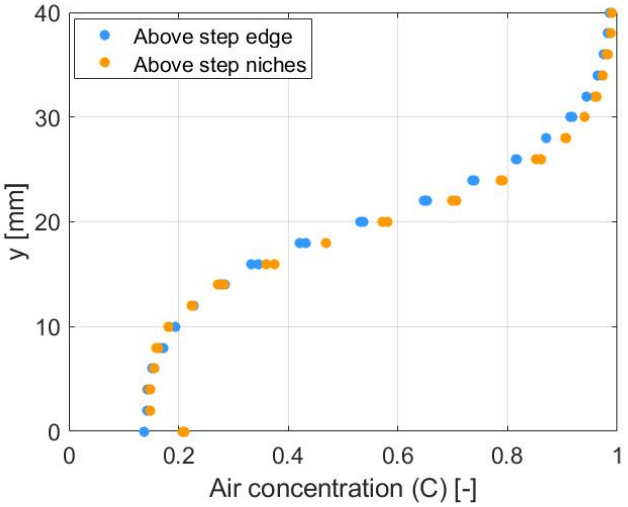

FIGURE 4.8: Comparison between above step edges and above step niches: Air concentration [-].

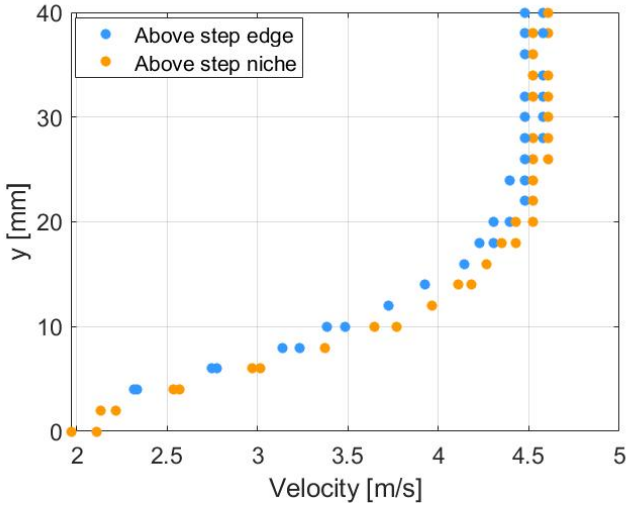

FIGURE 4.9: Comparison between above step edges and above step niches: Velocity [m/s].

Figures 4.8 and 4.9 show that there are some differences between the two positions. Indeed, the air concentrations taken above a step edge are smaller than those taken above a step niche. This observation was also made by Bung, 2011. This phenomenon is due to a higher aeration created by the recirculating zones. The difference is not very important because it is correlated with the vertical step height. In this case, this height equals to $3cm$ which is small, therefore the difference in air concentration between the two positions is also low. Moreover, the velocity is slower in the case of measurements taken above the step edge.

4.3 Air concentration

The first flow property studied is the air concentration. Firstly, the results for the different configurations at the first section with x=1.76m are shown in Figures 4.10 to 4.15. As a reminder, x is the coordinate whose origin is at the top of the spillway and the direction is parallel to the spillway. Then, the results for different x-coordinates are going to be shown, they correspond to Figures 4.17 to 4.20.

4.3.1 Results for different positions across the channel width

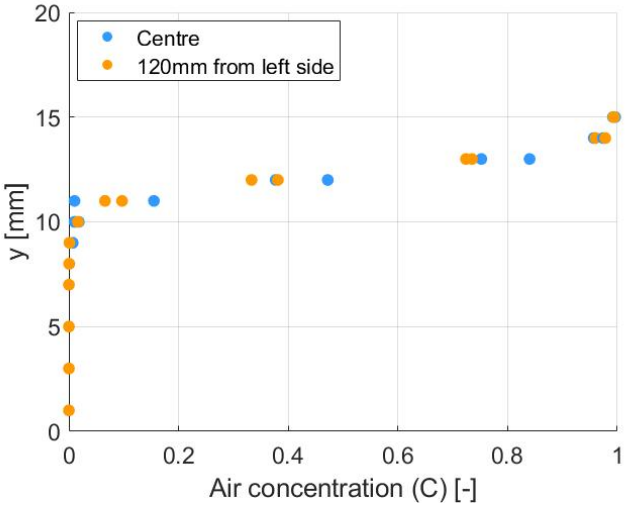

FIGURE 4.10: Creager weir and smooth spillway: Air concentration [-] at x=1.76m.

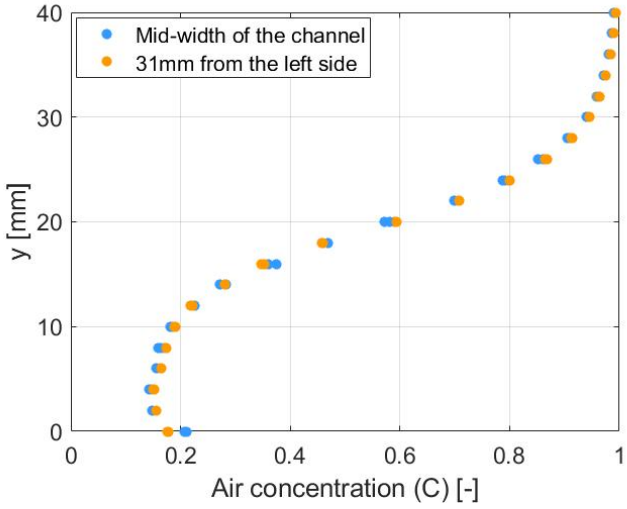

FIGURE 4.11: Creager weir and stepped spillway: Air concentration [-] at x=1.76m.

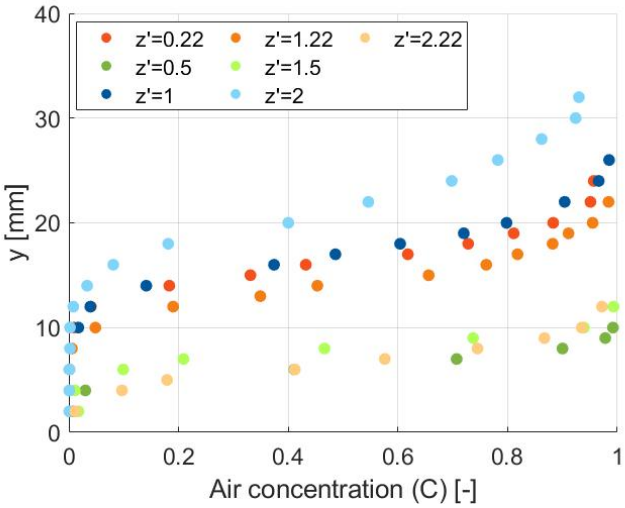

FIGURE 4.12: PKW1 and smooth spillway: Air concentration [-] at x=1.76m.

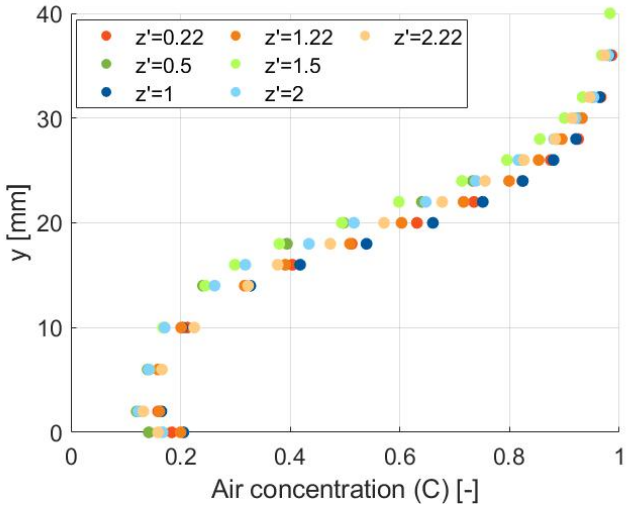

FIGURE 4.13: PKW1 and stepped spillway: Air concentration [-] at x=1.76m.

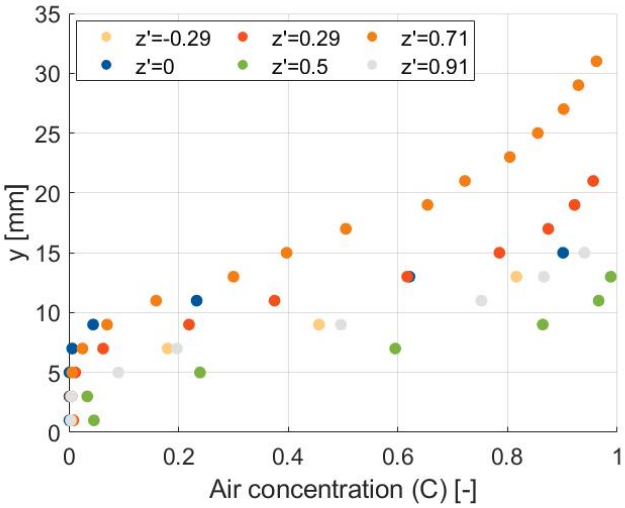

FIGURE 4.14: PKW2 and smooth spillway: Air concentration [-] at x=1.76m.

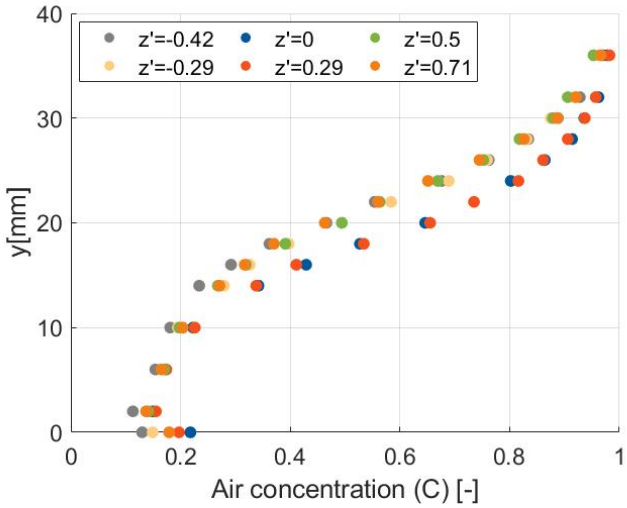

FIGURE 4.15: PKW2 and stepped spillway: Air concentration [-] at x=1.76m.

Figures 4.10 to 4.15 represent the air concentration profiles as a function of the y-coordinate. As a reminder, the y-coordinate originates at the bottom of the channel for the smooth spillway and at the pseudo-bottom for the stepped spillway. Its direction is perpendicular to these bottoms.

All air concentration profiles have one thing in common: their shape. Indeed, they can all be assimilated to an S-shape, even if it is clear that all the S-shape are not the same. It can be observed that transitions between the mainly clear water flow ($C < 0.3 - 0.4$) to the mainly air flow ($C > 0.6 - 0.7$) are more or less fast depending on the configuration. However, depending on the configurations and the position of the probe according to the width, it can be seen that y_{90} (y which corresponds to an air concentration equal to 0.9) is not the same. This has the direct impact that the clear water depths are not the same depending on the configurations and the z-coordinate.

Firstly, for the Creager weir (Figures 4.10 and 4.11), it can be observed that the probe position across the width has no impact on the air concentration profile as the dots of different colours are very close. Figure 4.10 shows slight discrepancies between the results, but the difference between the orange and blue points is not higher than the difference between two dots of the same colour (measures taken at the same position). This means that these small shifts are problems of inaccuracy in the measurements. This can be explained by the very fast change between the mainly clear water flow to the mainly air flow: a very small change in y leads to a large change in air concentration. For the configuration with the Creager weir and the smooth spillway, the conclusion is that there is almost no air entrained.

Then, Figure 4.12 represents the configuration with the PKW1 and the smooth spillway. Thanks to this figure, it is clear that the air concentration and thus the water depths are not uniform across the width of the channel. Indeed, the maximum of the lowest curve is under $10mm$ while the maximum of the highest curve is located above $30mm$. However, some trends can be drawn from this figure: the blue shade curves, which correspond to the position under the middle of the inlets, are the highest while the green shade curves (middle of the outlets) are located in the bottom of the graph. In the case of the orange shades (separation between the inlets and the outlets), it is more difficult to find a trend because the lightest one is located near

the curves which represent the positions downstream the outlets (green shades) while the other two are located closer to the blue shades which represent the positions downstream the inlets. In order to have a better understanding of the variation in water levels across the width of the channel, more positions were tested for this configuration. On Figure 4.16, y_{90} is represented for the different z-coordinates tested.

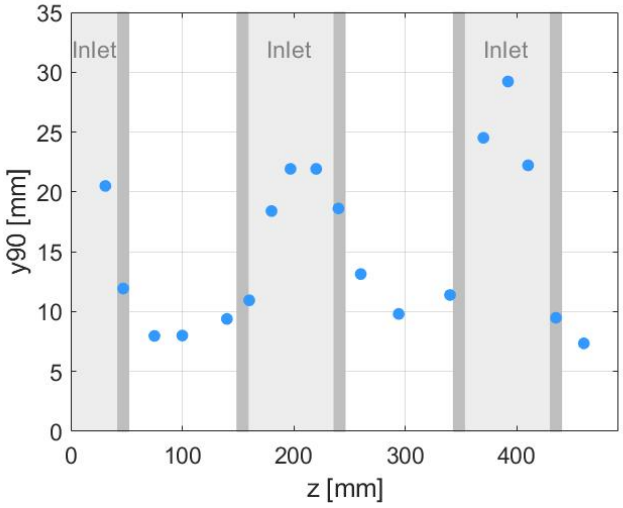

FIGURE 4.16: Vertical depth for air concentration equal to 0.9 (y_{90} [mm]) across the width of the channel for the PKW1 and the smooth spillway.

Figure 4.16 clearly shows that the highest water depths are downstream of the inlets, while the smallest are downstream of the outlets. It can also be observed that the results are not perfectly symmetric downstream an inlet, which explains that the results under the separating sides (orange shade curves) are quite different on Figure 4.12.

The next configuration is with the PKW1 and the stepped spillway, which is Figure 4.13. It can be seen that there is slight difference between the curves, but the maximum air concentration difference between two dots at the same y is 0.166 for $y = 20mm$. Furthermore, it is complicated to find trends for this configuration. The air concentrations downstream the outlets (green shade dots) are smaller than the other positions, but nothing can be concluded for the positions downstream the inlets and the separations between the inlets and the outlets.

Finally, Figures 4.14 and 4.15 represent the air concentration profiles for the last weir: PKW2. For the smooth spillway, the variation of depth is important. Indeed, the maximum of the lowest curve is under $15mm$, while the maximum of the highest curve is located above $30mm$. Moreover, the water depth downstream the outlet is the smallest, but it is not the one under the inlet which is the highest. It can be observed that the highest water depth is under a separation between inlet and outlet (orange colour). The last configuration with the PKW2 and the stepped spillway is represented on Figure 4.15. In this case, there is a difference between the curves but for the same y the more important one is 0.192 for $y = 20mm$.

4.3.2 Results for different positions along the flow

After the discussion about the different configurations at a constant x-coordinate, the results of air concentration profiles are going to be analysed for a position downstream the middle of an inlet (blue shade curves) and an outlet (green shade curves) for different x-coordinates. Three x-coordinates are going to be tested: $x = 140cm$, $x = 158cm$ and $x = 176cm$. These results are shown at Figures 4.17 to 4.20.

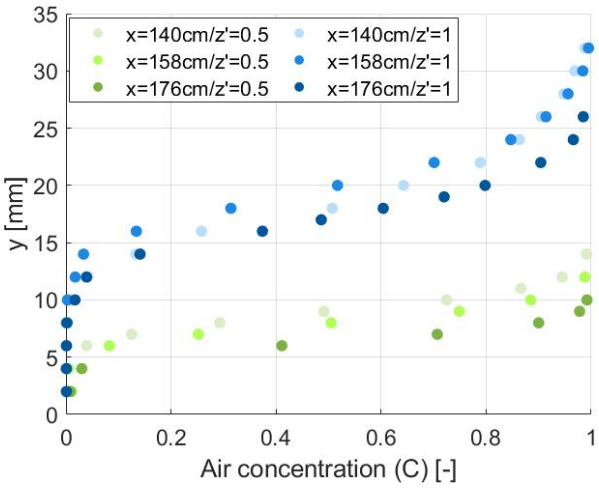

FIGURE 4.17: PKW1 and smooth spillway: Air concentration [-].

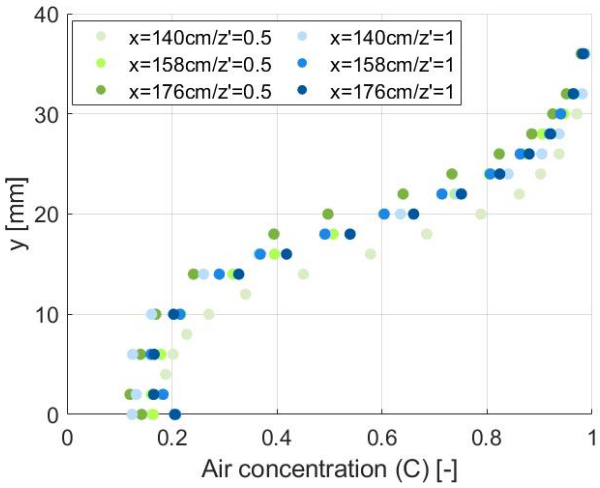

FIGURE 4.18: PKW1 and stepped spillway: Air concentration [-].

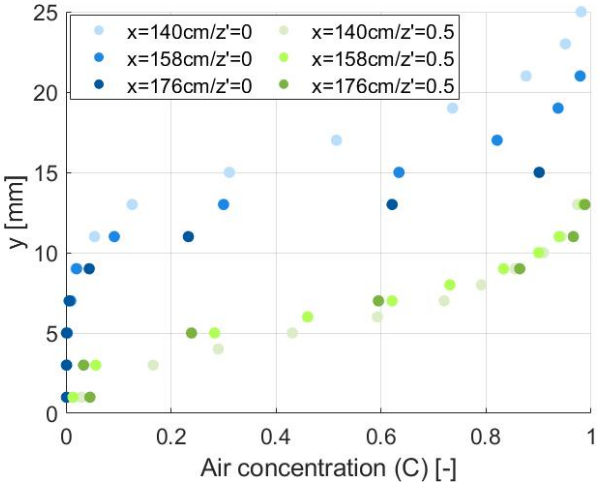

FIGURE 4.19: PKW2 and smooth spillway: Air concentration [-].

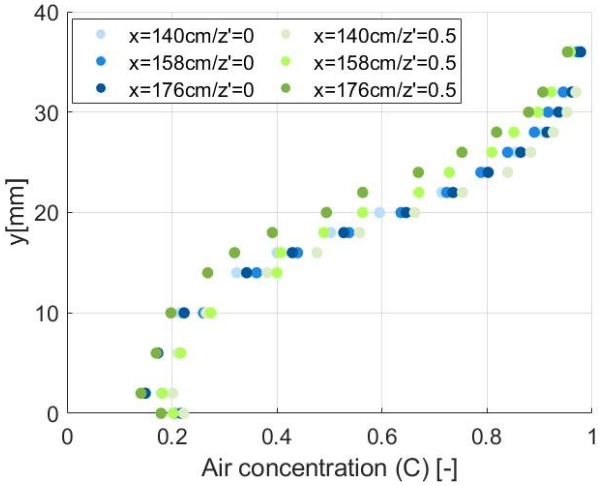

FIGURE 4.20: PKW2 and stepped spillway: Air concentration [-].

For the first configuration with the PKW1 and the smooth spillway (Figure 4.17), it can be observed that the water depths are always greater downstream the inlets (blue shade curves) than downstream the outlets (green shade curves). However, shifts between curves of the same colour can be observed. Downstream the outlet, the further you are from the top of the spillway, the greater air concentration you have at the same height (y) which means a smaller water depth. Downstream the inlet, the same conclusion can not be reached, but the lowest water depth corresponds to the further position from the top of the spillway also. Moreover, the difference between the y_{90} with the most gaps is $3.84mm$ for the curves downstream the inlet and $3.43mm$ for the outlet.

When the aluminium plate is removed to have the stepped spillway with the PKW1 (Figure 4.18), the air concentration profiles are very close to each other, no matter if the probe is downstream of the inlet or the outlet. On the other hand, the dispersion of the results downstream of the outlet is more important than the one downstream of the inlet. Indeed, the maximum difference of air concentration between two blue dots is 0.056 for the same y, while it is 0.291 for the green ones. Moreover, for the tests downstream the outlet, the smaller water depth corresponds to the further position from the top of the spillway. All these conclusions can also be found in the case of the PKW2 and the stepped spillway at Figure 4.20.

Then, Figure 4.19 shows the results for the PKW2 and the smooth spillway. The air concentration profiles are very close for the different positions downstream the outlet, contrary to those downstream the inlet, which are more scattered. This can be explained by looking at Figure 4.22. It can be observed that the whiter jets, which correspond to higher air concentration and higher water depth, are not parallel between them, and it can be seen that the jets are not at the same z-coordinate depending on the x-coordinate.

Moreover, a comparison can be done between PKW1 and PKW2 for the smooth spillway with Figure 4.17 and 4.19 or with Figure 4.21 and Figure 4.22. It is possible to conclude that the changes in jet positions depending on the x-coordinates tested are more important for the PKW2 than the PKW1.

FIGURE 4.21: Flow downstream PKW1.

FIGURE 4.22: Flow downstream PKW2.

Indeed, downstream of the PKW1, the position of the jets on the width seems more or less constant over a certain length, which is not the case downstream of the PKW2. However, it's impossible to say that the flow is uniform because of the different water depths on the width. Indeed, if the spillway was infinitely long, the different water depths would offset each other and a uniform height on the width would be reached.

4.4 Velocity

The second flow property studied is the velocity. Firstly, the results for the different configurations at the first section with x=1.76m are shown from Figure 4.23 to Figure 4.28. As a reminder, x is the coordinate whose origin is at the top of the spillway and the direction is parallel to the spillway. Then, the results for different x-coordinates are going to be shown, they correspond to Figure 4.29 to 4.32.

4.4.1 Results for different positions across the channel width

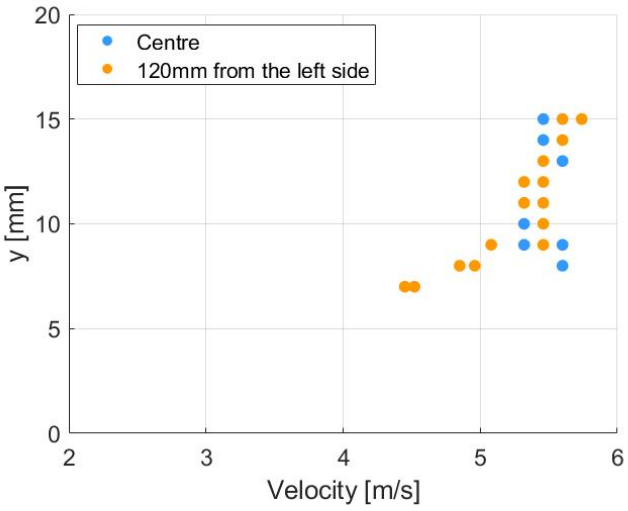

FIGURE 4.23: Creager weir and smooth spillway : Velocity [m/s] at x=1.76m.

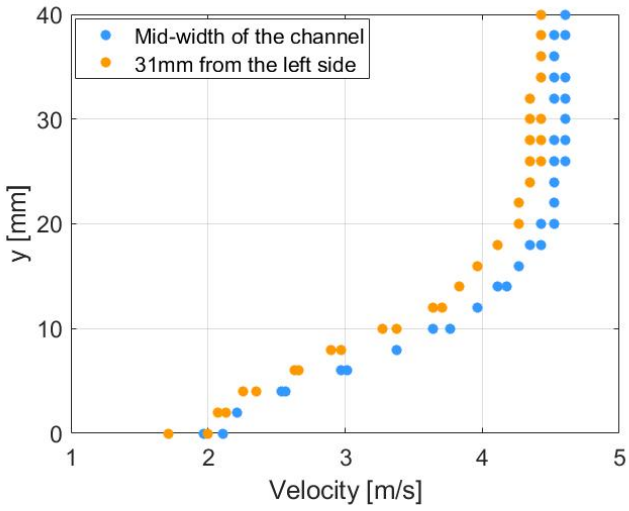

FIGURE 4.24: Creager weir and stepped spillway : Velocity [m/s] at x=1.76m.

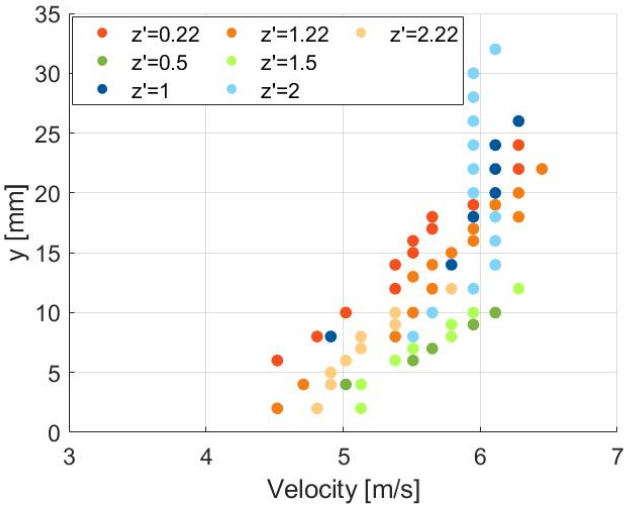

FIGURE 4.25: PKW1 and smooth spillway : Velocity [m/s] at x=1.76m.

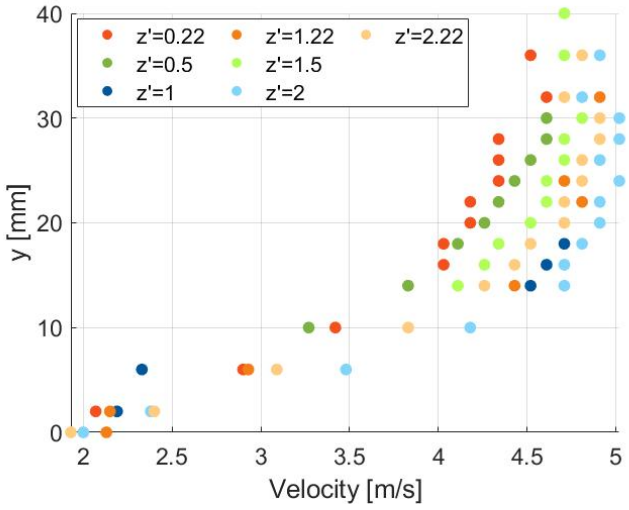

FIGURE 4.26: PKW1 and stepped spillway : Velocity [m/s] at x=1.76m.

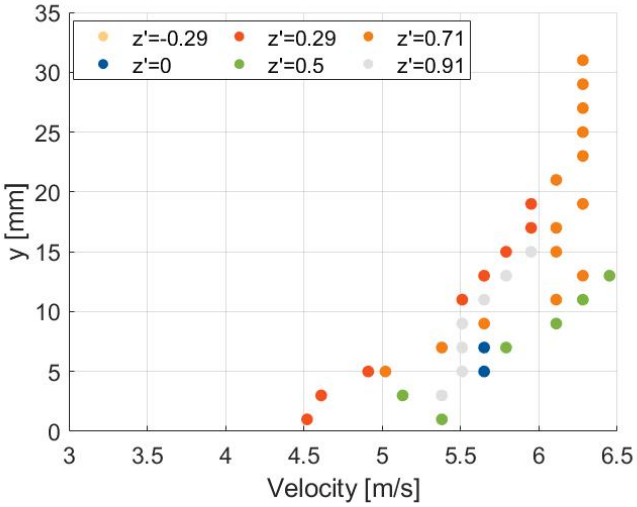

FIGURE 4.27: PKW2 and smooth spillway : Velocity [m/s] at x=1.76m.

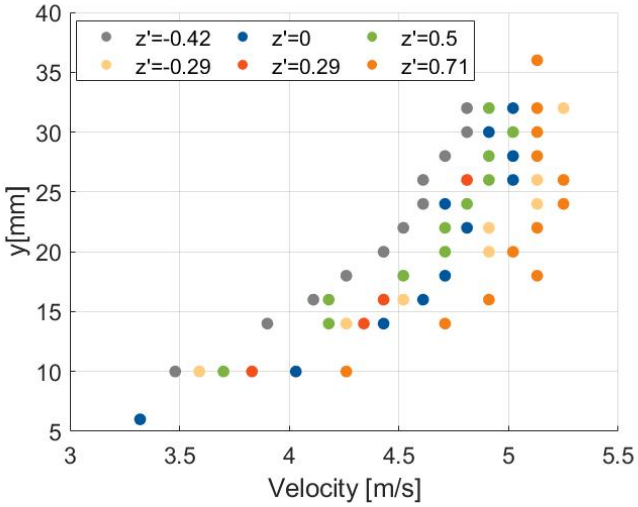

FIGURE 4.28: PKW2 and stepped spillway : Velocity [m/s] at x=1.76m.

All velocity profiles have one thing in common: their shape. Indeed, they can be assimilated to a power law. However, for each configuration and for different positions on the spillway, the values of the velocity are not the same.

The first configuration with the Creager weir and the smooth spillway is represented on Figure 4.23. Foremost, it can be observed that the results begin at $y = 7mm$. This can be explained by the poor flow aeration. Indeed, the conclusion about the air concentration for this configuration was that almost no air was entrained. This has for impact that there is a small amount of bubbles in the flow, and thus the probe has difficulties to find a correlation between the air concentration at the two tips. Without a correlation, it is impossible to find a correct velocity, which explains why only dots above $y = 7mm$ are shown on Figure 4.23. Moreover, the velocities measured at the channel centre and at $z = 120mm$ are overlaid, which means that the velocity is constant on the width for this configuration.

Then, Figure 4.24 shows the velocity profiles for the Creager weir and the stepped spillway. This figure allows to draw a conclusion about edge effects. Indeed, for the air concentration, no difference was found between the measures taken at $31mm$ from the left side and the measures taken at the centre of the channel, but it's not the case for the velocities. Indeed, the values for $z = 31mm$ are shifted to the left in relation to those taken in the middle of the channel, and thus the velocities near the side are slower. This can be explained by the friction between the flow and the side of the channel made of Plexiglass. As a reminder, a distance of $31mm$ from the left side corresponds to the closest possible position of the probe to the side because of the probe holder.

The next configuration is the PKW1 with the smooth spillway. On Figure 4.25, it can be observed that the velocity range for each configuration is more or less the same, i.e. from $4.52m/s$ to $6.28m/s$. As a reminder, the perpendicular height from the bottom y is very different depending on the position across the width. This explains that the maximum velocity is reached, for example, at $y = 32mm$ for $z' = 1$ (downstream an inlet) and at $y = 10mm$ for $z' = 0.5$ (downstream an outlet). For this reason, it is impossible to compare velocities with each other with Figure 4.25. A scaling has to be realised.

However, if the configuration for the same PKW but for the stepped spillway is observed (Figure 4.26), the vertical heights (y) are very similar, thus some conclusions can be drawn from this figure. It would be important to verify these conclusions with a scaling representation too. It can be seen on Figure 4.26 that the velocities downstream of the inlets (blue shade curves) are the fastest, while the velocities downstream of the outlets (green shade curves) are slower. For the other positions, it is complicated to draw a conclusion given that one curve is the slowest, while the other two are located between the blue and green curves.

For the last weir, the conclusions for Figure 4.27 are the same as the PKW1 and smooth spillway: the range of velocity is more or less the same no matter the position on the width, but a scaling has to be done to draw other conclusions. However, for the PKW2 and the stepped spillway (Figure 4.28), given that the height y are very similar, some conclusions can be drawn even if a verification will be done with the scaling results. It can be observed that the fastest velocities are located downstream two separations between inlet and outlet (orange shade curves). Moreover, velocities downstream inlet and outlet are not extreme velocities and are close to each other. Finally, the slowest velocity is located at $31mm$ from the left side. This can be explained by the side effects also observed on Figure 4.24.

4.4.2 Results for different positions along the flow

After the discussion about the different configurations at a constant x-coordinate, the results of velocity profiles are going to be analysed for a position downstream the middle of an inlet (blue shade curves) and an outlet (green shade curves) for different x-coordinates. Three x-coordinates are going to be tested: $x = 140cm$, $x = 158cm$ and $x = 176cm$. These results are shown at Figure 4.29 to Figure 4.32.

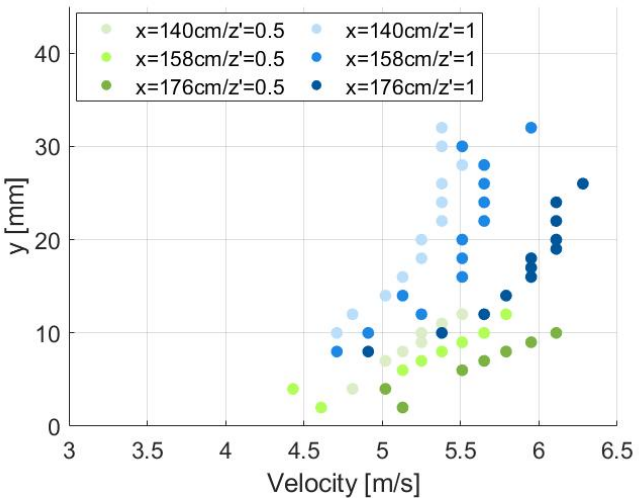

FIGURE 4.29: PKW1 and smooth spillway : Velocity [m/s].

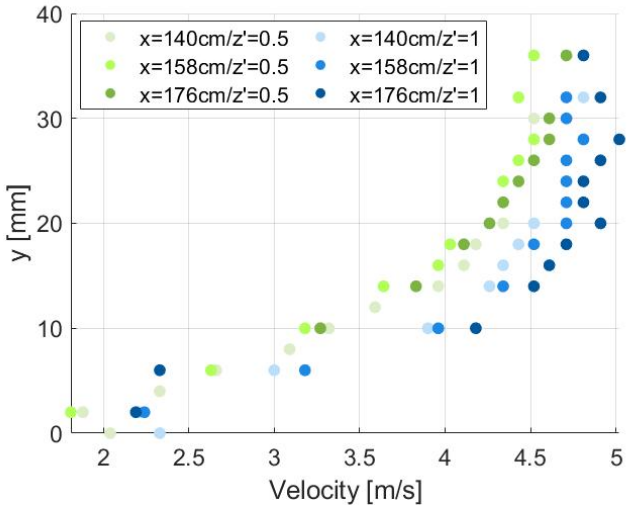

FIGURE 4.30: PKW1 and stepped spillway : Velocity [m/s].

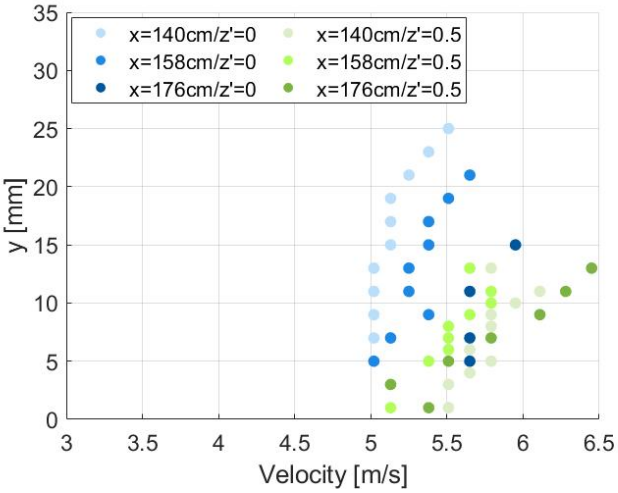

FIGURE 4.31: PKW2 and smooth spillway : Velocity [m/s].

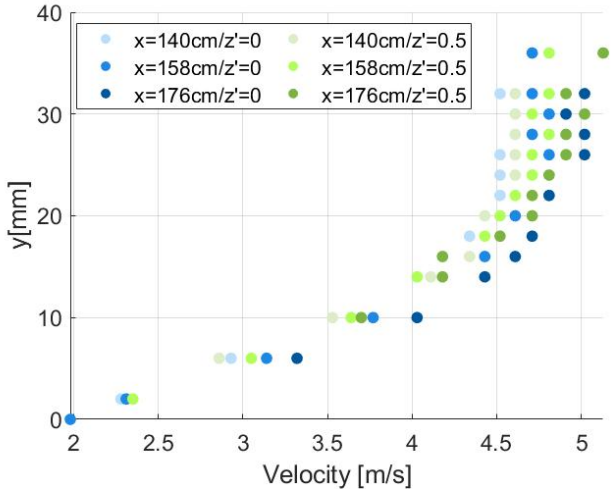

FIGURE 4.32: PKW2 and stepped spillway : Velocity [m/s].

As a reminder, on Figure 4.29 to Figure 4.32, the blue shade curves correspond to the positions downstream an inlet and the green ones to the positions downstream an outlet.

For the configuration with PKW1 and smooth spillway (Figure 4.29), it can be seen that for the same position on the width, the velocities increase when the probe is located further downstream on the spillway. Indeed, the lightest colours correspond to the slowest velocities, while the darkest colours correspond to the fastest velocities. Moreover, the velocities measured for the same x-coordinate appear to be in the same velocity range: the lightest colours go up to a value equal to $5.5m/s$, then they go up to $5.8m/s$ and finally, the darkest ones go up to $6.1m/s$. However, as explained above, it is impossible to compare the velocities with each other on this figure because of the different heights on the width of the channel.

Then, Figure 4.29 represents the configuration with the PKW1 and the stepped spillway. In this case, it is clear that the velocities downstream the outlet are slower than those downstream the inlet. Moreover, the results for the different x-coordinates downstream the inlet can be seen as similar, contrary to those downstream the outlet which are more scattered. For these dots, the velocities increase when the probe moves away from the top of the spillway (light blue correspond to the slowest values, while dark blue correspond to the fastest values).

Like the first two figures, the velocities increase when the probe is placed further downstream for the positions downstream the inlet, but this conclusion can not be found for the positions downstream the outlet (green shade curves). Indeed, the lightest green does not correspond to the slowest velocities. Moreover, some curve shapes on Figure 4.31 are not the same as other configurations. All these differences with the other configurations can be explained by the 3D flow characteristic shown in Figure 4.22. Indeed, on this picture, it can be observed that the jets change position on the width. This has the effect that the probe is not oriented parallel to the flow, which can lead to erroneous results.

Finally, the last configuration with the PKW2 and the stepped spillway (Figure 4.32) confirms once again the fact that the further downstream the measurement, the greater the speed both for positions downstream of inlet and outlet. Furthermore, the velocities measured at the same x-coordinate are very close to each other even if one is taken downstream an inlet and the other one is taken downstream an outlet.

4.5 Errors

For all the results, it is important to quantify the error on the air concentration and the velocity calculated by the conductivity probe. In order to realise it, the errors between two similar tests is are calculated. The analysed results are those measured for the Creager weir and the stepped spillway. These results can be seen on Figures 4.33 and 4.34.

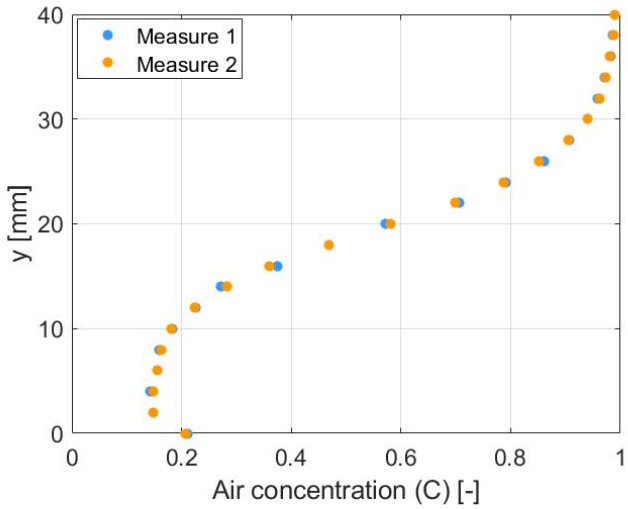

FIGURE 4.33: Air concentration [-] for two measures taken exactly at the same position.

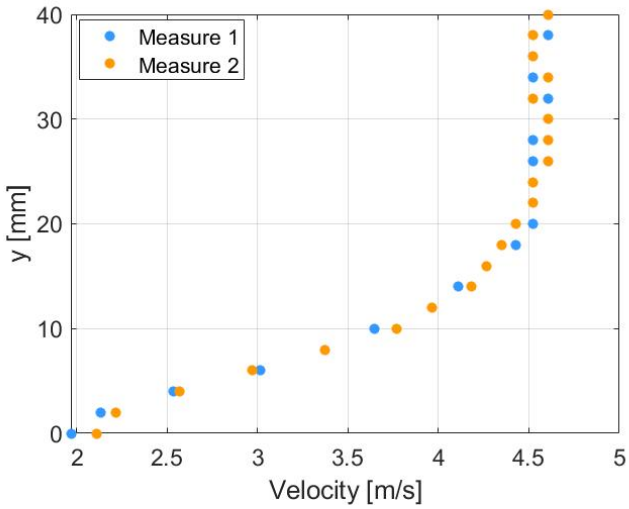

FIGURE 4.34: Velocity [m/s] for two measures taken exactly at the same position.

The means, maxima and minima of the errors calculated between the points located at the same perpendicular height to the pseudo-bottom are displayed in Table 4.2.

	Mean	**Maximum**	**Minimum**
Air concentration	1.13%	4.23%	0%
Velocity	1.53%	7.37%	0%

TABLE 4.2: Means, maxima and minima of the errors [%] for the air concentration and the velocity of two tests realised at the same position.

Chapter 5

Analyses and Discussions

In this chapter, the results are going to be analysed in order to compare the different configurations. Firstly, the air concentration profiles for each configuration are compared. Then, the discharges are calculated. The clear water depths and the average velocities are compared. Finally, dissipated energy is discussed.

5.1 Dimensionless air concentration profiles

In order to compare the air concentration profiles for each configuration individually, a solution has to be found to scale the flow height (y) in view of the different heights along the width of the channel. This solution is to divide the flow height (y) by the flow height which corresponds to the flow height where the air concentration equal to 0.9 (y_{90}). Figures 5.1 to 5.6 show the results for each configuration.

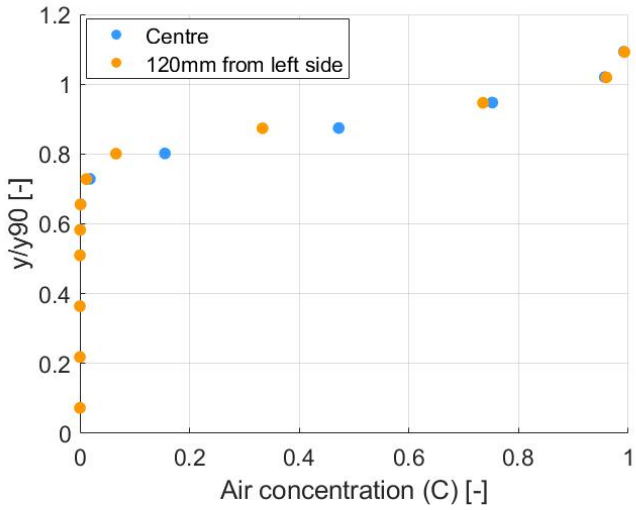

FIGURE 5.1: Creager weir and smooth spillway: Air concentration [-] depending on the dimensionless flow heigth [-].

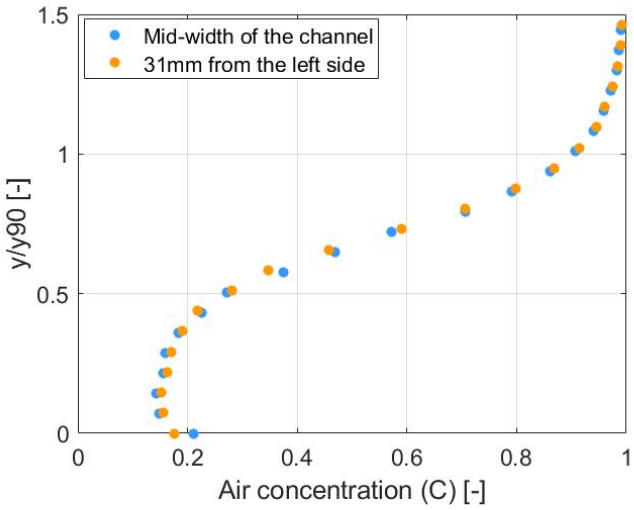

FIGURE 5.2: Creager weir and stepped spillway: Air concentration [-] depending on the dimensionless flow height [-].

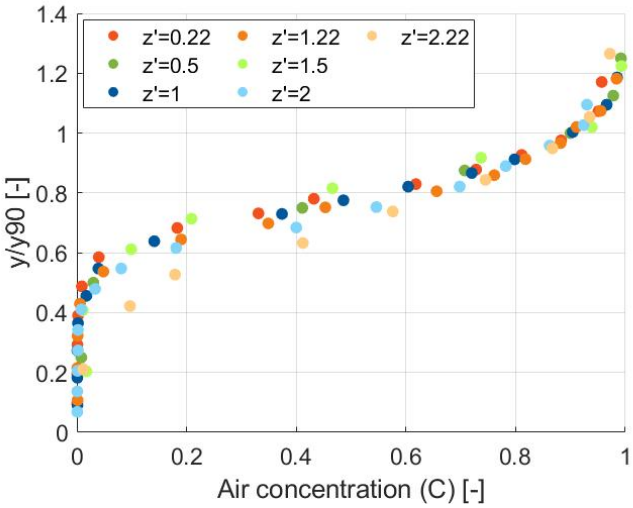

FIGURE 5.3: PKW1 and smooth spillway: Air concentration [-] depending on the dimensionless flow height [-].

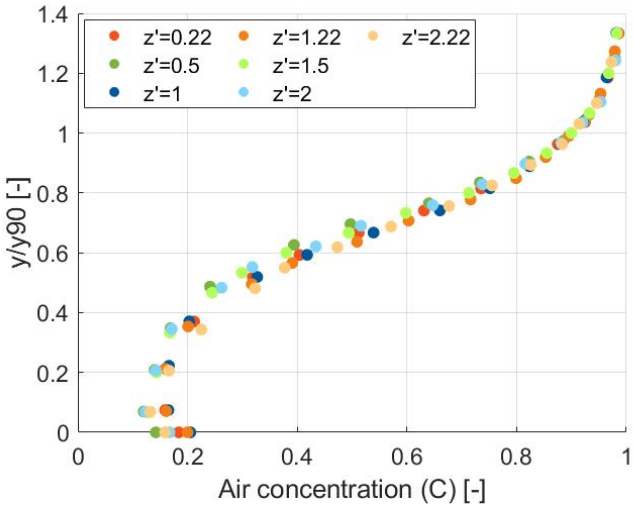

FIGURE 5.4: PKW1 and stepped spillway: Air concentration [-] depending on the dimensionless flow heigth [-].

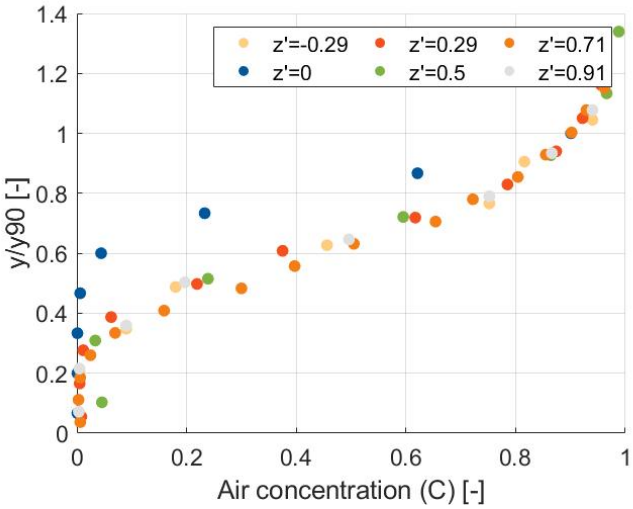

FIGURE 5.5: PKW2 and smooth spillway: Air concentration [-] depending on the dimensionless flow height [-].

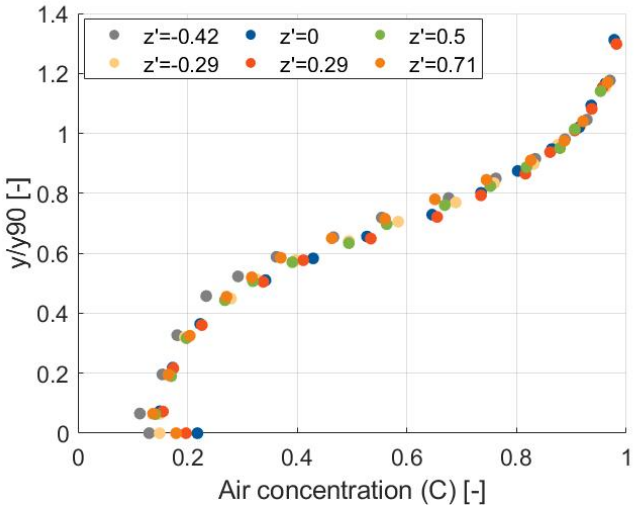

FIGURE 5.6: PKW2 and stepped spillway: Air concentration [-] depending on the dimensionless flow height [-].

In Figures 5.1 to 5.6, the dimensionless flow heights allow the curves to overlap for each configuration, regardless of the measure position. There are two exceptions: the first one is $z' = 2.22$ on Figure 5.3 and the second is $z' = 0$ on Figure 5.5. However, even with these two exceptions, the following conclusion is drawn: the air concentration profiles with a dimensionless flow height are the same in each configuration individually.

In order to compare the configurations, an average curve is calculated for each configuration from the results presented on Figures 5.1 to 5.6. Indeed, for several air concentrations, the average of the dimensionless flow heights is calculated. The average curves for all the configurations are plotted on Figure 5.7.

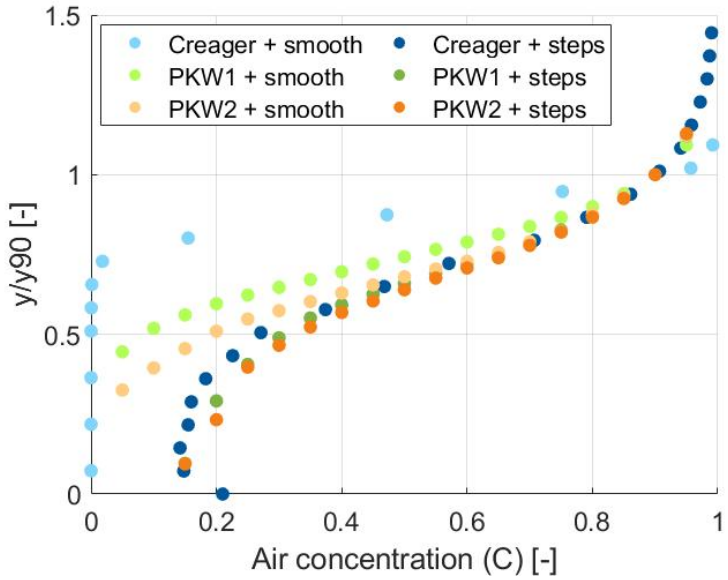

FIGURE 5.7: Comparison of the air concentration profiles depending on the dimensionless height (y/y_{90} [-]) for the six configurations.

The average air concentration profiles for the six configurations are represented on Figure 5.7. The lightest colours represent the smooth spillway, while the darkest colours represent the stepped spillway. The blue shade curves represent the Creager weir, the green ones the PKW1 and the orange ones the PKW2.

Firstly, Figure 5.7 illustrates that the configurations with a stepped spillway (dark colours) exhibit a greater degree of flow aeration until the air concentration reaches 0.9. Moreover, it can be seen that the air concentration around $y/y_{90} = 0$, thus near the bottom for the smooth spillway and near the pseudo-bottom for the stepped spillway, are not identical depending on the spillway. Indeed, the air concentration profiles for smooth spillways begin at an air concentration equal to 0 while those for steps spillways begin at approximatively $C = 0.15$.

Then, for the configurations with a smooth spillway, Figure 5.7 shows that PKW2 generates the most aeration in the flow, followed by PKW1 and finally the Creager weir. For the last one, the aeration is almost no-existent. Therefore, the difference of aeration between both PKWs is smaller than the difference between the Creager weir and the PKW1.

Finally, in view of the almost overlaid darker curves, it is possible to say that the flow aeration for stepped spillways does not depend on the weir placed at the top of the spillway.

In conclusion, the flow aeration firstly depends on the type of the spillway: more aeration is present for stepped spillways. Then, only in the case of smooth spillways, the weir has an importance: PKW2 generates the most aeration in the flow, followed by PKW1 and finally the Creager weir.

5.1.1 Comparison with theoretical models

The average air concentration profiles for the six configurations displayed in Figure 5.7 are compared with the theoretical models explained in Section 2.1.2. As a reminder, the various studied analytical models are:

- Chanson, 1995a
- Chanson and Toombes, 2002
- Wood, 1991

Figures 5.8 to 5.13 provide visual representations of the different comparisons. The air concentration axes are deliberately set at 0.9 because above this value, the theoretical models are no longer valid.

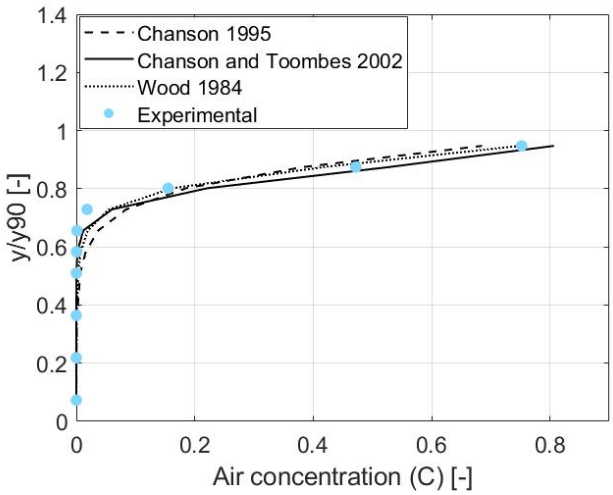

FIGURE 5.8: Creager weir and smooth spillway: Experimental and theoretical air concentration profiles.

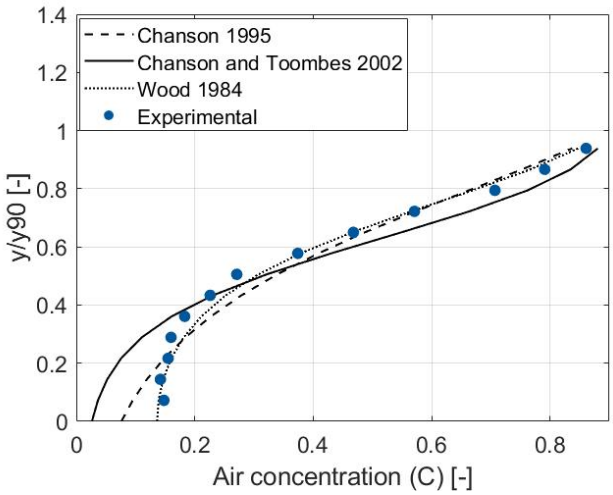

FIGURE 5.9: Creager weir and stepped spillway: Experimental and theoretical air concentration profiles.

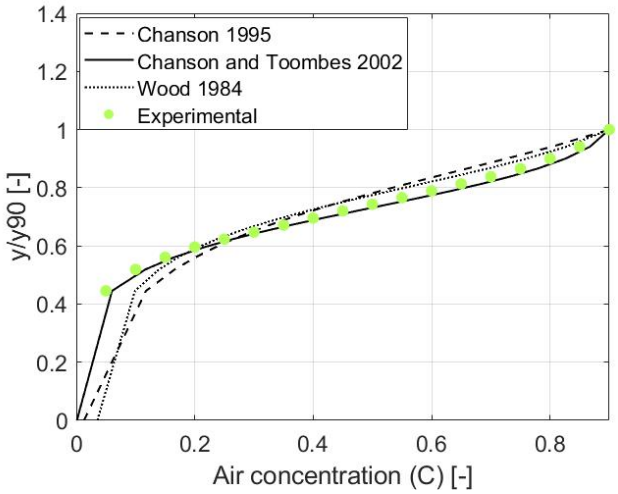

FIGURE 5.10: PKW1 and smooth spillway: Experimental and theoretical air concentration profiles.

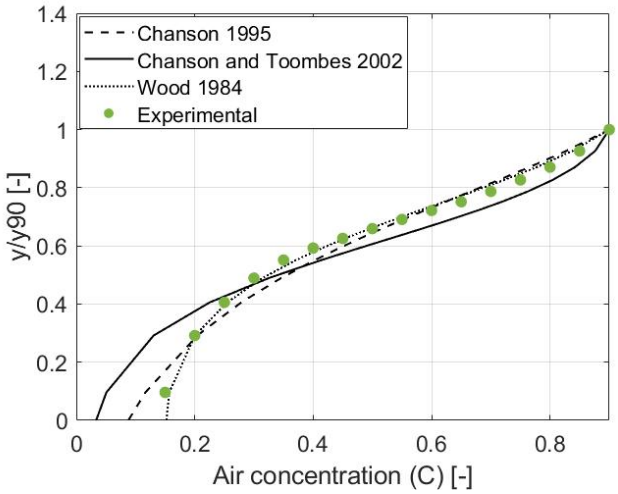

FIGURE 5.11: PKW1 and stepped spillway: Experimental and theoretical air concentration profiles.

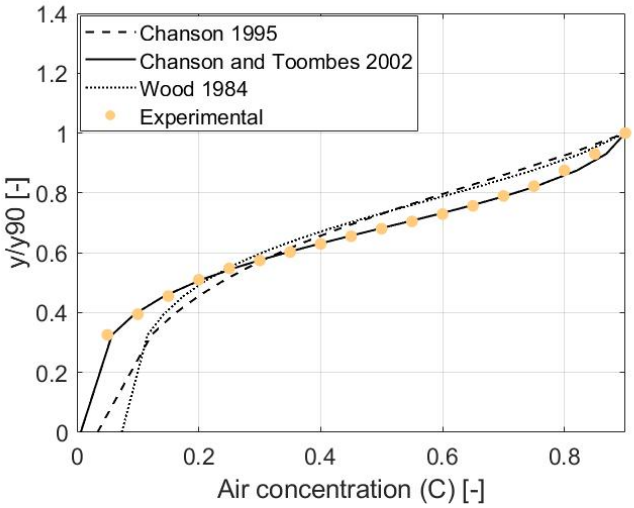

FIGURE 5.12: PKW2 and smooth spillway: Experimental and theoretical air concentration profiles.

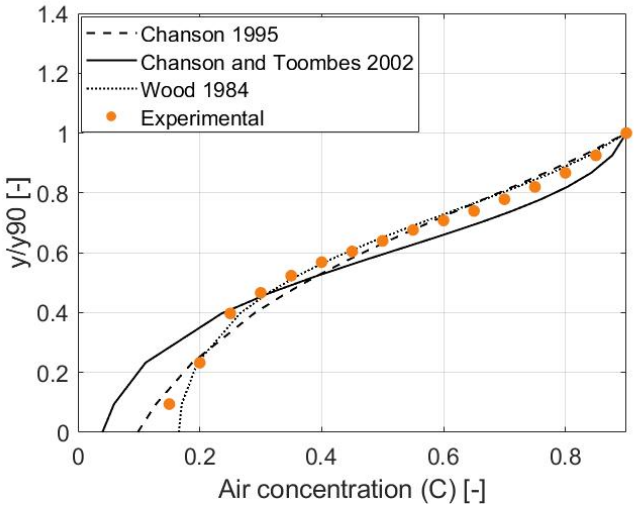

FIGURE 5.13: PKW2 and stepped spillway: Experimental and theoretical air concentration profiles.

Firstly, the different curves exhibit a consistent range of values for each configuration. To further validate this conclusion, Table 5.1 presents the average errors between the experimental data points and the analytic models.

Configuration	**Chanson, 1995a** [%]	**Chanson and Toombes, 2002** [%]	**Wood, 1991** [%]
Creager weir + smooth spillway	26.4	22.4	<u>20.5</u>
PKW1 + smooth spillway	15	<u>5.75</u>	12.2
PKW2 + smooth spillway	15.7	<u>2.2</u>	14.6
Creager weir + stepped spillway	15.6	28.2	<u>7.7</u>
PKW1 + stepped spillway	6.4	14.8	<u>2.76</u>
PKW2 + stepped spillway	6	13.6	<u>3.6</u>

TABLE 5.1: Average errors [%] between the experimental results and the theoretical models.

In Table 5.1, the underlined numbers are the minimum average errors depending on the analytic models. The Wood's model stands out as the most representative for the configurations with stepped spillways. On the other hand, the model of Chanson and Toombes is the most representative for the smooth spillways. The configuration with the Creager weir and the smooth spillway does not follow the drawn conclusion, but the difference between the models is 1.9%, which is low compared to the other configurations because the theoritical models are close for this configuration. Moreover, the minimum average errors are smaller for the PKWs than for the Creager weir.

5.2 Discharges

After the analysis of the air concentration profiles, a verification of the discharge is realised. Indeed, with the results of the air concentration and the velocity, it is possible to verify if the discharge calculated using the results is equal to the injected discharge (flowmeter value). In order to calculate the total discharge from the results, the different steps presented below are followed:

1. Calculating of the values of y_{90} which corresponds to the flow depths where the air concentration is equal to 0.9.
2. Calculating of the equivalent water depths h_w with Equations 5.1 and 5.2.

$$h_w = y_{90}(1 - C_{mean}) \tag{5.1}$$

$$C_{mean} = \frac{1}{y_{90}} \int_{y=0}^{y=y_{90}} C(z)dz \tag{5.2}$$

3. Calculating of the average velocities with Equation 5.3.

$$V_{mean} = \frac{1}{y_{90}} \int_{y=0}^{y=y_{90}} V(z)dz \tag{5.3}$$

4. Calculating of the specific discharges for each position on the width using Equation 5.4.

$$q = h_w V_{mean} \tag{5.4}$$

5. Calculating of the total discharge by integrating the specific discharges on the width (Equation5.5).

$$Q = \int_{z=0}^{z=L} q(z)dz \tag{5.5}$$

After following the various steps for each configuration, the total discharges are synthesised in Table 5.2.

Configuration	**Total discharge** [L/s]	**Percentage of injected discharge** [%]
Creager weir + smooth spillway	25.68	102.72
PKW1 + smooth spillway	24.78	99.12
PKW2 + smooth spillway	27.64	110.56
Creager weir + stepped spillway	30.3	121.2
PKW1 + stepped spillway	32.34	129.36
PKW2 + stepped spillway	34.23	134.23

TABLE 5.2: Total discharge [L/s] calculated from the experimental results for each configuration.

As a reminder, the injected discharge is the same for the six configurations and it is equal to $25L/s$. As it can be observable in Table 5.2, the discharge calculated from the results is up to 34.23% more important than the injected discharge. With such a difference, it is not possible to compare the configurations. The calculated discharges have to be changed and equal to $25L/s$. To do this, the water depths or the velocities have to be found with another method. Firstly, it is known that the double-tips conductivity probes lead to greater errors in measuring velocities than water depths. This can be explained by the fact that the velocity is calculated using the two tips of the probe, whereas the air concentration and consequently the height of water is calculated using a single tip. The error in velocity therefore comes from two sources, unlike the error in water height, which comes from a single. Furthermore, calculating velocity requires knowing the distance between the two tips, which is yet another error origin, even if it has been calculated using an optical microscope. In conclusion, the velocities must be calculated in another way in order to have total discharges equal to $25L/s$ for each configuration.

Using the discharge and water depths data, it is possible to calculate the resulting flow velocities. However, the first step is to distribute the total discharge ($25L/s$) across the width, as it is not uniform across the width. To find the discharge values at each measurement position (q), Equation 5.6 is used for each measurement point.

$$q = \frac{q_{measure}}{Q_{tot,measure}} Q_{tot,injrcted} \tag{5.6}$$

With

- q : discharge at each measurement point calculated from the injected discharge and the water depths.
- $q_{measure}$: discharge at each measurement point calculated from the velocities and water depths coming from the measurements (Equation 5.4).
- $Q_{tot,measure}$: Total discharge calculated by integrating $q_{measure}$, the different values are summarised at Table 5.2.
- $Q_{tot,injrcted}$: Total discharge injected and verify with the flowmeter. For reminder, in this work, $Q_{tot,injrcted} = 25L/s$.

Figure 5.14 is an example of q and $q_{measure}$ for the configuration with PKW1 and stepped spillway.

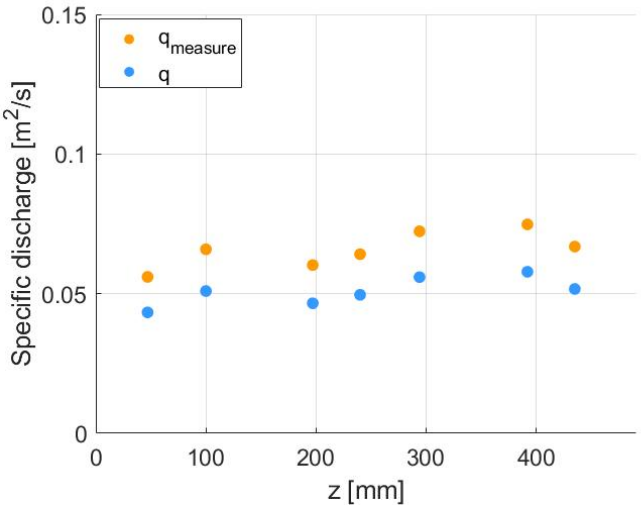

FIGURE 5.14: q [m^2/s] and $q_{measure}$ [m^2/s] for the configuration with PKW1 and stepped spillway.

In Figure 5.14, it is noticeable that the values of q are lower than those of $q_{measure}$. This discrepancy can be attributed to the fact that $Q_{tot,measure}$ is equal to 32.34 L/s which is too important compared with the flow actually injected (25L/s). The discharge must therefore be reduced but the non-uniformity across the width is kept.

This method is applied to all configurations: the results are presented in Figures 5.15 to 5.20.

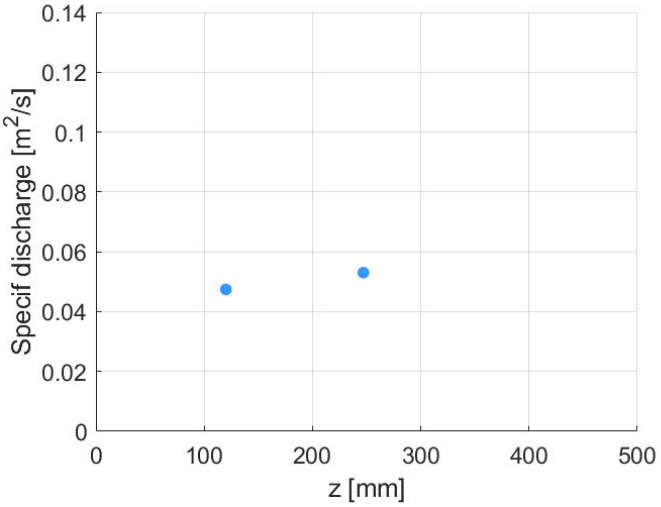

FIGURE 5.15: Creager weir and smooth spillway: Unit discharge [m^2/s].

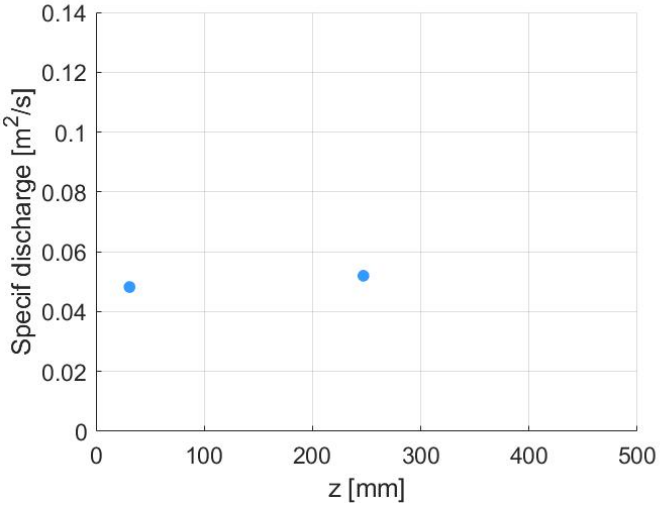

FIGURE 5.16: Creager weir and stepped spillway: Unit discharge [m^2/s].

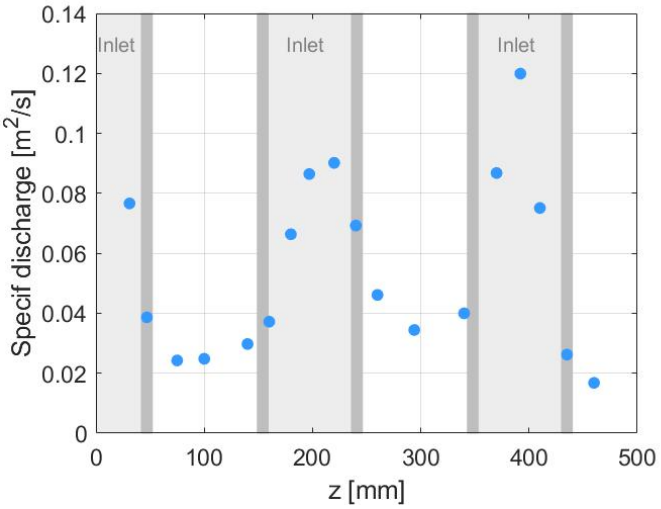

FIGURE 5.17: PKW1 and smooth spillway: Unit discharge [m^2/s].

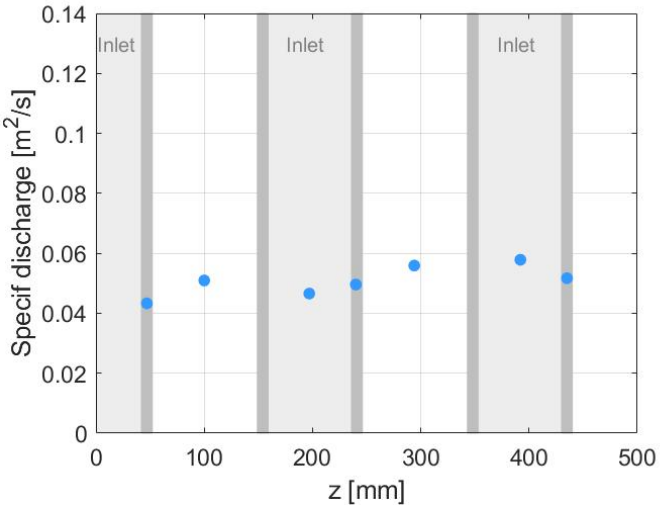

FIGURE 5.18: PKW1 and stepped spillway: Unit discharge [m^2/s].

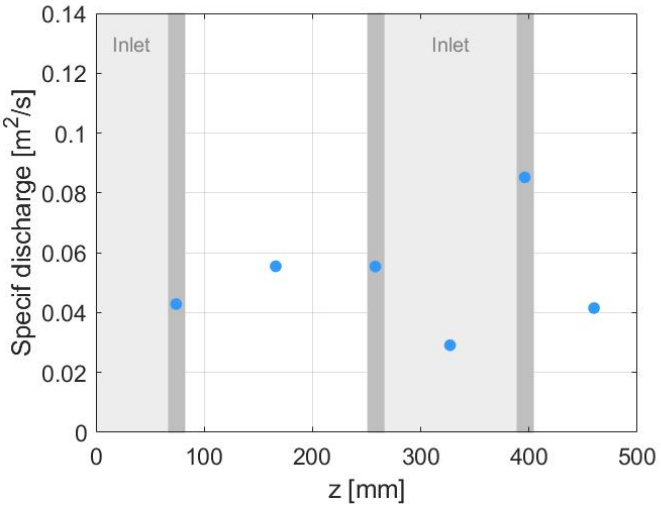

FIGURE 5.19: PKW2 and smooth spillway: Unit discharge [m^2/s].

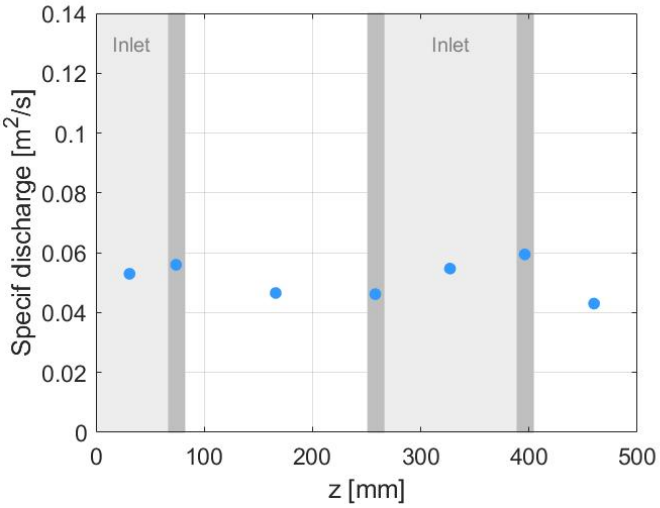

FIGURE 5.20: PKW2 and stepped spillway: Unit discharge [m^2/s].

In order to be able to compare the six configurations, the different discharges are reproduced on the same figure (Figure 5.21). On this figure, the lightest colours represent the smooth spillway, while the darkest colours represent the stepped spillway. The blue shade curves represent the Creager weir, the green ones the PKW1 and the orange ones the PKW2.

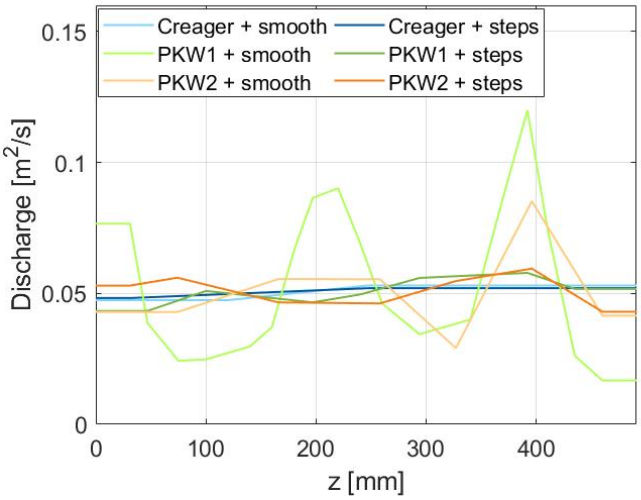

FIGURE 5.21: Comparison of the unit discharge [m^2/s] across the width of the six configurations.

On Figure 5.21 all the discharges are around 0.05 with more or less variations around this value. A comparison between the variations in discharges is realised. To carry out this analysis, Table 5.3 summarises the maximum, the minimum, the difference between them and the standard deviation of equivalent water depths for the six configurations.

Configuration	**Maximum** $[m^2/s]$	**Minimum** $[m^2/s]$	**Maximum-Minimum** $[m^2/s]$	**Standard deviation** $[m^2/s]$
Creager weir + smooth spillway	0.053	0.047	0.006	0.004
PKW1 + smooth spillway	0.12	0.017	0.103	0.029
PKW2 + smooth spillway	0.085	0.029	0.056	0.019
Creager weir + stepped spillway	0.052	0.048	0.004	0.003
PKW1 + stepped spillway	0.058	0.043	0.015	0.005
PKW2 + stepped spillway	0.059	10.043	0.016	0.006

TABLE 5.3: Maximum, minimum, difference between them and standard deviation of discharges [m^2/s] for the six configurations.

Based on the results of Table 5.3, it is concluded that the variations of discharge across the width are more important for the configurations with a PKW and a smooth spillway. This conclusion is based on the differences between the maximum and the minimum but also on the standard deviation. Moreover, it is remarkable that the differences between the maximum and the minimum are less important for the configurations with a Creager weir. Indeed, the discharges downstream Creager weirs are uniform across the width. The slight difference could be explained by the precision of the probe.

Then, the position of the maxima and minima in terms of discharge in relation to the geometry of the PKWs can be discussed. For the PKW1 and the smooth spillway, the maxima are located downstream of the inlets, while the minima are downstream of the outlets. For the three other configurations, no conclusion can be drawn as to the position of the maximum and minimum discharges.

5.3 Clear water depths

After the verification about the total discharge, the clear water depths are analysed regarding the six configurations. As a reminder, the flows obtained for the different configurations are air-water flows. However, in order to analyse other flow properties, like the discharge or the head, it is important to know the equivalent water depths, noted h_w. In those equations, y_{90} is the height from the bottom and perpendicular to it, for which the air concentration is equal to 0.9. The equivalent water depths are calculated with Equations 5.1 and 5.2 and showed on Figures 5.22 to 5.27.

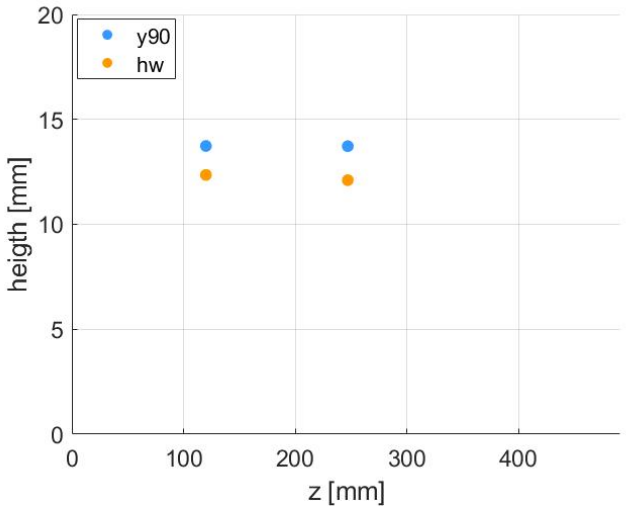

FIGURE 5.22: Creager weir and smooth spillway: Clear water depth [mm].

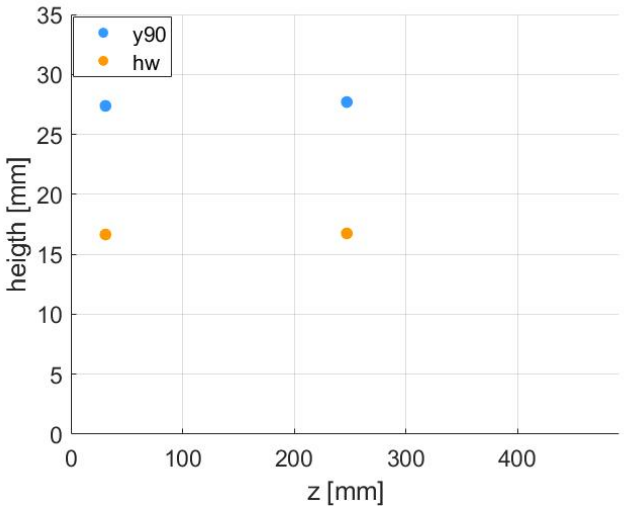

FIGURE 5.23: Creager weir and stepped spillway: Clear water depth [mm].

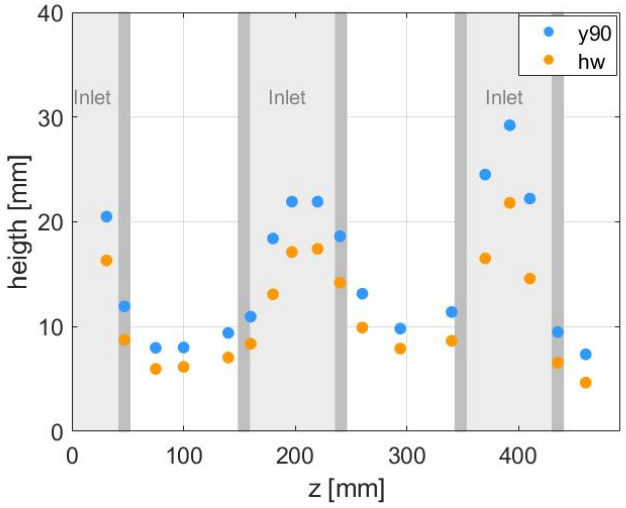

FIGURE 5.24: PKW1 and smooth spillway: Clear water depth [mm].

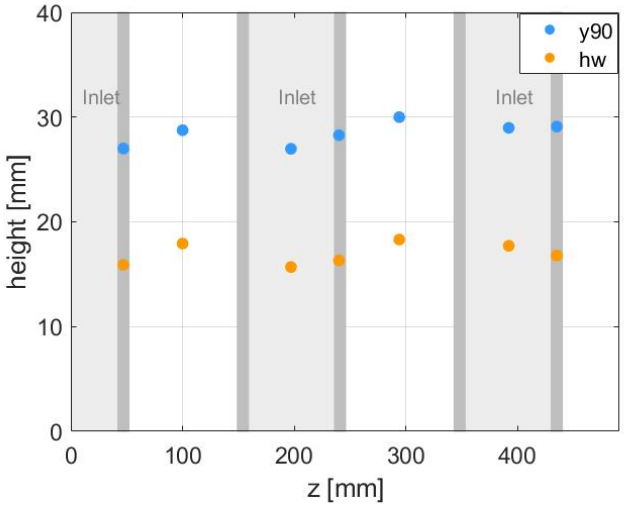

FIGURE 5.25: PKW1 and stepped spillway: Clear water depth [mm].

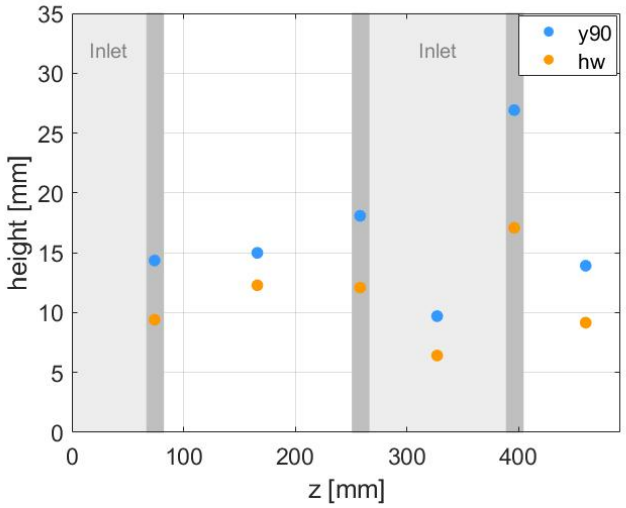

FIGURE 5.26: PKW2 and smooth spillway: Clear water depth [mm].

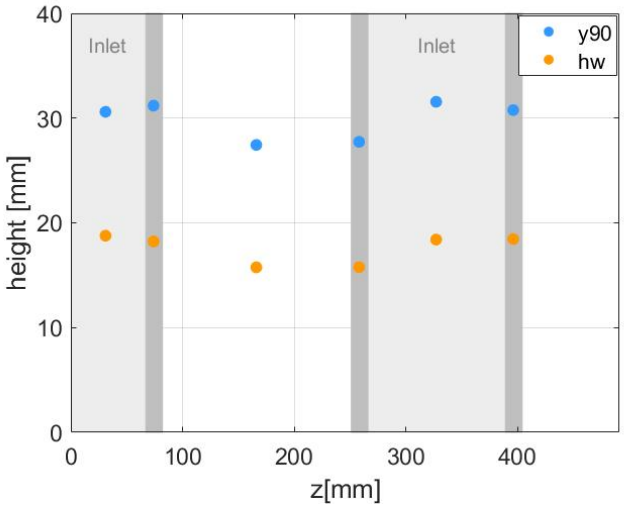

FIGURE 5.27: PKW2 and stepped spillway: Clear water depth [mm].

In order to be able to compare the six configurations, the different equivalent water depths are reproduced on the same figure (Figure 5.28). On this figure, the lightest colours represent the smooth spillway, while the darkest colours represent the stepped spillway. The blue shade curves represent the Creager weir, the green ones the PKW1 and the orange ones the PKW2.

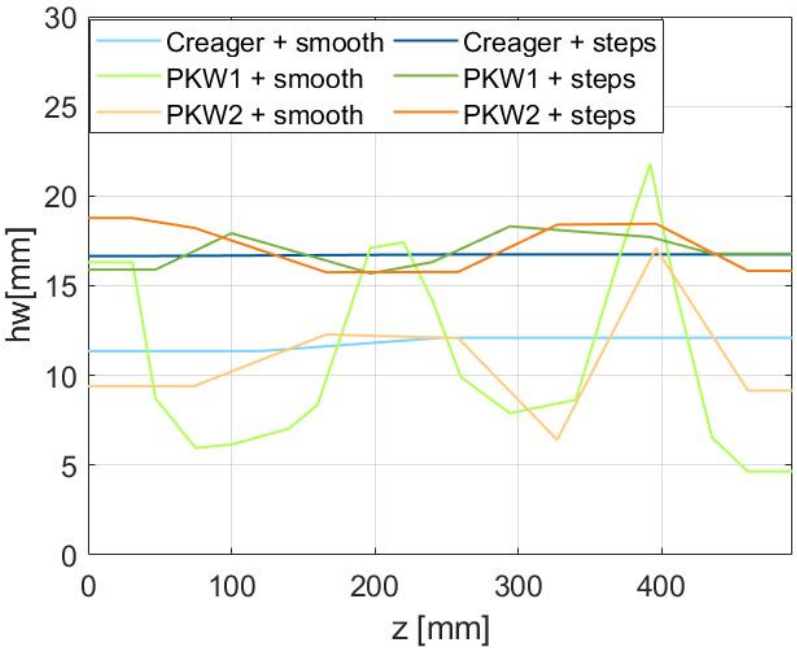

FIGURE 5.28: Comparison of the clear water depth profiles across the width of the six configurations.

On Figure 5.28 the equivalent water depths are generally higher for the configurations with stepped spillways (dark colours) than for smooth spillways (light colours). Some exceptions appear at peak heights for smooth spillways, but it does not change the trend.

The next step is the comparison between the variations in equivalent water depths. To carry out this analysis, Table 5.4 summarises the maximum, the minimum, the difference between them and the standard deviation of equivalent water depths for the six configurations.

Configuration	**Maximum [mm]**	**Minimum [mm]**	**Maximum-Minimum [mm]**	**Standard deviation [mm]**
Creager weir + smooth spillway	12.10	11.35	0.75	0.53
PKW1 + smooth spillway	21.81	4.65	17.16	5.04
PKW2 + smooth spillway	17.08	6.42	10.66	3.65
Creager weir + stepped spillway	16.74	16.65	0.09	0.06
PKW1 + stepped spillway	18.31	15.69	2.62	1.04
PKW2 + stepped spillway	18.77	15.75	3.02	1.44

TABLE 5.4: Maximum, minimum, difference between them and standard deviation of equivalent water depths [mm] for the six configurations.

Based on the results presented in Table 5.4, particularly the standard deviation values, it is evident that the dispersion of equivalent water depths is more pronounced for smooth spillways compared to stepped spillways. Indeed, Figure 5.28 further supports this observation, as the light-colored data points appear to be more scattered compared to the dark-colored data points. Furthermore, the standard deviations are higher for the PKWs compared to the Creager weir, which can be attributed to the fact that downstream of a Creager weir, the flow tends to be more uniformly distributed across the width. In fact, the obtained standard deviations for the Creager weir are $0.06mm$ and $0.53mm$, which can be explained by accuracy errors in measurements (the nearest mm). However, in the case of the PKWs, the standard deviation values are larger than $1mm$, which proves once again that PKWs create non-uniform flows over the width downstream them. Finally, it is not possible to draw a conclusion between the PKWs because in the case of smooth spillways, the standard deviation is higher for the PKW1, but it is the opposite for the stepped spillways.

Finally, the positions of maxima and minima clear water depths downstream the PKWs are analysed in relation to the PKWs geometry based on Figures 5.24 to 5.27. For the configurations with the PKW1 and the smooth spillway, the maxima are located approximately downstream of the middle of the inlets while the minima are downstream of the middle of the outlets. However, for the same PKW but with the stepped spillway, it is the opposite: the maxima correspond with the outlets and the minima with the inlets, even the difference between them is less pronounced than for the smooth spillway. For the second PKW and the smooth spillway, no conclusion can be drawn. Finally, for the PKW2 and the stepped spillway, the maxima are downstream of the inlets while the minima are downstream of the outlets. In the final analysis, it is impossible to draw any general conclusion on the position of the maxima and minima downstream of the PKWs unlike R. Eslinger and Crookston, 2020. Indeed, for a horizontal channel, his conclusion was that the PKW jets are aligned with the outlets key. This conclusion can't be drawn in this work.

5.4 Average velocities

After the analysis of the equivalent water depths, the analysis of the average velocities can be realised. Indeed, the used velocities are not the velocities obtained by the probe, but rather those calculated from the equivalent water depths and the distributed discharges calculated with Equation 5.4 in order to have a total discharge equal to $25L/s$. The velocities for each position on the width are calculated with Equation 5.7 and the results are presented in Figures 4.23 to 4.28.

$$V_{average} = \frac{q}{h_w} \tag{5.7}$$

Moreover, as explained in Section 4.4, the raw results do not allow a comparison of velocities over width because of the different flow depths across the width. The average velocities calculated with Equation 5.7 makes possible to carry out comparisons for each configuration, as well as comparisons between them.

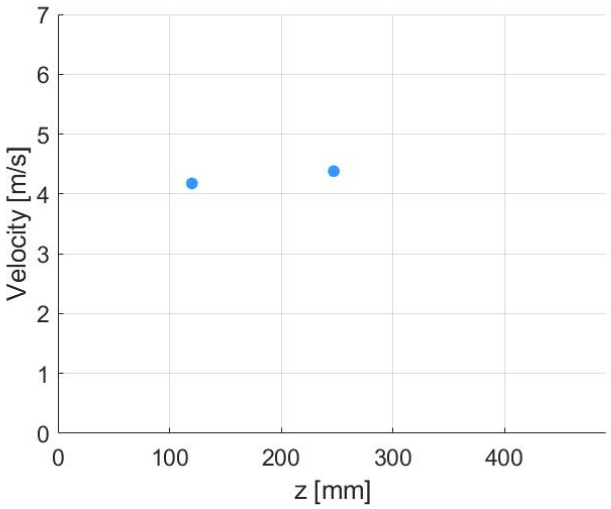

FIGURE 5.29: Creager weir and smooth spillway: Average velocity [m/s].

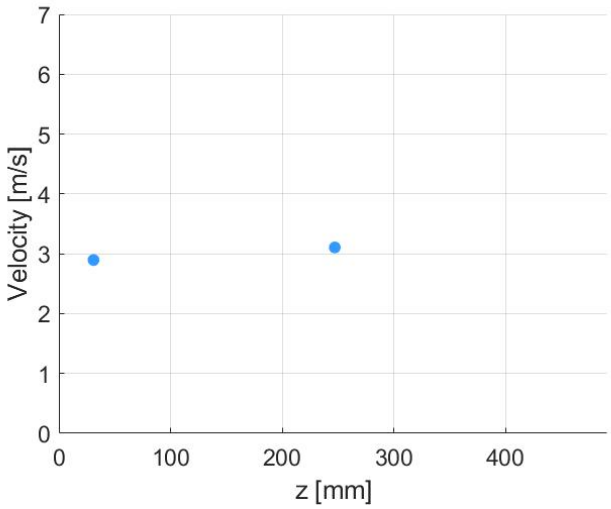

FIGURE 5.30: Creager weir and stepped spillway: Average velocity [m/s].

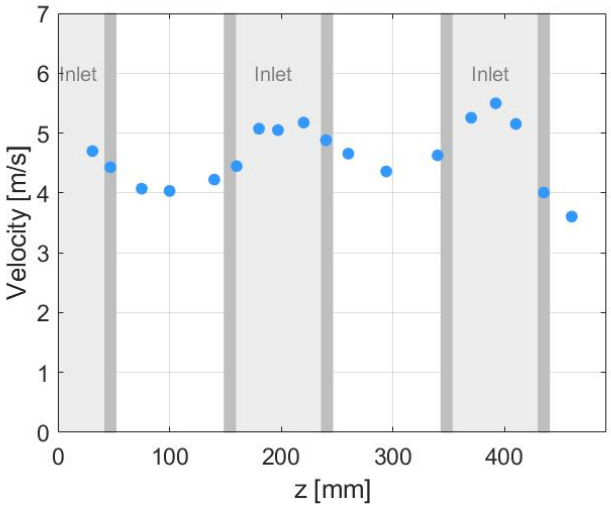

FIGURE 5.31: PKW1 and smooth spillway: Average velocity [m/s].

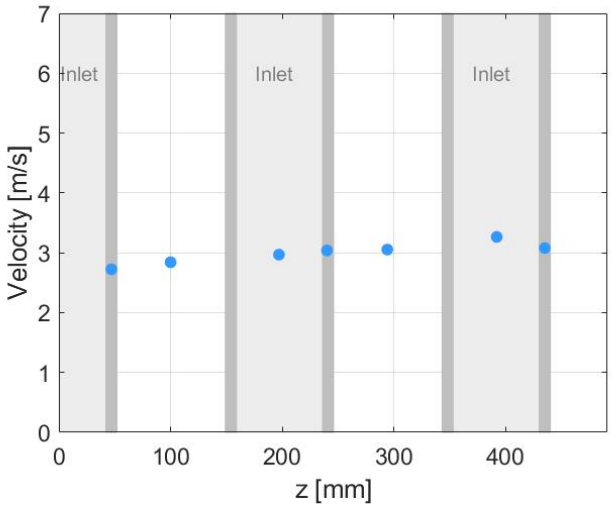

FIGURE 5.32: PKW1 and stepped spillway: Average velocity [m/s].

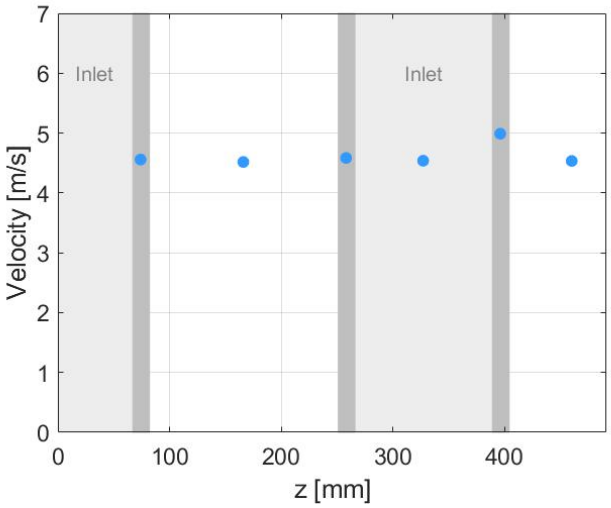

FIGURE 5.33: PKW2 and smooth spillway: Average velocity [m/s].

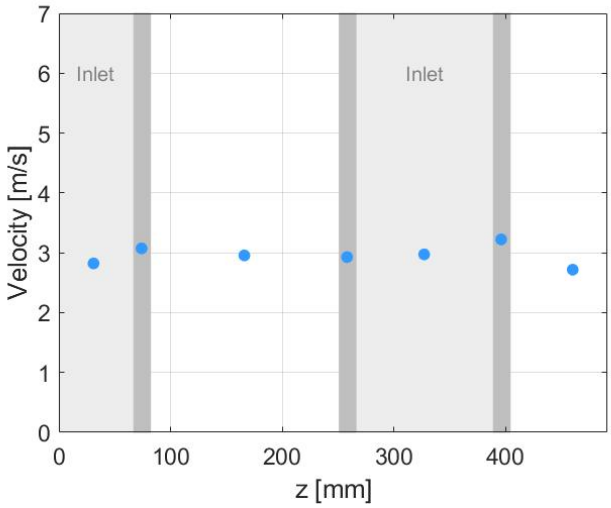

FIGURE 5.34: PKW2 and stepped spillway: Average velocity [m/s].

In order to be able to compare the six configurations, the different average velocities are reproduced on the same figure (Figure 5.35). On this figure, the lightest colours represent the smooth spillway, while the darkest colours represent the stepped spillway. The blue shade curves represent the Creager weir, the green ones the PKW1 and the orange ones the PKW2.

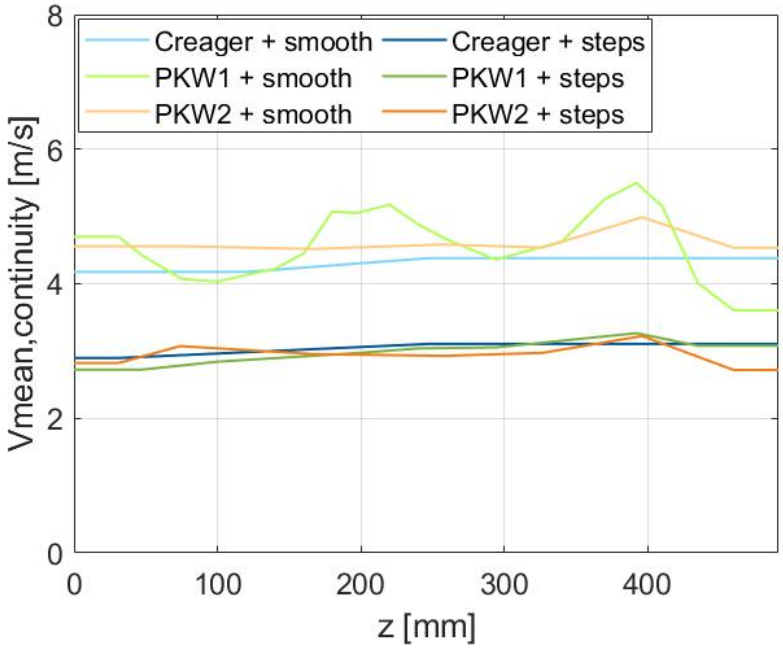

FIGURE 5.35: Comparison of the average velocity profiles across the width of the six configurations.

Firstly, Figure 5.35 clearly indicates that the average velocities are generally higher for configurations with smooth spillways (light colours) compared to stepped spillways (dark colours). This conclusion is the opposite to the one drawn for the equivalent water depths, which are greater for the stepped spillway.

The next step is the comparison between the variations in average velocity. To carry out this analysis, Table 5.5 summarises the maximum, the minimum, the difference between them and the standard deviation of average velocities for the six configurations.

Configuration	**Maximum [m/s]**	**Minimum [m/s]**	**Maximum-Minimum [m/s]**	**Standard deviation [m/s]**
Creager weir + smooth spillway	4.5	4.29	0.21	0.15
PKW1 + smooth spillway	5.45	3.57	1.88	0.51
PKW2 + smooth spillway	5.51	4.49	0.52	0.2
Creager weir + stepped spillway	3.76	3.51	0.25	0.18
PKW1 + stepped spillway	4.22	3.52	0.7	0.23
PKW2 + stepped spillway	4.41	3.72	0.69	0.22

TABLE 5.5: Maximum, minimum, difference between them and standard deviation of average velocities [m/s] for the six configurations.

Based on the results presented in Table 5.5, particularly the standard deviation values, and the observations from Figures 5.29 to 5.34, it is evident that the dispersion is relatively similar across all configurations, except for the PKW1 and smooth spillway case, where a notable difference can be observed. Indeed, the standard deviations are in the range 0.15-0.23 except for the PKW1 and the smooth spillway, for which it is equal to 0.51. Moreover, in this configuration, Figure 5.31 clearly shows that the maxima are positioned downstream of the inlets, while the minima are located downstream of the outlets. For the other configurations, no conclusion about the minima and maxima can be drawn.

5.5 Energy dissipation

An important property that can be studied is the energy dissipation depending on the type of weir. In order to know the dissipated energy and compare them, the upstream and downstream heads have to be calculated for the six configurations. An overview diagram is represented on Figure 5.36 with the positions of the three weirs and the different measurements used to calculate the heads.

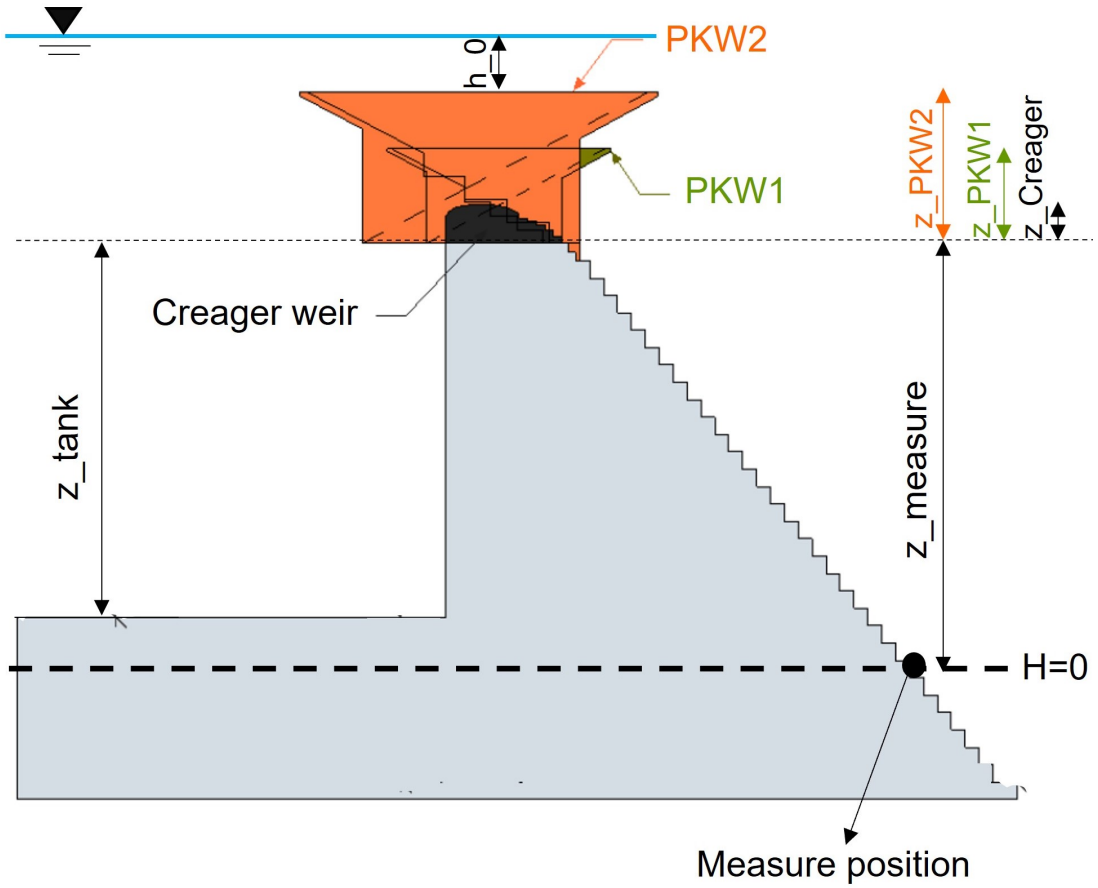

FIGURE 5.36: Overview diagram of the setup and the measurements used to calculate heads.

Firstly, it can be observed on Figure 5.36 that the head due to altitude is equal to 0 at the measure position. Then the different measurements are:

- z_{weir} : height of weirs. They are summarised in Table 5.6 for the different weirs.

$z_{Creager}$	z_{PKW1}	z_{PKW2}
6.7cm	16.3cm	26.2cm

TABLE 5.6: $z_{weir}[cm]$

- $z_{measure}$: distance between the measure position and the top of the spillway where the weirs are placed.
- z_{tank} : distance between the bottom of the tank to the top of the spillway where the weirs are placed.
- h_0 : water depth above the weirs.

5.5.1 Upstream head

In order to calculate the upstream heads, the water depths above the weirs have to be determined. These measurements are taken from Faure, 2015-2016. Indeed, the setup used for J.Faure's thesis was the same as the one used in this work, and a probe was placed above the tank in order to know depths above the weirs. The results are shown on Figure 5.37.

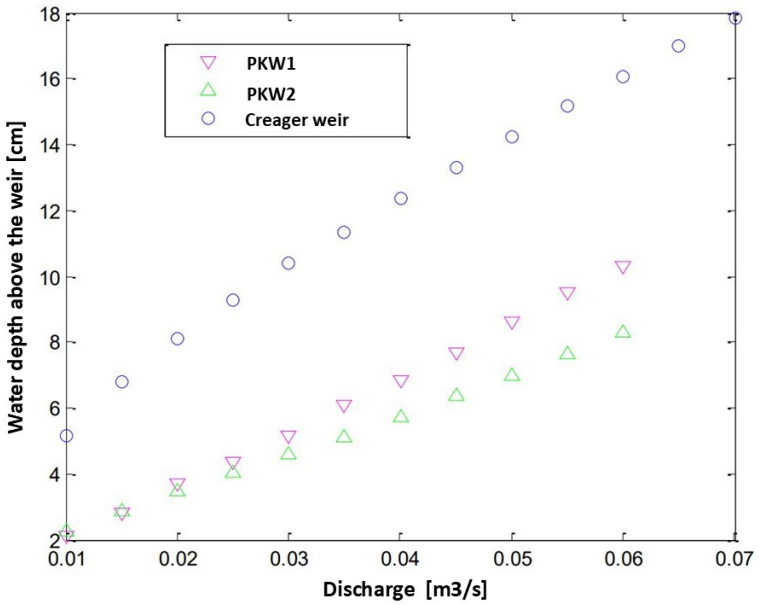

FIGURE 5.37: Changes in water depth [cm] over the weirs studied (Faure, 2015-2016).

In this work, the discharge is equal to $0.025m^3/s$. With Figure 5.37, it is therefore possible to obtain the water depth above the weirs. The results are summarised in Table 5.7.

$h_{0,Creager}$	$h_{0,PKW1}$	$h_{0,PKW2}$
9.31cm	4.39cm	4.08cm

TABLE 5.7: Water depth above the weirs (h_0 [cm]) for $Q = 0.025m^3/s$.

With h_0 known, it is possible to calculate the upstream heads depending on the weir with Equation 5.8. In this equation, L corresponds to the channel width, and it is equal to $0.492m$. The results for the three weirs are summarised in Table 5.8.

$$H_{upstream} = z_{measure} + z_{weir} + h_0 + \frac{Q^2}{2gL^2(z_{tank} + z_{weir} + h_0)^2} \tag{5.8}$$

Weir	$z_{measure}$ [m]	z_{weir} [m]	h_0 [m]	z_{tank} [m]	$H_{upstream}$ [m]
Creager	1.392	0.067	0.0931	0.52	1.552
PKW1	1.392	0.163	0.0439	0.52	1.599
PKW2	1.392	0.262	0.0408	0.52	1.695

TABLE 5.8: Upstream heads ($H_{upstream}$ [m]).

5.5.2 Downstream head

The heads at the measure point ($x = 1.76m$) can be calculated for the six configurations using Equation 5.9. In this equation, the altitude term is not taken into account because it was decided to set the altitude origin at the measurement point. Moreover, h_w and $V_{average}$ are taken respectively from Sections 5.3 and 5.4. The results for the six configurations are shown in Figures 5.38 to 5.43.

$$H_{measure} = h_w cos(\phi) + \frac{V_{average}^2}{2g} \tag{5.9}$$

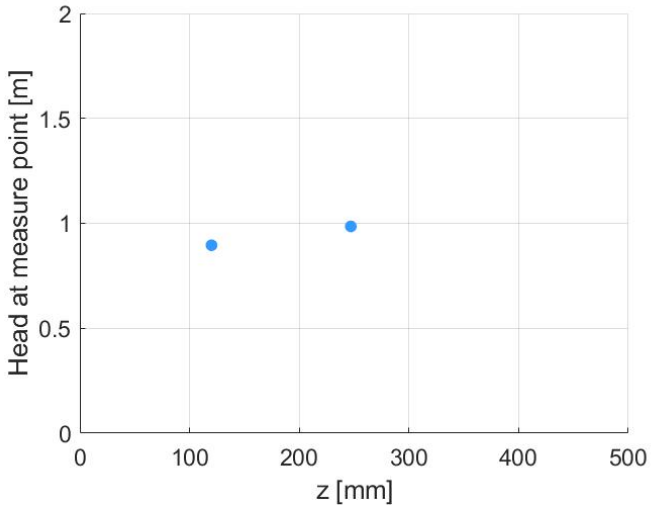

FIGURE 5.38: Creager weir and smooth spillway: Head [m].

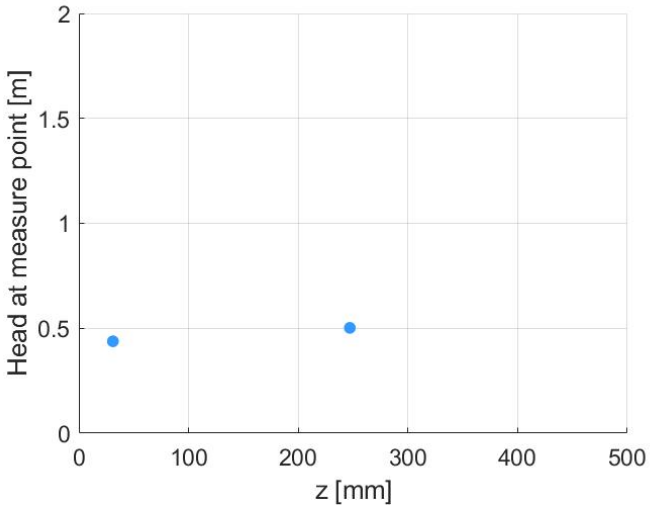

FIGURE 5.39: Creager weir and stepped spillway: Head [m].

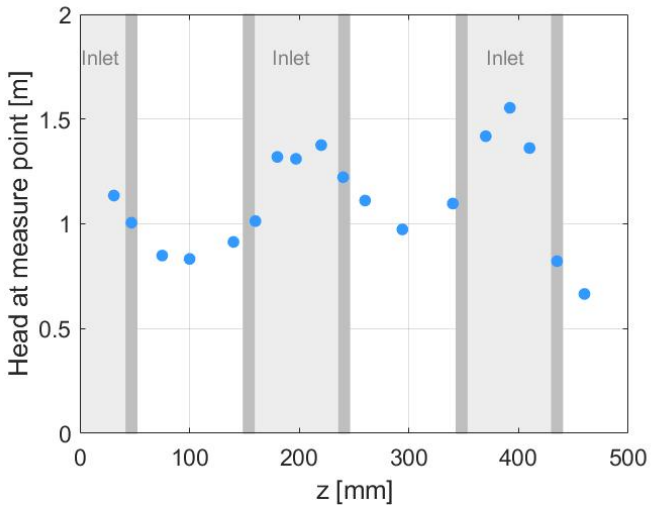

FIGURE 5.40: PKW1 and smooth spillway: Head [m].

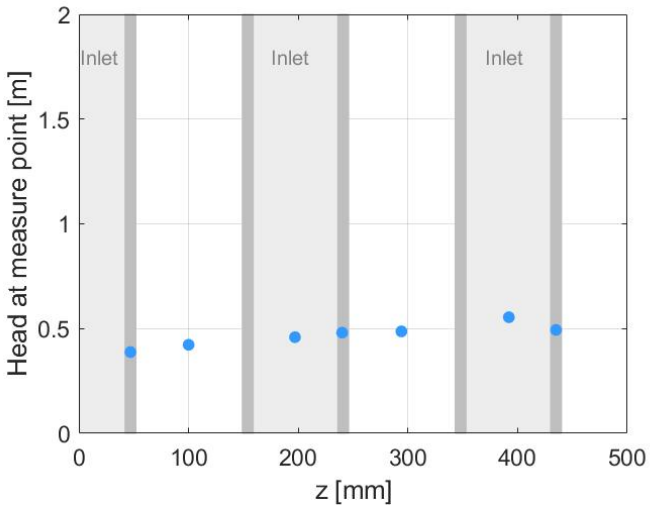

FIGURE 5.41: PKW1 and stepped spillway: Head [m].

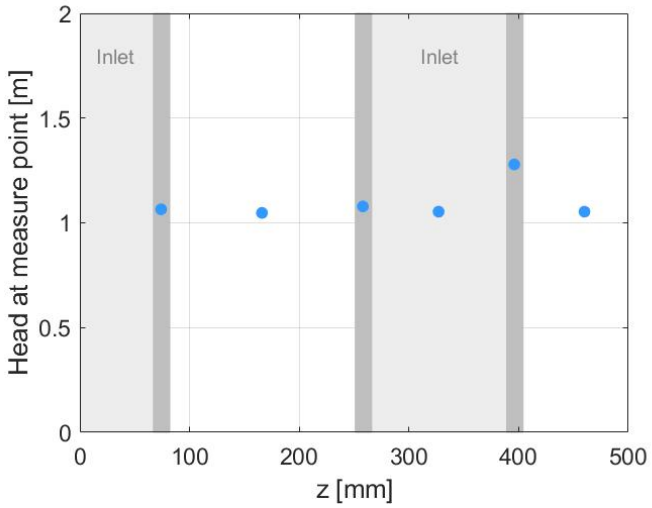

FIGURE 5.42: PKW2 and smooth spillway: Head [m].

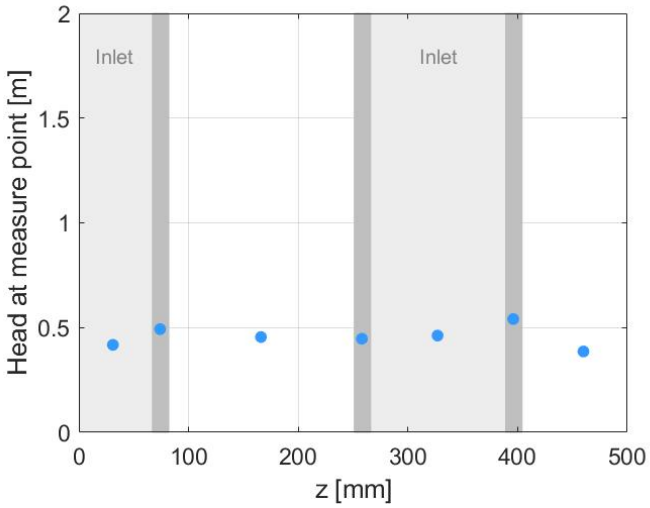

FIGURE 5.43: PKW2 and stepped spillway: Head [m].

In order to be able to compare the six configurations, the different heads are reproduced on the same figure (Figure 5.44). On this figure, the lightest colours represent the smooth spillway, while the darkest colours represent the stepped spillway. The blue shade curves represent the Creager weir, the green ones the PKW1 and the orange ones the PKW2.

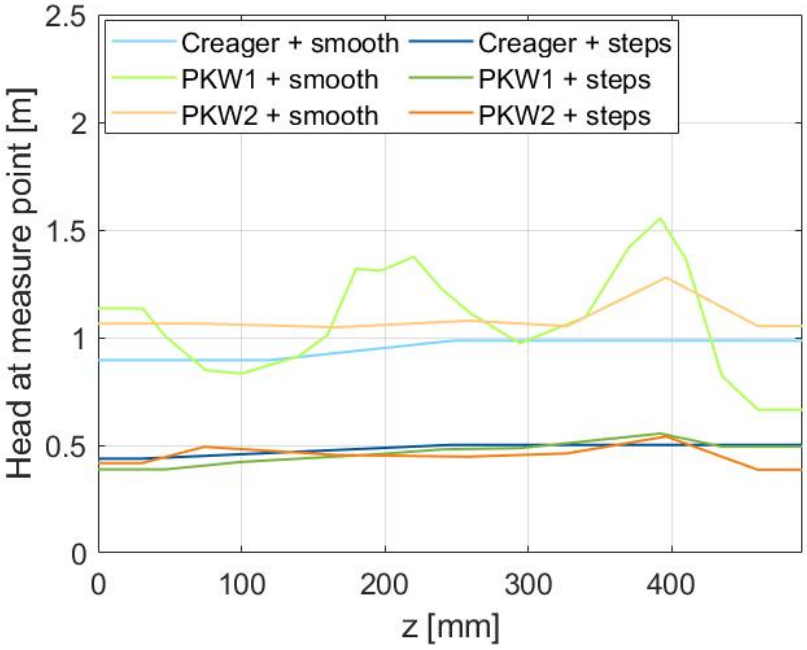

FIGURE 5.44: Comparison of the heads [m] across the width of the six configurations.

Figure 5.44 clearly illustrates that the heads are generally lower for configurations with stepped spillways (dark colors) compared to smooth spillways (light colors). This observation aligns with the conclusions drawn for velocities and stands in contrast to the results obtained for water depths. Indeed, the flow is supercritical, which means that the kinetic term ($V^2/2g$) is much more important than the water head term in the load ($h_w cos(\phi)$) calculation formula. It is therefore logical that the heads fit more the velocities than the water depths.

Then, like the for discharges, clear water depths and velocities, the comparison between the variations in heads are analysed. To carry out this analysis, Table 5.9 summarises the maximum, the minimum, the difference between them and the standard deviation of average velocities for the six configurations.

Configuration	**Maximum [m]**	**Minimum [m]**	**Maximum-Minimum [m]**	**Standard deviation [m]**
Creager weir + smooth spillway	0.9853	0.8954	0.0899	0.0636
PKW1 + smooth spillway	1.5538	0.6651	0.8887	0.2459
PKW2 + smooth spillway	1.2788	1.0475	0.2314	0.0903
Creager weir + stepped spillway	0.5018	0.4377	0.0641	0.0453
PKW1 + stepped spillway	0.5542	0.3878	0.1664	0.0535
PKW2 + stepped spillway	0.5407	0.386	0.1547	0.05

TABLE 5.9: Maximum, minimum, difference between them and standard deviation of heads [m] for the six configurations.

Based on the results of Table 5.9, especially on the difference between maximum and minimum and the standard deviation, the results indicate that the dispersion of heads is more significant for smooth spillways compared to stepped spillways. Moreover, the difference between the smooth and stepped spillways is more pronounced for PKW1, followed by PKW2, and finally for the Creager weir. In the case of the Creager weir, the standard deviation difference is only equal to $0.0183m$.

Then, the difference between the maximum and minimum values is observed to be smaller for configurations with a Creager weir compared to those with a PKW. However, the standard deviations for the configurations with a Creager weir and those with a PKW and a stepped spillway are very close to each other. It can therefore be concluded that the variations in head are more important in the case with a PKW and a smooth spillway, and particularly for the PKW1 in this work.

Finally, for the configurations with more important variations in head, the position of the maxima and the minima can be observed in relation to the geometry of the PKW. For the configuration with the PKW1 and the smooth spillway, Figure 5.40 shows that the maxima are located downstream of the inlets while the minima are located downstream of the outlets. However, in the case of the configuration with PKW2 and the smooth spillway, it is not possible to draw any conclusions about the positioning of the minima and maxima. This is because Figure 5.42 only displays one maximum, which is located downstream of a separation between an inlet and an outlet.

In order to calculate an energy dissipation for the six configurations, a total head is calculated by integrating the heads on the width. The total heads for the six configurations are summarised in Table 5.13.

Configuration	**Total head $H_{measure}$ [m]**
Creager weir + smooth spillway	0.9517
PKW1 + smooth spillway	1.0704
PKW2 + smooth spillway	1.0896
Creager weir + stepped spillway	0.4837
PKW1 + stepped spillway	0.4683
PKW2 + stepped spillway	0.4585

TABLE 5.10: Total head [m] calculated for each configuration.

Given that the upstream loads are not the same depending on the weir, it is not possible to draw conclusions between the configurations with different weirs. However, it is evident that the total head is higher for smooth spillways compared to stepped spillways for the same type of weir.

5.5.3 Propagation of uncertainty

In this section, the aim is to elaborate how the uncertainties propagate, especially for the heads. In view of the calculation of heads, uncertainty can have two origins:

- Measuring flow depths.
- Measuring discharges.

Assuming that the two uncertainties are independent, according to Bally and Berroir, 2010, Equation 5.10 is used to calculate the uncertainty on the heads depending on the uncertainties of the measuring flow depths and discharges.

$$\delta H(h,Q) = \sqrt{\left|\frac{\partial H}{\partial h}\right|^2 (\delta h)^2 + \left|\frac{\partial H}{\partial Q}\right|^2 (\delta Q)^2} \tag{5.10}$$

Firstly, the uncertainties are the following:

- $\delta h = 1.13\%$ (calculated in Section 4.5).
- $\delta Q = Q \times 1\%$ (the uncertainty is equal to 1% of the injected discharge).

Secondly, derivatives are calculated (Equation 5.12 and Equation 5.13). As a reminder, heads for the six configurations are calculated with Equation 5.11.

$$H_{measure} = h_w cos(\phi) + \frac{\left(\frac{Q}{h_w L}\right)^2}{2g} \tag{5.11}$$

$$\frac{\partial H}{\partial h} = cos(\phi) - \frac{Q^2}{h_w^3 L^2 g} \tag{5.12}$$

$$\frac{\partial H}{\partial Q} = \frac{Q}{h_w^2 L^2 g} \tag{5.13}$$

Given that the equivalent water depths are different depending on the configurations but because of the non-uniformity across the width, different heights of water exist also for the same configuration. The maximum uncertainty for each configuration are summarised in Table 5.11.

Configuration	**Uncertainty of H [m]**
Creager weir + smooth spillway	0.0309
PKW1 + smooth spillway	0.1841
PKW2 + smooth spillway	0.0968
Creager weir + stepped spillway	0.0143
PKW1 + stepped spillway	0.0161
PKW2 + stepped spillway	0.016

TABLE 5.11: Uncertainty of the total head [m] for the six configurations.

5.5.4 Dissipated energy

Once the upstream heads and the heads at the measure point are known, it is possible to calculate the dissipated energy for the six configurations. Firstly, it is important to remember that the vertical height between the measure point and the top of the different weirs are not the same depending on the weir. Table 5.12 summarises these vertical heights.

Weir	**Distance between the measure point and the top of the weir [m]**
Creager weir	1.459
PKW1	1.555
PKW2	1.654

TABLE 5.12: Vertical height [m] between the measure point and the top of the different weirs.

With these vertical heights and the heads for each configuration, it is possible to calculate the dissipated energy per vertical meter of dam with Equation 5.14.

$$\frac{H_{upstream} - H_{measure}}{z_{measure} + z_{weir}} \tag{5.14}$$

Configuration	$H_{upstream}$ [m]	$H_{measure}$ [m]	$z_{measure}$ [m]	z_{weir} [m]	$\Delta H/m$ [m/m]
Creager weir + smooth spillway	1.552	0.9517	1.392	0.067	0.411
PKW1 + smooth spillway	1.599	1.0704	1.392	0.163	0.34
PKW2 + smooth spillway	1.695	1.0896	1.392	0.262	0.366
Creager weir + stepped spillway	1.552	0.4837	1.392	0.067	0.732
PKW1 + stepped spillway	1.599	0.4683	1.392	0.163	0.727
PKW2 + stepped spillway	1.695	0.4585	1.392	0.262	0.748

TABLE 5.13: Dissipated energy per vertical meter [m/m] of dam for each configuration.

After the calculation of the dissipated energy per vertical meter of dam, it is possible to recalculate the heads $H_{measure}$ in order to have heads at the same vertical distance from the top of the different weirs. Indeed, at this point, the distance between the top of the dam to the point where the heads are measured is different. It is thus not correct to compare them with not the same height of dam. In order to have the same distance, the PKWs heads are calculated at a vertical distance of 1.459m from the top of their weir, which corresponds to the distance for the Creager weir. Knowing the height differences between the PKWs and the Creager weir and the dissipated energy per meter, it is thus possible to recalculate the heads at a distance equal to 1.459m from the top of each weir for each configuration. The results are summarised in Table 5.14.

Configuration	$H_{measure}$ [m]
Creager weir + smooth spillway	0.9517
PKW1 + smooth spillway	1.103
PKW2 + smooth spillway	1.161
Creager weir + stepped spillway	0.4837
PKW1 + stepped spillway	0.538
PKW2 + stepped spillway	0.604

TABLE 5.14: Heads [m] at a vertical distance from the top of the weirs equal to $1.459m$ for the six configurations.

The dissipated energy for the six configurations and at a vertical distance of $1.459m$ from the top of the weir are calculated using Equation 5.15. The results are summarised in Table 5.15.

$$1 - \frac{H_{measure}}{H_{upstream}} \tag{5.15}$$

Configuration	Dissipated energy [-]
Creager weir + smooth spillway	0.387
PKW1 + smooth spillway	0.31
PKW2 + smooth spillway	0.315
Creager weir + stepped spillway	0.688
PKW1 + stepped spillway	0.664
PKW2 + stepped spillway	0.643

TABLE 5.15: Dissipated energy [-] at a vertical distance from the top of the weirs equal to $1.459m$ for the six configurations.

Firstly, the dissipated energy is significantly higher (around 30%) for configurations with stepped spillways compared to those with smooth spillways. Then, for smooth spillways, the change in weir creates a difference in dissipated energy of 7.7% while this difference is equal to 4.5 %. The change in weir therefore generates a greater difference in the case of smooth spillways.

Then, the dissipated energy is slightly higher for Creager weirs compared to PKWs in both smooth and stepped spillway configurations.This conclusion is counterintuitive because the PKWs create three-dimensional flows downstream. In 3D flows, the turbulences are more important than in 2D flows (flows downstream Creager weirs, for example). More turbulence means more energy dissipation, but the obtained results do not confirm this hypothesis.

For the PKWs, it is impossible to know which one dissipates more energy because for smooth spillways, PKW2 dissipates more energy while for stepped spillways, PKW1 dissipates more energy. However, the dissipated energies are very close to each other (0.5% for smooth spillways and 2.1% for stepped spillways). However, the results of R. Eslinger and Crookston, 2020, represented in Figure 2.15, show that the dissipated energy depends on the ratio W_i/W_O and in this work, this ratio is equal to 1.26 for PKW1 and 1.37 for PKW2 which can explained that the dissipated energy is very close for these two PKWs.

In conclusion, the type of spillway has a greater influence than the type of weir on the dissipated energy. Indeed, switching from a smooth spillway to a stepped spillway enables a greater dissipated energy.

5.5.5 Comparison with theoretical models

In order to verify that the experimental results are in the right range, some comparisons with theoretical models are realised. These analyses are performed for the configurations with Creager weirs because some research has been carried out on PKWs.

Creager weir and smooth spillway

The fact that the flow is uniform at the measure point is hypothetised. The uniform depth is obtained when the friction slope is equal to the bottom slope (Equation 5.16).

$$J = i = sin(\phi) \tag{5.16}$$

The uniform depth is calculated from the empirical Manning-Strickler formula (Equation 5.17).

$$u = KJ^{1/2}R_h^{2/3} \tag{5.17}$$

In this equation,

- u : average cross-sectional velocity [m/s].
- K : Friction coefficient $[m^{1/3}/s]$ ($K = 90m^{1/3}/s$ in this work).
- J : friction slope [-].
- R_h : hydraulic radius [m] ($R_h = \frac{Lh}{L+2h}$).

$$\frac{Q}{h_u L} = K(i)^{1/2}\left(\frac{Lh_u}{L+2h_u}\right)^{2/3} \tag{5.18}$$

By solving Equation 5.18, the following uniform depth is found:

$$h_u = 12.33mm \tag{5.19}$$

The average velocity and the head are calculated at Equation 5.20 and Equation 5.21.

$$V_{average} = \frac{Q}{h_u L} = \frac{0.025}{12.33 \times 10^{-3} \times 0.491} = 4.13m/s \tag{5.20}$$

$$H = h_u cos(\phi) + \frac{V_{average}^2}{2g} = 0.877m \tag{5.21}$$

A comparison between the experimental and theoretical results is realised in Table 5.16.

	h_w [mm]	$V_{average}$ [m/s]	H [m]
Experimental results	12.1	4.38	0.9517
Theoretical results	12.33	4.13	0.877
Error	1.9%	6.05%	8.5%

TABLE 5.16: Creager weir and smooth spillway: comparison between experimental and theoretical results.

Creager weir and stepped spillway

For this configuration, the uniform flow is reached because the discharge was chosen in Section 3.4 to have a uniform flow at the measure point. According to Boes and Hager, 2003a, Equations 5.22 to 5.29 are used in order to find the residual head H_{res}. Moreover, Equations 2.4 and 5.30 are used to calculate respectively the uniform depth and the average velocity.

$$\frac{H_{\text{res}}}{H_{\max}} = \frac{F}{\frac{H_{\max}}{h_c} + F} \tag{5.22}$$

$$F = \left(\frac{f_b}{8\sin\phi}\right)^{1/3} \cos\phi + \frac{\alpha}{2}\left(\frac{f_b}{8\sin\phi}\right)^{-2/3} \tag{5.23}$$

$$\frac{1}{\sqrt{f_b}} = \frac{1}{\sqrt{0.5 - 0.42\sin(2\phi)}}\left[1.0 - 0.25\log\left(\frac{K}{D_{h,w,u}}\right)\right] \tag{5.24}$$

$$h_c = \left(\frac{q^2}{g}\right)^{1/3} \tag{5.25}$$

$$\alpha = 1.1 \tag{5.26}$$

$$K = s.cos(\phi) \tag{5.27}$$

$$D_{h,w,u} \approx 4h_{w,u} \tag{5.28}$$

$$h_{w,u} = 0.23s\left(\frac{q_w}{\sqrt{gsin\phi s^3}}\right)^{0.65} \tag{5.29}$$

$$V_{average} = \frac{Q}{h_u L} \tag{5.30}$$

A comparison between the experimental and theoretical results is realised in Table 5.17.

	h_w [mm]	$V_{average}$ [m/s]	H [m]
Experimental results	16.74	3.105	0.484
Theoretical results	15.6	3.26	0.536
Error	7.3%	4.99%	10.7%

TABLE 5.17: Creager weir and stepped spillway: comparison between experimental and theoretical results.

Tables 5.16 and 5.17 confirm that the obtained results for the Creager weir are in the right range of values. Indeed, the difference between the clear water depths for the stepped spillway is 1.14mm but as a reminder, measurements are accurate to within a millimetre. Then, the error values for velocities and heads have two origins: measurement errors in water levels and discharges.

Chapter 6

Conclusion and Future work

The principal purpose of this work was to characterize the flow properties downstream Piano Key Weirs (PKW), particularly for a steep slope. For this characterization, flows downstream three different weirs were studied : a Creager weir, and two PKWs with different geometries. Moreover, these weirs were combined with two types of spillways: smooth spillways and stepped spillways. At the end, six configurations were tested with the aim of comparing them and drawing conclusions about the flow properties depending on the used weir and spillway.

Firstly, a general introduction about the dams was presented: their history, their different functions, their current state. Then, some explanations about the spillways were provided: their usefulness, their importance and the different possible geometries. This has led to a summary diagram of notations for stepped spillways.

Secondly, a state of the art was realized, particularly for stepped spillways and Piano Key Weirs which are the subject of this work. In the stepped spillways part, the various advantages of this type of spillway were mentioned and the three flow regimes were presented. A particular attention has been paid to skimming flow as this is the regime targeted in this work. Theoretical models were presented in order to calculate the flow properties for this flow regime. In the second part, the PKWs were the main topic. Their history, their advantages, the different types, the notation for their geometry and the flow patterns were discussed. All these discussions have led to the purpose of this work.

The third step is the methodology. This chapter begins with the description of the experimental setup used during this work. Then, the different instrumentals used were described: the double-tips conductivity probe, the probe holder and the flowmeter. Moreover, the summary of the different tested configurations and the experimental protocol were presented. Finally, preliminary calculations were carried out to determine the discharge used during the entire period of the work.

Then, the results obtained using the double-tips conductivity probe were presented. Firstly, the comparison of the results given by the two probes and the comparison between the results above a step niche or a step edge were realised. Furthermore, the results of air concentrations and velocities profiles for the six configurations were shown. For each configuration, several positions across the width of the channel and approximately far from the top of the dam were tested. For each configuration, some conclusions about the presence and the position of extremes were drawn. Moreover, the evolution of the flow properties along the flow was analysed for each configuration.

The next step was the most important part of this work: the analyses and discussions of the results. The first studied property was the dimensionless air concentrations profiles. Indeed, in order to be able to compare the shapes of the air concentrations profiles, the y-coordinates were divided by the mixture-flow depth at 90% air concentration for each test. For each configuration, these profiles were almost overlaid. Average curves were thus elaborated in order to compare the six configurations and each average curve with theoretical models. The second studied flow property was the discharge. The total discharge was calculated from the air concentrations and velocities results. However, this discharge did not correspond to the injected discharge ($25L/s$). The specific discharges were therefore recalculated on the basis of the injected discharge, and these could be compared with each other in terms of variations. Then, the clear water depths were calculated from the air concentration profiles. Some comparisons between the six configurations were realized in terms of values, variations and positions of the extremes in relation to the geometry of the weirs. Using discharges and clear water heights, the average velocities were calculated and also compared between them. Finally, the last analysed property was the dissipated energy. In order to know it, the upstream heads and the heads at the measure point were calculated.

At the end, different important conclusions were drawn from the results obtained in this work. Firstly, more air is entrained in the flow for stepped spillways than for smooth spillways. Moreover, in the case of smooth spillways, the air entrainment is more important for the PKW2, than for PKW1 and finally the air entrainment for the Creaser weir is almost non-existent. For stepped spillways, the air entrainment can be considered to be the same for the different weirs. Then, a non-uniformity of the clear water depth and velocity across the width can be observed for PKWs. This results in non-uniformity of heads across the width of the channel, which is greater for smooth spillways than for stepped spillways. This non-uniformity is also more important for the PKW1 than the PKW2. Finally, this work enabled a comparison to be made of the energy dissipated as a function of the weirs and spillway types. The conclusion is that the stepped spillways dissipate more energy than smooth spillways. Moreover, the type of weir seems to have a small influence on the dissipated energy. Even if the difference is not very important, the dissipated energy is slightly greater in the case of a Creager weir than PKWs. This conclusion is counterintuitive because the PKWs create 3D flows downstream. In 3D flows, the turbulences are more important than in 2D flows (flows downstream Creager weirs). More turbulence means more energy dissipation, but the obtained results do not confirm this hypothesis.

The obtained results and the corresponding conclusions provide some perspectives for the future. Indeed, it would be interesting to investigate more positions over the length of the flow in order to have a better idea of the properties of the 3-dimensional flow that appears downstream of PKWs. Moreover, testing several discharges and several PKWs could enable to see how the 3-dimensional flow evolves depending on the PKWs geometry and the discharge. Another perspective would be to consider the design of dissipation basins for non-uniform flows over the width of the basin. Indeed, until now, the dissipation basins are designed for uniform flow across the width of the channel, but the results obtained show that, downstream of PKWs, the head is not uniform across the width.

Nomenclature

Symbols	Unities	Significations
B	m	Lateral crest length of a piano key weir
B_i	m	Upstream overhang lengths of a piano key weir
B_o	m	Downstream overhang lengths of a piano key weir
C	-	Air concentration
C_{mean}	-	Mean air concentration
C_w	-	Discharge coefficient
D'	-	Turbulent diffusivity
D_0	-	Dimensionless coefficient in diffusivity model
$D_{h,w,u}$	m	Hydraulic diameter of uniform flow
F	-	Coefficient used in Boes and Hager,2003 method
$F*$	-	Characteristic roughness Froude number
f_b	-	Friction factor
g	m^2/s	Gravity acceleration
H	m	Total upstream head
h_0	m	Water depth above weirs
$h_{90,u}$	m	Uniform mixture-flow depth for an air concentration equals to 90%
h_c	m	Critical height
H_{dam}	m	Vertical height of the dam
$H_{dam,u}$	m	Vertical height from the top to reach the uniform flow
H_{max}	m	Energy head at spillway crest
$H_{measure}$	m	Energy head at x=1,76m
H_{res}	m	Residual energy head
$H_{upstream}$	m	Energy head at spillway crest
h_w	m	Clear-water flow depth
$h_{w,u}$	m	Uniform equivalent clear water depth
i	-	Bottom slope
J	-	Head loss
K	$m^{1/3}/s$	Strickler coefficient
K'	-	Integration constant
L	m	Channel width
L_i	m	Location of the inception point
N	-	Exponent of power-law velocity profile
P	m	Weir height of a piano key weir
q	m^2/s	Discharge at each measurement point calculated from the injected discharge and the water depths

Q	m^3/s	Water discharge
$q_{measure}$	m^2/s	Discharge at each measurement point calculated from the velocities and water depths
Q_{PKW}	m^3/s	PKW discharge
$Q_{tot,injected}$	m^3/s	Total discharge injected and verify with the flowmeter
$Q_{tot,measure}$	m^3/s	Total discharge calculated by integrating $q_{measure}$
q_w	m^2/s	Unit discharge
Q_W	m^3/s	Sharp crested weir discharge correspondent
r	-	Discharge enhancement ratio
R_h	m	Hydraulic radius
s	m	Step height
T_s	m	Wall thickness of a piano key weir
u	m/s	Average flow velocity
V	m/s	Flow velocity in x-direction
V_{90}	m/s	Characteristic flow velocity at h90
$V_{average}$	m/s	Average flow velocity
V_{mean}	m/s	Average flow velocity
W_i	m	Inlet widths of a piano key weir
W_o	m	Outlet widths of a piano key weir
W_u	-	Number of "PKW unit" of a piano key weir
x	m	Coordinate originating at the top of the spillway and parallel to the (pseudo-)bottom
y	m	Transverse coordinate originating at the (pseudo-)bottom and perpendicular to it
y'	-	Dimensionless depth
y_{90}	m	Mixture-flow depth at 90% air concentration
z	m	Coordinate on the width of the spillway
z'	-	Dimensionless z-coordinate
$z_{measure}$	m	Distance between the measure position and the top of the spillway where the weirs are placed
z_{tank}	m	Distance between the bottom of the tank to the top of the spillway where the weirs are placed
z_{weir}	m	Weirs depth
α	-	Coefficient used in Boes and Hager,2003 method
β	-	Constant in the air demand equation of Wood
γ	-	Constant in the air demand equation of Wood
Δx	m	Cistance between the two tips of the probe
ϕ	-	Channel slope

Bibliography

Anderson, R., & Tullis, B. (2013). Piano key weir hydraulics and labyrinth weir comparison. *Journal of Irrigation and Drainage Engineering*, *139*(3), 246–253.

Bally, F.-X., & Berroir, J.-M. (2010). Incertitudes expérimentales. *ENS, Université Paris*, *6*(7).

Baylar, A., Emiroglu, M., & Bagatur, T. (2009). Influence of chute slope on oxygen content in stepped waterways. *Gazi University Journal of Science*, *22*(4), 325–332.

Bhukya, R. K., Pandey, M., Valyrakis, M., & Michalis, P. (2022). Discharge estimation over piano key weirs: A review of recent developments. *Water*, *14*(19), 3029.

Boes, R. M., & Hager, W. H. (2003a). Hydraulic design of stepped spillways. *Journal of Hydraulic Engineering*, *129*(9), 671–679.

Boes, R. M., & Hager, W. H. (2003b). Two-phase flow characteristics of stepped spillways. *Journal of hydraulic engineering*, *129*(9), 661–670.

Bung, D. B. (2011). Developing flow in skimming flow regime on embankment stepped spillways. *Journal of Hydraulic Research*, *49*(5), 639–648.

Carosi, G., & Chanson, H. (2008). Turbulence characteristics in skimming flows on stepped spillways. *Canadian Journal of Civil Engineering*, *35*(9), 865–880.

Cfbr. (accessed in June 2023). Evacuateurs de crue [https://www.barrages-cfbr.eu/Evacuateurs-de-crue.html].

Chanson, H. (1995a). Air bubble diffusion in supercritical open channel flow.

Chanson, H. (1995b). Air bubble entrainment in free-surface turbulent flows: Experimental investigations.

Chanson, H. (2001). Hydraulic design of stepped spillways and downstream energy dissipators. *Dam Engineering*, *11*(4), 205–242.

Chanson, H. (1994). Hydraulics of nappe flow regime above stepped chutes and spillways. *Australian Civil/Structural Engineering Transactions*, (1), 69–76.

Chanson, H., & Felder, S. (2010). Turbulence measurements in air-water self-aerated flows: Basic analysis and results. *Proc. 7th International Conference on Multiphase Flow ICMF*.

Chanson, H., & Gonzalez, C. A. (2005). Physical modelling and scale effects of air-water flows on stepped spillways. *Journal of Zhejiang University-Science A*, *6*(3), 243–250.

Chanson, H., & Toombes, L. (2002). Air–water flows down stepped chutes: Turbulence and flow structure observations. *International Journal of Multiphase Flow*, *28*(11), 1737–1761.

Crookston, B. M., Erpicum, S., Tullis, B. P., & Laugier, F. (2019). Hydraulics of labyrinth and piano key weirs: 100 years of prototype structures, advancements, and future research needs. *Journal of Hydraulic Engineering*, *145*(12), 02519004.

Defi12. (accessed in June 2023). Pkw for the oule dam (france) [https://defi-12.com/wp-content/uploads/2021/06/eco-Industrie_PDF-DEFI-12.pdf].

Dewals, B., André, S., Schleiss, A., & Pirotton, M. (2004). Validation of a quasi-2d model for aerated flows over mild and steep stepped spillways. In *Hydroinformatics: (in 2 volumes, with cd-rom)* (pp. 63–70). World Scientific.

Erpicum, S., Machiels, O., Archambeau, P., Dewals, B., Pirotton, M., & Daux, C. (2011). Energy dissipation on a stepped spillway downstream of a piano key weir–experimental study. *Labyrinth and piano key weirs-PKW 2011*, 105–112.

Erpicum, S., Lempérière, F., Ouamane, A., Ho Ta Khanh, M., Laugier, F., Tullis, B., & Crookston, B. (2020). From labyrinth to piano key weird: The story.

Faure, J. (2015-2016). Evacuateurs de crue de type pkw - etude expérimentale de l'énergie résiduelle en aval. In *Master thesis, university of liège.*

finartamerica. (accessed in June 2023). *Beaver dam spillway gates (us)* [https://fineartamerica.com/featured/beaver-dam-spillway-gates-james-pinkerton.html].

IAHR. (accessed in June 2023). Riou dam (france) - stepped spillway [https://www.iahrmedialibrary.net/the-library/applied-hydraulics/hydraulic-structures/riou-dam-france-stepped-spillway-3/976].

ICOLD. (accessed in March 2023). International commission of large dam [https://www.icold-cigb.org/GB/dams/dams.asp].

Laugier, F., Vermeulen, J., & Lefebvre, V. (2013). Overview of piano key weirs experience developed at edf during the past few years. *Labyrinth and piano key weirs II*, 213–226.

Lempérière, F., & Ouamane, A. (2003). The piano keys weir: A new cost-effective solution for spillways. *International Journal on Hydropower & Dams*, *10*(5), 144–149.

LeProgrès. (accessed in June 2023). Pkw and smooth spillway for the charmines dam (france) [https://www.leprogres.fr/ain/2015/08/14/touches-de-piano-et-nouvelle-partition-pour-le-barrage-de-charmines].

Lopes, R., Matos, J., & Melo, J. (2011). Flow properties and residual energy downstream of labyrinth weirs. *Labyrinth and Piano Key Weirs; Erpicum, S., Laugier, F., Boillat, JL, Pirotton, M., Reverchon, B., Schleiss, A., Eds*, 97–104.

Merkel, J., Belzner, F., Gebhardt, M., & Thorenz, C. (2018). Energy dissipation downstream of labyrinth weirs.

Ouamane, A., & Lempérière, F. (2006). Nouvelle conception de déversoir pour l'accroissement de la capacité des retenues des barrages. *Colloque international sur la protection et la préservation des ressources en eau, Bilda, Algérie.*

Pfister, M., & Hager, W. H. (2011). Self-entrainment of air on stepped spillways. *International Journal of Multiphase Flow*, *37*(2), 99–107.

Pralong, J., Vermeulen, J., Blancher, B., Laugier, F., Erpicum, S., Machiels, O., Pirotton, M., Boillat, J.-L., Leite Ribeiro, M., & Schleiss, A. (2011). A naming convention for the piano key weirs geometrical parameters. *proceedings of the International Conference Labyrinth and Piano Key Weirs*, 271–278.

R. Eslinger, K., & Crookston, B. M. (2020). Energy dissipation of type a piano key weirs. *Water*, *12*(5), 1253.

Schleiss, A. (2011). From labyrinth to piano key weirs: A historical review. *Proc. Int. Conf. Labyrinth and Piano Key Weirs Liège B*, 3–15.

Silvestri, A., Archambeau, P., Pirotton, M., Dewals, B., & Erpicum, S. (2013). Comparative analysis of the energy dissipation on a stepped spillway downstream of a piano key weir. *Labyrinth and piano key weirs II*, 111–120.

Silvestri, A. (2011-2012). Étude de la dissipation d'énergie sur un coursier en marches d'escalier en aval d'un évacuateur de crue de type pkw. *Master Thesis at the University of Liège.*

Singh, D., & Kumar, M. (2022). Energy dissipation of flow over the type-b piano key weir. *Flow Measurement and Instrumentation*, *83*, 102109.

Van Alwon, J., Borman, D., Sleigh, A., & Kapur, N. (2017). Experimental and numerical modelling of aerated flows over stepped spillways. *Proceedings of IAHR 2017.*

Wikipedia. (accessed in March 2023). Barrage [https://fr.wikipedia.org/wiki/Barrage].

Wood, I. R. (1991). *Air entrainment in free-surface flow: Iahr hydraulic structures design manuals 4.* Balkema.